Investigating the molecular mechanism underpinning the neurodegenerative disease Charcot-Marie-Tooth disease, and the frameshifting mechanism of C9-FTD/ALS

DISSERTATION

Zur Erlangung des akademischen Grades
"Doctor rerum naturalium"

Dr. rer. nat.

Eingereicht an der

Fakultät für Mathematik, Informatik und Naturwissenschaften der Universität Hamburg

Vorgelegt von

Robin J Thompson, M.Sci

Hamburg

6th June 2023

The work presented here was carried out from 14th February 2019, to 31st December 2023 at the Institute for Biochemistry and Molecular Biology, a part of the Faculty of Mathematics, Computer Science, and Natural Sciences, at the University of Hamburg. The work was supervised by Prof. Dr. Zoya Ignatova.

Reviewers

Prof. Dr. Zoya Ignatova	Dr. Marie Sissler
University of Hamburg	University of Strasbourg
Martin-Luther-King Platz 6	21 rue René Descartes
20146 Hamburg	67000 Strasbourg
Germany	France

Publications

- Zuko, A., Mallik, M., Thompson, R., Spaulding, E. L., Wienand, A. R., Been, M., Tadenev, A. L. D., van Bakel, N., Sijlmans, C., Santos, L. A., et al. (2021). tRNA overexpression rescues peripheral neuropathy caused by mutations in tRNA synthetase. Science 373(6559): 1161-1166.
- 2. Das, S., Zuko, A., Thompson, R., Storkebaum, E. and Ignatova, Z. (2022). Immunoprecipitation Assay to Quantify the Amount of tRNAs associated with Their Interacting Proteins in Tissue and Cell Culture. *Bio-protocol* 12(4): e4335.

Contents

Ab	stract	1
Zus	sammenfassung	3
1 -	Introduction	5
	1.1 - Initiation and elongation phases in translation	5
	1.2 - How tRNA abundance and prevalence of codons affects translational speeds	10
	1.3 - tRNA aminoacylation and charging fidelity	11
	1.4 - Structure of neuronal cells	16
	1.5 - Local Translation in Neuronal cells	18
	1.6 - Charcot-Marie-Tooth disease	21
	1.7 - C9-orf72-mediated ALS/FTD	22
	1.8 - Other neurodegenerative diseases with links to translation	25
2 -	Aims of the thesis	28
3 -	tRNA sequestration as an underlying mechanism of CMT2 neuropathy associated with	h
ger	netic mutations in GARS	29
	3.1 - Introduction	30
	3.2 - Results & Discussion	30
	3.3 - Conclusion	40
	3.4 - Materials and Methods	40
4 -	CMT-YARS mutant variants increased ribosome occupancy at Tyr codons	46
	4.1 - Introduction	46
	4.2 - Results and Discussion	48
	4.3 - Conclusion	54
	4.4 - Materials and Methods	55

5 – Length dependent decrease of translation along neurites is exacerbated in cells
expressing CMT-GARS variants57
5.1 - Introduction57
5.2 - Results & Discussion59
5.3 - Conclusion67
5.4 - Materials and Methods68
$6-C9 \textit{Orf72} ALS$ -associated G_4C_2 repeat regions caused ribosomal queuing behind start
codon72
6.1 - Introduction72
6.2 - Results and Discussion74
6.3 – Conclusion81
6.4 - Materials and Methods82
7 – Discussion
7.1 - Charcot-Marie-Tooth disease84
7.2 - C9Orf72 mediated ALS/FTD87
7.3 - Conclusion90
8 – Bibliography91
9 - List of hazardous substances
Acknowledgements
Eidesstattliche Versicherung
Affidavit114

List of abbreviations

A Adenine

aa Amino acid

aaRS Aminoacyl-tRNA-Synthetase

AARS Alanyl-tRNA-synthetase

aa-tRNA Aminoacyl-tRNA

ALS Amyotrophic lateral sclerosis

A site Aminoacyl site

ATP Adenosine triphosphate

bp Base pair

C Cytosine

C9 or C9-ALS C9*Orf72* mediated FTD/ALS

CHIR CHIR99021

CMT Charcot-Marie-Tooth Disease

CNS Central nervous system

DMEM Dulbecco's modified eagle medium

DNA Deoxyribonucleic acid

DPR Di-peptide repeat protein

eEF Eukaryotic elongation factor

elF Eukaryotic initiation factor

E-site Exit site

FTD Frontotemporal dementia

FXS Fragile X syndrome

G Guanine

GARS Glycyl-tRNA-synthetase

Gly Glycine

GTP/GDP Guanosine tri/di-phosphate

Htt Huntingtin

IP Immunoprecipitation

iPSC Induced pluripotent stem cells

ISR Integrated stress response

MARS Methionyl-tRNA-Synthetase

Met Methionine

MNs Motor neurons

mRNA Messenger RNA

NCV Nerve conduct velocity

nt Nucleotide

PiC Pre-initiation complex

PMA Purmorphamine

PNS Peripheral nervous system

P site Peptidyl site

RAN Repeat-associated non-AUG

RNA Ribonucleic acid

rRNA Ribosomal RNA

SEC Size exclusion chromatography

smNPC Small-molecule neural progenitor cells

SNs Sensory neurons

T Thymine

TC Ternary complex

tRNA Transfer RNA

tRNAi Initiator transfer RNA

Tyr Tyrosine
U Uracil

WT Wild type

YARS Tyrosyl-tRNA-synthetase

Abstract

The molecular mechanisms underlying the progression and the development of the neurodegenerative disease: Charcot-Marie-Tooth (CMT), and C9*Orf72*-mediated amyotrophic lateral sclerosis (ALS), is still not fully understood. CMT is a prevalent (1:2500) inherited disease, though the term describes a number of disorders with a plethora of different genetic causes, though all of which lead to motor and sensory neuronal defects. In this study we focused on CMT2, the axonal dystrophy form which shows a phenotype of length-dependant, distal axonal degeneration. Proteins involved in this form of CMT are the aminoacyl-tRNA-synthetases (aaRS), though why mutations in ubiquitously expressed enzymes such as the aaRSs cause defects specifically in motor and sensory neurons, is not understood, and proposed hypotheses to-date do not fully capture a unified mechanism among all the different CMT-relevant mutations of aaRSs that have been found in patients. Repeat expansions in the C9Orf72 gene are a frequent cause for the development of the devastating neurodegenerative disease, ALS. These repeat-expansions cause production of cytotoxic di-peptide repeat proteins (DPRs) as the ribosomes translate the expansion regions. Evidence suggests that the ribosome frameshifts on this repeat-region, causing production of a variety of different DPRs, which lead to a variety of toxic effects inside the cell. The cause of this frameshifting is still unclear, and while a number of possible reasons are proposed, it still lacks a fully explored mechanism. Therefore, in this study then we aim to explore the molecular mechanisms causing these diseases.

The most studied cause of CMT2 are mutations of the glycyl-tRNA-synthetase (GARS), with variants of the protein leading to a wide range of clinical outcomes, such as disease onset as early as a few years, to the second or third decade in life, with severity in symptoms as well. So far, a single explanation capturing how these wide-ranging effects can bring out the same disorder, has been elusive. Here, we show that tested GARS variants have a 50% increased affinity to its cognate tRNA^{Gly}, and in an in vitro study, showed that the mutant variants show a slow release of the tRNA. Ribosome profiling analysis of mice^{C201R/+} spinal cord samples, showed a 40% increased ribosomal dwelling time at Gly codons. This indicates a possible 'sequestration' effect by the mutant GARS, wherein cognate tRNA is held for a longer than usual time, possibly leading to translational slowdown. This effect was also shown for CMT-

relevant YARS variants in *Drosophila* models. In cultured neuronal cells transfected with CMT-GARS variants, a length-dependant translational decrease was seen, with distal areas of the cell showing less relative translation, with some mutants having a ~50% decreased translation as compared to wild type, at a distance of 170µm away from the somata. Transfecting the cell with equimolar concentrations of tRNA^{GIy} alleviated the translational slowdowns at the distal end. Taken together, then, mutant-GARS shows a higher affinity to its cognate tRNA, which depletes the available pool of tRNA in the cell leading to translation defects. This is potential aberrant translational rate is felt more strongly in the distal areas of the cell, linking a molecular mechanism of this protein to the clinical progression.

Alternate start codons that are implicated in the non-canonical translation in the C9Orf72 gene, were used in a construct in cell culture, followed by a ribosome profiling experiment to determine frameshifting under conditions of excess pre-initiation complexes, and stalled initiation. While the work carried out here for C9-ALS was unfortunately limited in its scope, a number of interesting facts can be seen. The addition of Met-tRNAi^{Met} to the cell is followed by an increased clustering of initiation complexes upstream of the start codon. In the 'CUG+tRNA' sample, frameshift analysis also shows a shift to the +1 frame, when compared to the transcriptome. However, lack of read-depth, possibly due to inefficient initiation at the non-canonical start codons, leaves the data inconclusive, though indicative of further work needed to fully investigate this effect.

Zusammenfassung

Die molekularen Mechanismen welche dem Fortschreiten und der Entwicklung der neurodegenerativen Krankheiten Charcot-Marie-Tooth (CMT) und C9Orf72-vermittelte amyotrophe Lateralsklerose (ALS) zugrunde liegen, sind noch immer nicht vollständig verstanden. CMT ist eine häufige auftretende Erbkrankheit (1:2500). Der Begriff beschreibt eine Reihe von Störungen mit einer Fülle unterschiedlicher genetischer Ursachen, welche jedoch alle zu motorischen und sensorischen neuronalen Defekten führen. In dieser Studie konzentrierten wir uns auf CMT2, die Form der axonalen Dystrophie die einen Phänotyp der längenabhängigen distalen axonalen Degeneration zeigt. Bei den an dieser Form der CMT beteiligten Proteinen handelt es sich um die Aminoacyl-tRNA-Synthetasen (aaRS). Warum jedoch Mutationen in ubiquitär exprimierten Enzymen wie den aaRSs Defekte speziell in motorischen und sensorischen Neuronen verursachen ist nicht geklärt. Die bisher vorgeschlagenen Hypothesen erfassen nicht vollständig einen einheitlichen Mechanismus der verschiedenen CMT-relevanten aaRS Mutationen, welche bei Patienten gefunden wurden. Repeat-Expansionen im C9Orf72-Gen sind eine häufige Ursache für die Entwicklung der verheerenden neurodegenerativen Krankheit ALS. Diese Repeat-Expansionen verursachen die Produktion von zytotoxischen Di-Peptid-Repeat-Proteinen (DPR), wenn die ribosomen die Expansionsregionen translatieren. Es gibt Hinweise darauf, dass das Ribosom an dieser Repeat-Region einem Frameshifting unterliegt, was zur Produktion einer Vielzahl verschiedener DPRs führt welche eine Reihe von toxischen Wirkungen innerhalb der Zelle hervorrufen. Die Ursache für dieses Frameshifting ist noch unklar, und obwohl eine Reihe möglicher Gründe vorgeschlagen werden ist der Mechanismus noch nicht vollständig erforscht. In dieser Studie wollen wir daher die molekularen Mechanismen erforschen, welche diese Krankheiten verursachen.

Die am besten untersuchte Ursache von CMT2 sind Mutationen der Glycyl-tRNA-Synthetase (GARS), wobei Varianten des Proteins zu einem breiten Spektrum von klinischen Ergebnissen führen z. B. Ausbruch der Krankheit bereits im Alter von wenigen Jahren bis zum zweiten oder dritten Lebensjahrzehnt, als auch Symptome die unterschiedlich stark ausgeprägt sind. Bislang gab es keine einheitliche Erklärung dafür, wie diese weitreichenden Auswirkungen zu ein und derselben Erkrankung führen können. Hier zeigen wir, dass die getesteten GARS-

Varianten eine um 50 % erhöhte Affinität zu ihrem kognitiven tRNAGly haben, und in einer invitro-Studie konnten wir zeigen, dass die mutierten Varianten eine langsame Freisetzung der tRNA aufweisen. Ribosome profiling-Analysen von Mäusen mit C201R/+ Rückenmarksproben zeigten eine um 40 % erhöhte ribosomale Verweildauer an Gly-Codons. Dies deutet auf einen möglichen "Sequestrations"-Effekt durch die GARS-Mutante hin, bei dem die kognitive tRNA länger als üblich festgehalten wird, was möglicherweise zu einer Verlangsamung der Translation führt. Dieser Effekt wurde auch für CMT-relevante YARS-Varianten in Drosophila-Modellen gezeigt. In kultivierten neuronalen Zellen, welche mit CMT-GARS-Varianten transfiziert wurden, wurde ein längenabhängiger Rückgang der Translation beobachtet. Hierbei weisen die distalen Bereiche der Zelle eine geringere relative Translation auf, bei einige Mutanten im Vergleich zum Wildtyp eine bis zu ~50% verringerte Translation, und zwar in einer Entfernung von 170µm von den Somata. Die Transfektion der Zelle mit äquimolaren Konzentrationen von tRNAGly milderte die Translationsverlangsamung am distalen Ende. Insgesamt zeigt die Mutanten-GARS also eine höhere Affinität zu ihrer kognitiven tRNA, wodurch der verfügbare tRNA-Pool in der Zelle erschöpft wird, was zu Translationsdefekten führt. Diese potenziell abweichende Translationsrate macht sich in den distalen Bereichen der Zelle stärker bemerkbar, was einen molekularen Mechanismus dieses Proteins mit dem klinischen Verlauf in Verbindung bringt.

Alternative Startcodons, die für die nicht-kanonische Translation im C9Orf72-Gen verantwortlich sind, wurden in einem Konstrukt in Zellkultur verwendet, gefolgt von einem ribosomalen Sequenzierungsexperiment, um Frameshifting unter Bedingungen eines Überschusses an Prä-Initiationskomplexen und einer blockierten Initiation zu bestimmen. Obwohl die hier durchgeführten Arbeiten für C9-ALS in ihrem Umfang leider begrenzt waren lassen sich doch eine Reihe interessanter Fakten feststellen. Nach der Zugabe von MettRNAiMet in die Zelle kommt es zu einer verstärkten Anhäufung von Initiationskomplexen vor dem Startcodon. In der 'CUG +tRNA'-Probe zeigt die Frameshift-Analyse im Vergleich zum Transkriptom ebenfalls eine Verschiebung zum +1-Frame. Aufgrund der mangelnden Lesetiefe, die möglicherweise auf eine ineffiziente Initiation an den nicht-kanonischen Startcodons zurückzuführen ist sind die Daten jedoch nicht schlüssig, obwohl sie auf weitere Arbeiten zur vollständigen Untersuchung dieses Effekts hinweisen.

1 - Introduction

Translation in eukaryotes is a strictly regulated process in which mRNA molecules - which are initially transcribed from the DNA sequences on the chromosomes in the nucleus and transported into the cytoplasm - are decoded into peptide chains by a ribosome [1]-[3]. The ribosome scans along the mRNA molecule, reading the mRNA three nucleotides at a time [4], or a codon, and from this generates a peptide chain, the sequence of which is determined by the mRNA sequence. At every step of this process there are myriad factors involved, and many different types of regulatory processes that ensure efficient and correct translation of mRNA molecules into their coded protein [5]. A critical component of this entire process is the tRNA, the molecule that brings the amino acid - the singular component of peptide chains - to the ribosomes to be added to the growing peptide chain [6]. The tRNA thus forms a key link between the genetic code and the proteome which carries out the functions as detailed by their corresponding genes. Disruptions then of the tRNA; either their availability, ability to carry their cognate tRNA, or processing, can lead to translational defects inside the cell and has links to many diseases which can arise in humans [7]. Translation of the mRNA by the ribosome can be thought of as two distinct phases: initiation and elongation. The first being the stage of ribosomal binding to the mRNA where it scans along the molecule until reaching the start codon - an AUG nucleotide sequence on the mRNA that signals the ribosome to begin elongation. At this stage, the ribosome recruits more factors, and the synthesis of the peptide chain can begin. The ribosome moves down the mRNA codon by codon, elongating the peptide chain as it goes, until reaching a stop codon, wherein translation is terminated and the ribosome is dissociated from the mRNA and the peptide released.

1.1 - Initiation and elongation phases in translation

A number of factors are involved in the accurate and correct formation of the pre-initiation complex (PiC) and scanning fidelity along the mRNA. These include: eIF1, eIF1a, eIF2, eIF3, eIF4F complex, eIF5, eIF5B, and the Poly(A)-binding protein [8]. Initiation is first preceded by the formation of the Ternary complex(TC), wherein the initiation factor eIF2-GTP, binds to the initiator tRNAi^{Met}, and forms a complex with the small ribosomal 40S subunit [9]. This process is facilitated by eIF1 & eIF1a [10] and together with eIF3 and eIF5, forms the 43S complex [11].

The eIF4F complex and eIF3 mediate the loading of 43S onto the 5'-methyl cap of mRNA [12], [13], completing the 48S pre-initiation complex formation. After mRNA loading, the PiC investigates every nucleotide in a 5' to 3' direction along the mRNA [14], during which the GTP bound to eIF2 becomes hydrolysed, but remains in the PiC, and free Pi is not allowed to leave [11]. The scanning mechanism of the PiC, while still not fully understood, requires a very specific conformation and spatial structure of all of the different initiation factors involved to effectively allow for the scanning process to occur, and also to allow for the transition from initiation to elongation, once the PiC has reached an AUG start codon. For example, the initiation factor eIF4A, an RNA helicase [15], is positioned downstream of the PiC to help unwind mRNA before it encounters the ribosome. eIF4G is positioned upstream of the ribosome, and interacts with the mRNA and also eIF4a, effectively scaffolding the PiC together during scanning [16]. Once the AUG start codon is reached, the tRNAi^{Met} moves to fully accommodate into the P site, triggering rearrangement of eIF1 and release of free Pi [11] causing commitment of the 48S ribosome to transition from initiation to elongation. eIF5B mediates the dissociation from the PiC of eIF1, eIF1a, and eIF2-GDP, and recruits the 60S subunit [15], [17].

The first AUG encountered is generally favoured along the sequence, but context around the start codon is vital for correct conformational changes needed to trigger correct AUG recognition. Kozak sequences such as: (A/G)CCaugG, which critically feature a purine in position -3 and a guanine in position +4, relative to the start codon, interact with specific residues on the ribosome and stabilise the mRNA-ribosome interactions [8], [18]. Now, with the ribosome properly situated at an AUG start codon, with the tRNAi^{Met} base-paired to the mRNA in the P site, and the 60S subunit joining, the translation competent 80S ribosome is now fully formed and can carry on to the elongation phase. Peptide synthesis is carried out during the elongation phase of translation, in which the fully assembled, translationally-competent 80S ribosome [19], moves along the mRNA molecule, one codon at a time, decoding the sequence as it moves with the aid of aminoacyl-tRNA(aa-tRNA) which carries an amino acid corresponding to the specific anticodon on the tRNA [20]. The amino acid from the tRNA is incorporated onto the C-terminal end of the growing peptide nascent chain that extends from the peptidyl-transfer centre(PTC) of the ribosome, and out of the exit tunnel which spans the length of the larger 60S ribosome subunit [21], [22].

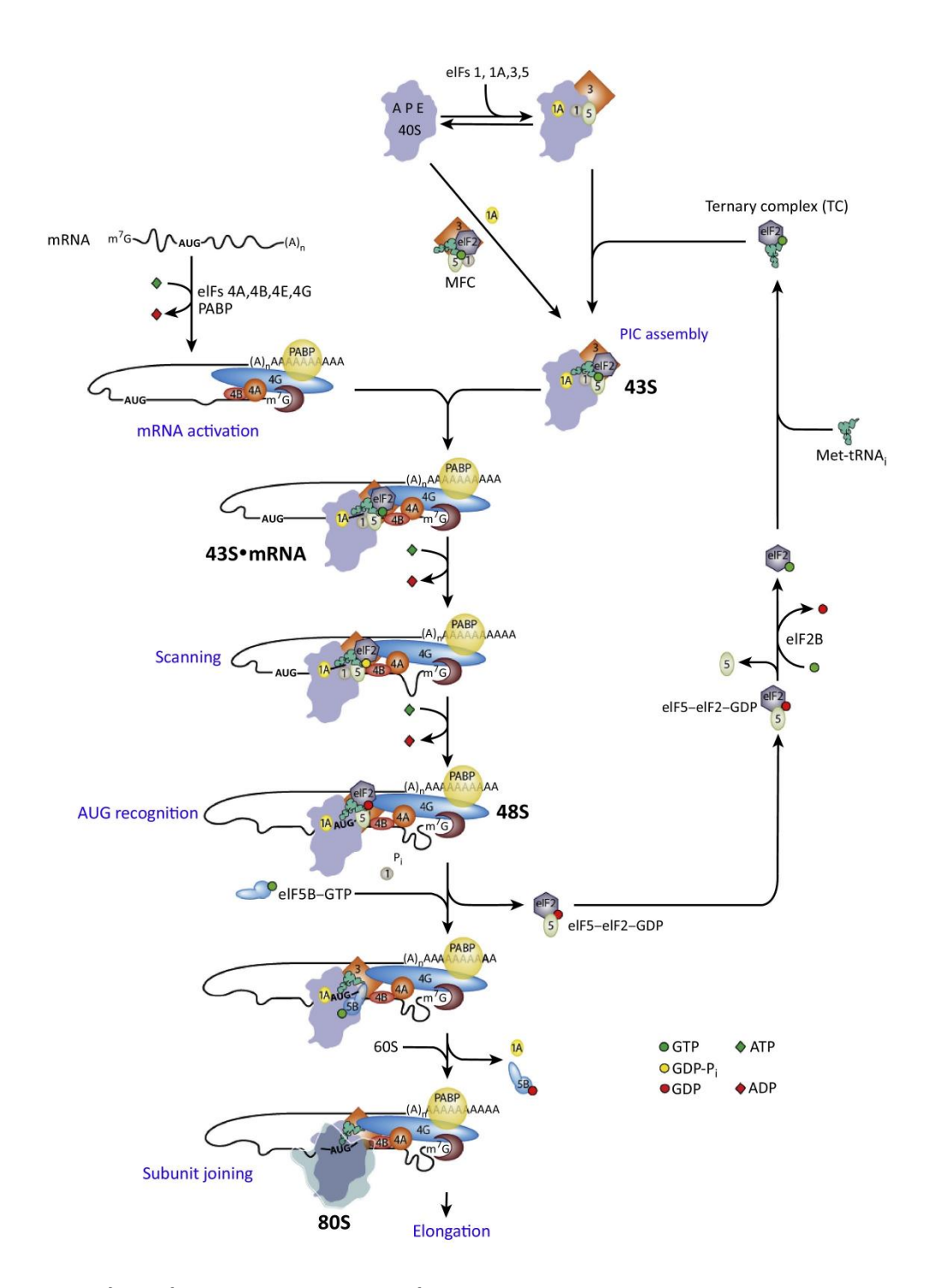


Figure 1.1 – The eukaryotic initiation pathway.

The 43S is initially formed from the TC, eIF1, 1a, 3 and 5. The mRNA is 'activated' by PABP, and eIF4F complex and is loaded onto the 43S at the 5'-cap end. The PiC then scans along the mRNA, triggering hydrolysis but retention of free Pi until the AUG codon is recognised. eIF1 is rearranged, and eIF2-GDP and Pi is released mediated by eIF5B. eIF5B also aids 60S subunit joining and formation of the translationally competent 80S subunit. eIF2-GDP is recycled by eIF2B into eIF2-GTP, allowing new TC to form. Figure taken from: [8].

The tRNA is then released from the E site of the ribosome - one of the three sites in the ribosome [23] - as it continues on to the next codon, commencing decoding of the rest of the coding-sequence. Canonical elongation is terminated once the ribosome reaches a stop codon – three codons with the sequence: UGA, UAA, UAG [24]. The 80S ribosome is then disassembled and can be utilised again in another round of initiation and elongation [25]. At the beginning of the elongation phase of translation, the 80S ribosome has an empty A site as the Met-tRNAi^{Met} is positioned and bound to the start codon in the P site [26]. The A site is the entry site for aa-tRNA and the site for the initial base-pair recognition between the tRNA and its cognate codon sequence on the mRNA molecule that is strung through the core of the ribosome [6], [27]. The 18s rRNA ensures accurate incorporation of the correct aa-tRNA for the codon in the A site, by inspecting the correct geometry of the codon-anticodon helix, carried out by the bases A1824, A1825, and G626 on the rRNA. These bases stabilise the aatRNA in the A site on correct Watson-Crick base pairing in the 1+ and 2+ position [28], while providing tolerance on the 3+ position – the 'wobble' base [29]. The tRNA itself is escorted to the A site as a ternary complex (eEF1A(GTP)-aa-tRNA) with the elongation factor, eEF1a1 [30] or eEF1a2 in neuronal cells [31], and GTP. Upon binding to the ribosome and A site entry, the tRNA undergoes a conformational change, positioning the anticodon to interact with the mRNA and the acceptor end bound to eEF1A [32]. The eEF1A can then dock on the GTPase activating centre on the 60S subunit, triggering GTP hydrolysis by eEF1a [30], [33], [34]. Hydrolysis of GTP and release of aa-tRNA from the ternary complex, allows entry of the aminoacylated 3'CCA tail of the tRNA into the PTC, causing peptide bond formation between the nascent chain polypeptide and the amino acid on the A-site tRNA, swapping the bond from the P-site tRNA [34] [35]. This pre-translocation state of the ribosome, where a tRNA is bound in the A site and a deacetylated-tRNA in the P site is swiftly moved into the posttranslocation state by the activity of the GTPase, eEF2. This elongation factor induces a 'ratcheting' motion on the ribosome, with the small subunit in a different orientation to the large subunit [36]. This is followed by another conformational change causes a 'swivelling' of the small subunit, moving the anticodon ends of the tRNA into the E and P sites, leaving the A site empty to receive another aa-tRNA [37], [38] and allowing the tRNA in the E site to be recycled for further translation.

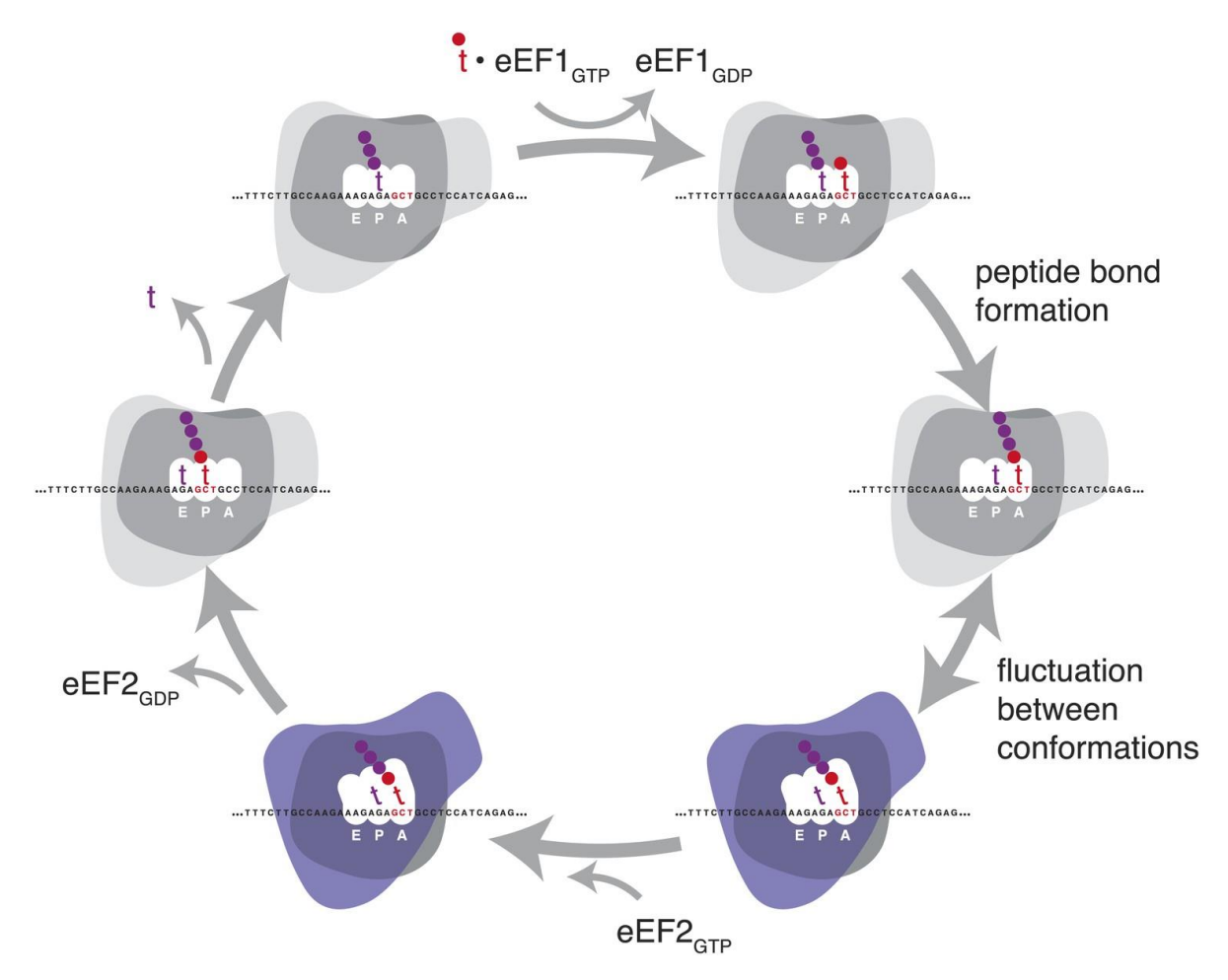


Figure 1.2 – The complete eukaryotic elongation cycle on the ribosome.

eEF1-GTP brings aminoacyl-tRNA to the ribosome where it is accommodated into the A site of the ribosome. The A-site tRNA forms a peptide bond with the nascent peptide in the exit tunnel, leaving the P-site tRNA unacylated. The ribosome moves one codon downstream, aided by eEF2, shifting the tRNAs from A>P and P>E. The empty A site is now ready to accommodate another tRNA. Figure taken from: [39].

This repeated cycle continues across the entire coding sequence on the mRNA, moving a codon each time, and elongating the nascent polypeptide with every addition. Eventually the ribosome will encounter a termination or 'stop' codon, donated by the codons: UGA, UAG, and UAA. The stop codons in the A site is recognised by the release factor, eRF1 [24] accommodating into the A site of the ribosome, extending its GGQ motif [40] into the PTC of the ribosome and triggering hydrolysis of the peptidyl-tRNA bond [41]. The subunits can then be dissociated by release factors to be used again in translation, and the completed polypeptide can be released from the ribosome [42].

1.2 - How tRNA abundance and prevalence of codons affects translational speeds tRNA is a vital molecule in the translation process then, and forms a critical bridge between the genetic code and its expression in the form of proteins. Therefore, the regulation, expression, and maintenance of tRNA can be a critical determining factor in how fast or slow, or how error-free the elongation process is [43], [44]. In fact, avoiding Ribosomal slowdowns during elongation is a necessity for the cell, as chronic slowdowns can lead to Ribosomal stalling, or even collisions [45], which forces the cell to undergo an energy expensive pathway to clear and recycle the ribosomes [46], [47] and inevitably leads to a decreasing amount of protein expression of the stall-inducing transcript. As tRNA plays a pivotal role in the rate of elongation, since the ribosome cannot continue to translocate without an occupied A site, the supply of aa-tRNA needs to meet the demand of the individual codons that make up the coding sequences.

Table 1.1 – Codon usage bias in humans.

Amino acid corresponding to the respective codon is indicated. Numbers are frequency of codon per one thousand. Data obtained from Codon usage database: [48].

Phe	UUU	17.6
Phe	UUC	20.3
Leu	UUA	7.7
Leu	UUG	12.9
Leu	CUU	13.2
Leu	CUC	19.6
Leu	CUA	7.2
Leu	CUG	39.6
Ile	AUU	16
Ile	AUC	20.8
Ile	AUA	7.5
Met	AUG	22
Val	GUU	11
Val	GUC	14.5
Val	GUA	7.1
Val	GUG	28.1

Ser	UCU	15.2
Ser	UCC	17.7
Ser	UCA	12.2
Ser	UCG	4.4
Pro	CCU	17.5
Pro	CCC	19.8
Pro	CCA	16.9
Pro	CCG	6.9
Thr	ACU	13.1
Thr	ACC	18.9
Thr	ACA	15.1
Thr	ACG	6.1
Ala	GCU	18.4
Ala	GCC	27.7
Ala	GCA	15.8
Ala	GCG	7.4

Tyr	UAU	12.2
Tyr	UAC	15.3
Stop	UAA	1
Stop	UAG	0.8
His	CAU	10.9
His	CAC	15.1
Gln	CAA	12.3
Gln	CAG	34.2
Asn	AAU	17
Asn	AAC	19.1
Lys	AAA	24.4
Lys	AAG	31.9
Asp	GAU	21.8
Asp	GAC	25.1
Glu	GAA	29
Glu	GAG	39.6

Cys	UGU	10.6
Cys	UGC	12.6
Stop	UGA	1.6
Trp	UGG	13.2
Arg	CGU	4.5
Arg	CGC	10.4
Arg	CGA	6.2
Arg	CGG	11.4
Ser	AGU	12.1
Ser	AGC	19.5
Arg	AGA	12.2
Arg	AGG	12
Gly	GGU	10.8
Gly	GGC	22.2
Gly	GGA	16.5
Gly	GGG	16.5

As can be seen in table 1.1, due to the degeneracy of the genetic code, each codon, even though coding for the same amino acid, has an individual usage, or put simply, a specific

prevalence in the coding sequence, a 'codon usage bias'. Generally, codons with a stronger bias across the genome correlates with higher amounts of available tRNA, as would be logical as they would impose a higher translational burden on the cell which needs to be met [44]. In practical terms, this means that highly expressed proteins will have greater numbers of codons with higher usage biases, as it can make use of the larger available tRNA pool to meet the need for more of the protein to be synthesised. One way to help meet this demand for some codons is to increase the gene number [49] and allow for multiple isodecoders to express (tRNAs with the same anticodon but a different tRNA body), increasing the available tRNA pool [50]. Another is to allow for a wobble base position [51], allowing for tRNAs to decode multiple different codons, such as with the tRNAGIY-TCC/ACC wobble. However, Ribosomal elongation speed itself is a controlled process, with an evolutionary pressure to ensure distinct translational rates at different points on the mRNA [52]. Slow or fast patches of translation on certain stretches of transcripts are necessary for the correct folding of the nascent chain [53], as the peptide chain can be given enough time to properly fold into its secondary and tertiary structures that give proteins their function [54]. Thus, tRNA abundance and prevalence of specific codons across the coding sequence are inextricably linked to the generation of the correct translatome of the cell, and any perturbations in abundance or processing of tRNA could potentially lead to widespread dysfunctions of the cell.

1.3 - tRNA aminoacylation and charging fidelity

For tRNA to carry out their role in translation, they first need to be loaded with an amino acid so as to deliver it to the ribosome during each elongation cycle. This process, called charging, is carried out by a ubiquitously expressed group of tRNA-ligase enzymes, also named as aminoacyl-tRNA synthetases (aaRS) [20]. These enzymes — which can be broadly classified as either Class 1 or Class 2 aaRS [55]—[57] - specifically charge each tRNA species with their cognate amino acid. For example, Glycyl-tRNA synthetase (GARS) will only charge tRNA^{Gly} with the amino acid glycine (Gly). This process is done by forming an ester bond between the amino acid and the adenine nucleotide on the 3' end of the CCA-tail of the tRNA in the catalytic site of the aaRS [58]. The reaction has two steps: first, the amino acid needs to be 'activated', where a nucleophilic attack is carried out on the C-terminal end of the amino acid of the acarboxylate oxygen to the a-phosphate group on an ATP molecule, generating an activated

aminoacyl-adenylate(aa-AMP) molecule bound to the catalytic site of the aaRS. The aaRS can then transfer the amino acid to the adenine on the CCA tail of the tRNA – the 2'-OH group (or 3', depending on the aaRS [59]) attacks the carbonyl carbon of the adenylate, which releases the bound AMP molecule, and forms a bond between the amino acid and the nucleotide (figure 1.3) [20]. The charged aa-tRNA can now bind to eEF1a and will be transported to the ribosome to take part in translation.

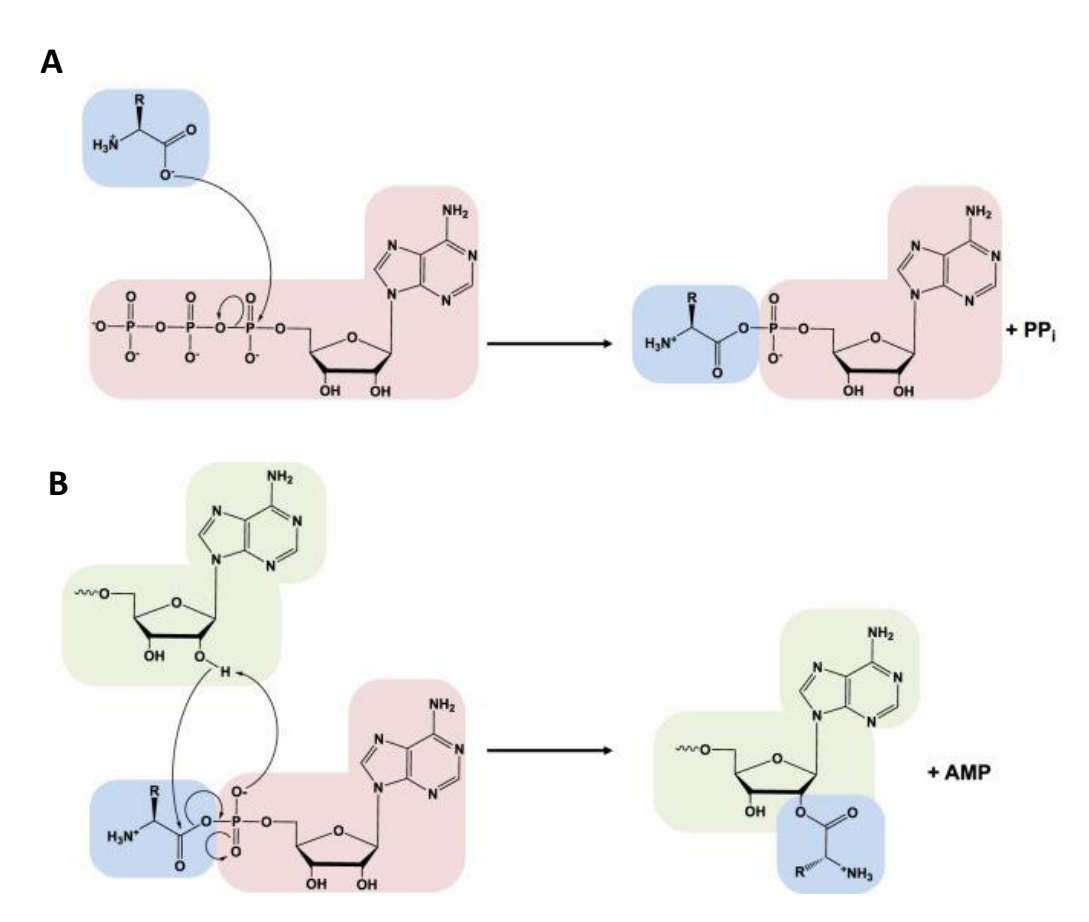


Figure 1.3 – Aminoacylation reaction on the CCA tail of the tRNA with a Class I aaRS, transferring the amino acid to the 2'OH group on the tRNA.

In **(A)** the amino acid (blue) is activated with ATP (red), releasing the free phosphates and forming aa-AMP. **(B)** The activated aa-AMP is transferred to the tRNA(green), releasing AMP. Figure taken from: [20].

The fidelity of this process must be strictly regulated and controlled. If the aaRS charges tRNAs with the incorrect amino acid, this will ultimately be incorporated into a growing peptide, which may lead misfolded and toxic proteins being produced by the cell, and lead to a decoupling of the codon sequence to the sequence of the peptide chain. To prevent this, the synthetases have mechanisms in place to distinguish both their cognate tRNA and also the amino acid [60], [61]. Failing this, some synthetases also contain editing mechanisms that error-checks for the correct tRNA-amino acid pairing and can hydrolyse the bonds between the pair to prevent the incorrect tRNA being used in translation [62]. Each synthetase carries out these processes in slightly different manners, mostly due to the nature of their cognate amino acid or tRNA. For discrimination of cognate tRNA, each species of tRNA has differences in their sequence, which the synthetases can utilise to identify the correct one. The first step of aaRS-tRNA bonding is driven mostly by unspecific, electrostatic interactions between phosphate backbone on the tRNA and peptides on the protein [63]. However, once the synthetase is in close proximity to the tRNA, it will try to bond more tightly, forcing a conformational change on the tRNA, allowing accommodation of the CCA-tail into its catalytic site. This process is lead more by identity elements on the tRNA, such as bases 35, 36, and 37 on the anticodon stem loop on the tRNA, which seems to be common among almost all aaRS [64]. As each tRNA species will have a different anticodon corresponding to the codon it needs to decode at the ribosome, the anticodon loop is a useful identity element to readily discriminate from the majority of the tRNA species. Though more specific, synthetase-specific elements also exist: For example, the well-known G3-U70 base pairing on a tRNA marks it for charging with AARS, which in fact is so well conserved that mutating other tRNAs to harbour the G3-U70 base-pairing will also mark it for charging with alanine [60], [65] regardless of anticodon identity. tRNAs also contain a discriminator base in the position directly 5' to the CCA tail (NCCA). All tRNAs of the same family in an individual organism will have the same discriminator base, for example all human tRNA^{Ser} will be: 5'GCCA'3 [66], and shows another filtering mechanism for the aaRSs. The base itself is used in aiding tRNA-aaRS binding, such as with the G73 discriminator in tRNAAsp where it hydrogen bonds with residues on the synthetase [67].

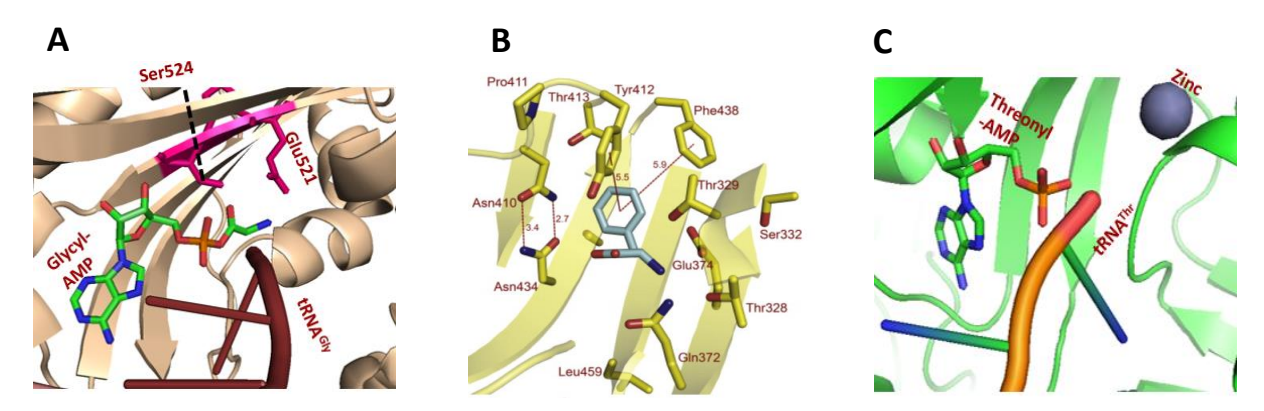


Figure 1.4 – Distinct recognition methods for different aaRSs.

Catalytic sites of **(A)** the GARS, **(B)** FARS (Phenylalanyl-tRNA-synthetase), and **(C)** TARS (Threonyl-tRNA-synthetase). Amino acid is shown in the catalytic site, along with the specific residues or ions that are important for amino acid recognition in their respective catalytic sites. Figure for FARS taken from: [68]. Images for GARS and TARS made using Pymol with data from PDB entries: GARS - 4QEI [69], and TARS - 1QF6 [70].

Amino acids are smaller molecules and often with similar physiochemical properties, making discrimination by the aaRS more difficult. There are three main types of strategies that are employed to discriminate for the cognate amino acid: charge exclusion, size exclusion, and metal ion aided exclusion. All of which are employed specifically by each aaRS to independently discriminate only its cognate amino acid. For example, in the negatively charged binding pocket of the GARS, two residues, Ser524 and Glu521, extend their sidechains into the open space, which interact and stabilise specifically Gly due to its neutral state and small size. This prevents non-cognate alanine binding, an amino acid with a hydrophobic sidechain, but of similar size to Gly (figure 1.4a) [71]. Metal ions, such as Zinc, imbedded into the active site of TARS aid the enzyme in discriminating against valine incorporation into the active site [61]. Another example is FARS, where the structure of the binding pocket specifically allows only the distinctly structured Phe to enter and bind [68]. Though this does lead to problems in the enzyme as Tyr has a very similar shape and size to Phe. A conserved Ala residue in the pocket helps to reduce Tyr binding, but misincorporation for FARS can still be high [72].

Despite the enzymes attempts to recognise and only bind their cognate amino acid and tRNA, misbinding can happen. For enzymes that seem particularly susceptible to this, a 'proof-

reading' step before the aa-tRNA can be released is carried out which can edit the mischarged tRNA. FARS is demonstrative of this need since the FARS can still successfully activate Tyr if it is incorporated into the active site which can lead to mischarging of Tyr-tRNA^{Phe} [73].

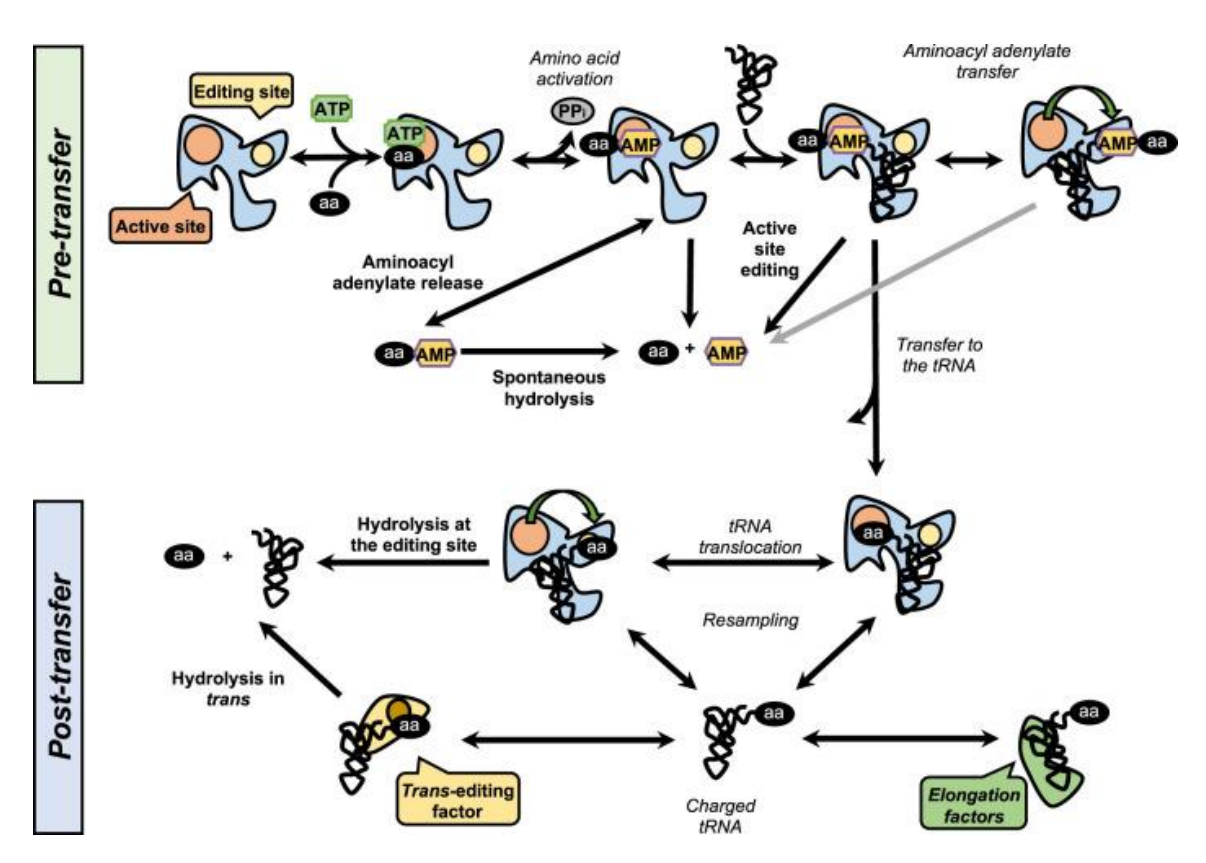


Figure 1.5 – Editing pathways possible by the aaRSs.

There are two distinct pathways the enzymes can take: pre or post-transfer editing. In Pretransfer the aa-AMP bond is the main target, which can undergo hydrolysis at different steps before it has been added onto the tRNA. tRNA is not generally required for this step, though some aaRS such as LARS require tRNA binding [74]. Post-transfer editing targets the ester bond between the aa-tRNA and involves a secondary domain in the aaRS to 'proof read' the charged tRNA. In some organisms, trans-editing factor proteins act as an additional barrier before the mischarged aa-tRNA can enter translation [20], [75]. Figure taken from: [20].

While not all aaRS carry out this editing ability, it has been described in: Valine synthetase (YARS), phenylalanine synthetase (FARS), leucine synthetase (LARS), methione synthetase (MARS), threonine synthetase (TARS), alanine synthetase (AARS), proline synthetase (PARS), lycine synthetase (KARS), and serine synthetase (SARS) [73]. This is done either in a

pretransfer editing by hydrolysis of misactivated amino acids, or post-transfer editing by hydrolysis of the ester bond on misacylated tRNA [76], [77]. Proofreading aaRS contain a separate active site away from the aminoacylation centre, and in post-transfer editing, conformational rearrangements move the misacylated tRNA into this site which can be as far as 40 Å away [78]. This extra step ensures a more accurate delivery of the correct amino acid to the ribosome, ensuring fidelity of the translation of the genetic code.

1.4 - Structure of neuronal cells

The nervous system in humans is made up of neuronal cells; a cell capable of passing along an electrical 'action potential' down their membrane, which can elicit specific physiological responses dependant on the stimuli [79]. There are three main neuronal cell types: Sensory neurons (SN), Motor neurons (MNs), and Interneurons (INs). Generally, a SN, or an afferent neuron, will receive a signal from an external stimuli, both physical such as touch, or chemical as in the olfactory response [80]. The SN will then send the signal to the Central Nervous System (CNS) [81]. MNs, or efferent neurons, will receive a signal, and depending on the response needed, will pass the signal to effector organs to respond to the stimuli, such as muscles or glands [82]. MNs can be either lower motor neurons or upper motor neurons, the former have their cell body in the spinal cord and innervate muscles and glands in the body, and the later extend from the cerebral cortex and extend down into the spinal cord or brain stem. INs are the intermediaries, and will receive a signal from SNs and can pass it along multiple pathways to elicit a response from different motor neurons [83]. For example, when a hand comes into contact with a hot surface, heat sensitive SNs will activate. For an action potential to be transduced along the neuronal cell, the activating stimuli must reach above a certain threshold (which can be different for specific type of cells and stimuli in which they respond [84]) to cause the depolarisation of the neuronal cell membrane. This activates voltage-gated sodium channels on the membrane of the neuronal cell, generating an electrical pulse that can pass along the membrane [85]. The action potential is passed along until it reaches a terminus at the synapse, causing neurotransmitter release (such as glutamate) via vesicle release into the synaptic cleft [86].

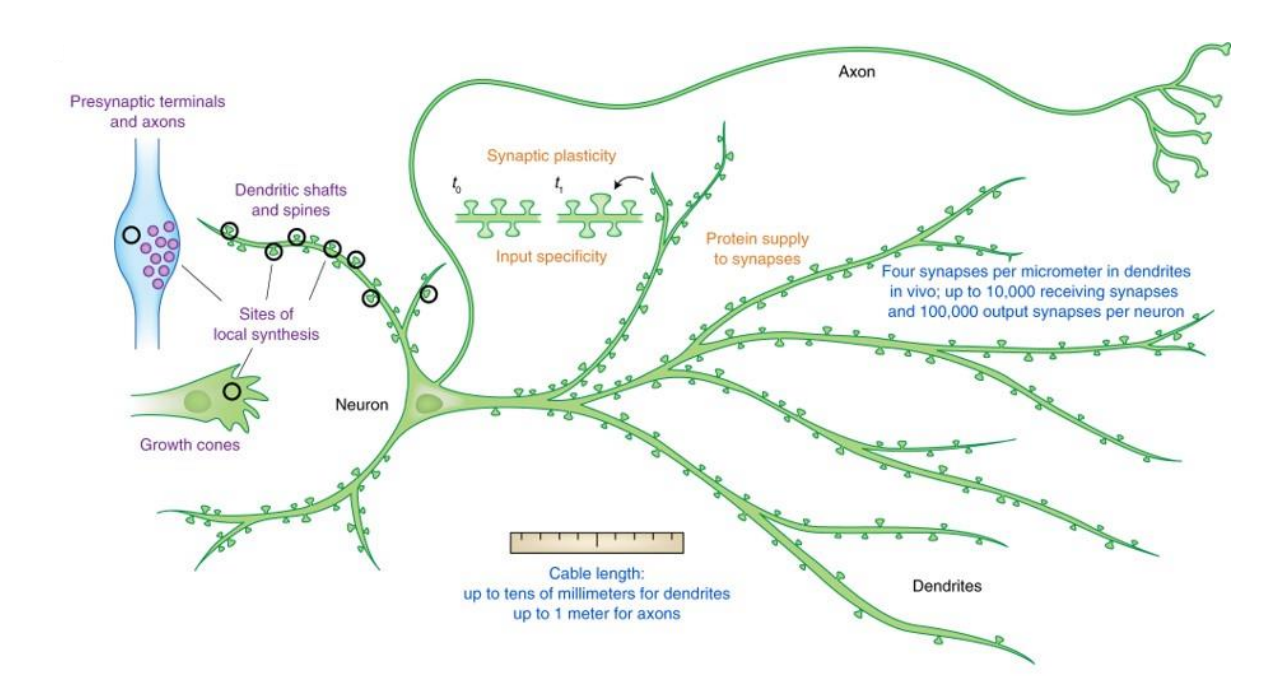


Figure 1.6 – Anatomy of a neuronal cell.

Main processes and physical features are highlighted, as well as sites of specific local translation in the cell. Dendritic spines are the postsynaptic membrane and the areas where the signals are received in the cell. Signal travels down the axon into the presynaptic terminals. Local translation happens at the growth cones – the developing terminal of the neuronal cell, as well as the pre and postsynaptic membranes in the axons and dendrites, respectively. Figure taken from: [87].

The signal is then picked up on the post-synaptic membrane, causing a new action potential on the receiving neuron, such as in spinal cord where it will be picked up by INs, which will send the signal back to the hands via the MNs to contract muscles and move the hand out of the way, while also send the signal to the brain to activate the pain receptors. The types of response elicited depends on the type of stimuli and to what severity it is being perceived. Stimuli which do not reach the threshold electrically fade and do not cause the depolarisation of the membrane. Thus, the neuronal cell is highly specialised and structured in a very specific way as to allow this sending and receiving signals (figure 1.6). The neuronal cells, as is the case for all human cells, have a cytoplasmic cell body(somata) which contains a nucleus, and all the typical organelles to carry out metabolism, maintenance, and transcription/translation of proteins necessary for cellular function. Though due to the specialised function of the neuronal cell, it also has a number of extended cellular protrusions that are the signal

transduction sites of the cell. These are either dendrites or axons, which are the signal receiving or sending fibres of the cell, respectively. Dendrites have a number of 'spines' along their membrane, which are the 'post-synaptic' sites of signal transduction, where the signal is passed to the cell [88]. Neuronal cells have only one axon, and depending on where in the body it is, can extend upwards to 1 metre in length. For instance, the somata of SN and MNs in the PNS are typically found in the Dorsal root ganglion in the spinal cord, and extend their axons to their respective tissue [89] which can extend towards the distal limbs. At the most distal end of the axon are synaptic terminals. This is where the signal is transmitted and will often be passed onto a specific organ or muscle.

1.5 - Local Translation in Neuronal cells

Despite most of the neuronal cell translation and protein synthesis happening in the somata; discreet, local translation happens all along the dendritic and axonal lengths, even at the most distal ends of the neurons, such as at the synaptic terminals [90]-[92]. This was first outlined decades ago, with the discovery of polysomes in dendrites and axons [93]. Soon after this, localised mRNA species were then also discovered, such as microtubule-associated protein 2 (Map2a) [94], and calcium/calmodulin- dependent protein kinase 2 alpha (Camk2α) [95], among many others [7]. It became clear that the distal projections of neuronal cells were carrying out differential gene expression as compared to the main cell body. Why this occurs could be due in part from the possible length of the axons, but also because of the need for site specific plasticity of the synapses(the dynamic modulation of connection strength between neurons) [96] and axonal homeostasis[97]. Local protein synthesis thus solves a logistical issue in neuronal cells. Instead of having to synthesise every protein at the somata and transport it along distant microfilaments, the cell can have a pool of locally reserved ribosomes and translation factors to carry out translation directly at the site the proteins will be needed. It has even been shown that local translation aids in the development and directionality of growing neurons in response to external stimuli [98]. In one study, DCC, a receptor implicated in axon growth and guidance, physically interacts with translational machinery and mediates local translation upon netrin-1 stimulation [99]. Even in astrocytes – glial cells that maintain neuronal brain homeostasis – it has been shown that local translation helps to maintain specific interfaces between astrocytes and the brain vascular system [100].

Studies have also shown that this differential gene expression has slightly different patterns than traditional translation in the somata, with the monosomes actively taking a more major part in axonal translation [101]. It is clear then that this compartmentalisation is necessary for developing neuron motility, synaptic plasticity, differentiation and specialisation of specific cell types, and response to injury or other external stimuli. How the cell can maintain this diverse compartmentalisation, and selectively choose which mRNAs need to be packaged and transport is an ongoing field of research. What determines which mRNA will be localised to the neurite projections, is still somewhat unknown, though studies have suggested that neuronal process localised mRNA contains longer, unique 3' UTR regions which may signal transport to the neurites [102]. What is known, is that for the transport of these mRNAs, the cells form membrane-less RNA granules [103], which harbour translationally repressed mRNA, ribosomes, and other translational machinery, and transport them down long microtubule stretches to be distributed to their targeted areas [104]. The RNA granules assemble from mRNA and RNA binding proteins (RBPs) and form phase separated structures [103]. These structures interact with dynein and kinesin motor proteins to transport along the microtubule network in the axon, linked to lysosomal structures and tethered together by ANXA11 [105]. ribosomes in these granules are transported fully assembled and stalled at the pre-translocation state by binding of the RBP G3BP2 at the ribosome E site [106].

Defects in the transport of transcripts to sites of local protein synthesis, have been implicated in multiple neurodegenerative diseases, most notably with FUS mutations linked to ALS(amyotrophic lateral sclerosis), which has been shown to reduce translation specifically in neurite processes through an eIF2a-phosphorylated manner, while leaving cell bodies of neurons undisturbed [107]. FUS, an RNA-binding protein, is implicated in a number of processes, such as splicing, transcription, DNA damage repair, and RNA localisation [108], but exerts its disease phenotype by binding and aggregating RNA and proteins inside granules, preventing proper localisation and transport of RNA granules in neuronal cells [109], [110]. Another protein, SMN(survival of motor neurons) is linked to regulation of local transport and assembly of RNPs [111]. Defects in this protein also lead to misregulation of local protein synthesis and axon and development of Spinal muscular atrophy (SMA) [112]. The correct RNA granule assembly and transport towards the distal neuron then is vital for both maintaining local protein synthesis, and defects in this choreographed system is directly linked to the development of a number of neurodegenerative diseases.

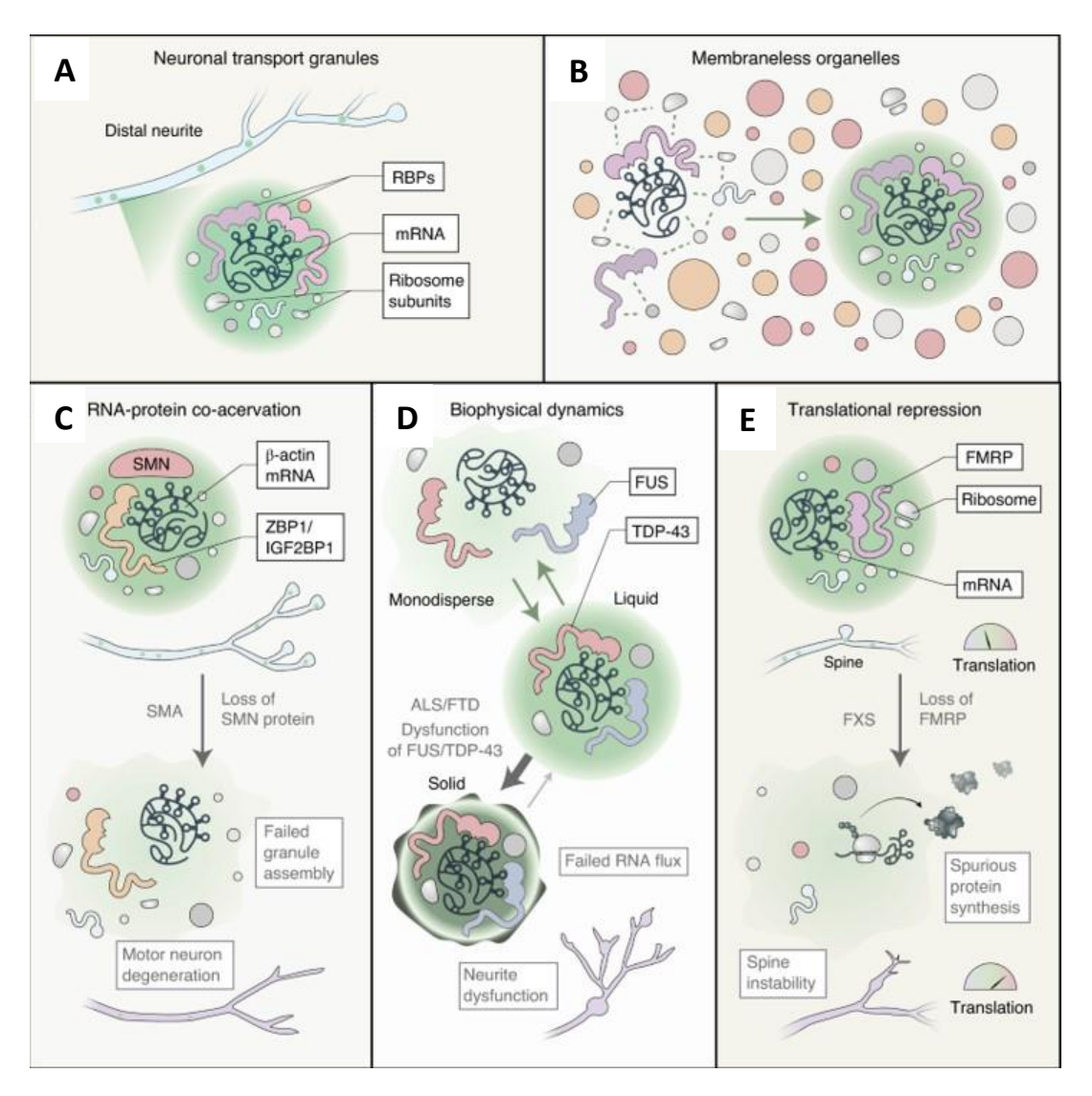


Figure 1.7 – Neuronal RNA granule components and known dysfunctions linked to neurodegenerative diseases.

(A) Major components of the RNA granule: RNA binding proteins (RBP), mRNA, and ribosome subunits. (B) Phase-separated RNA granules assemble as membraneless organelles, but can exchange dynamically with the cytoplasm. (C) Accumulation of RBPs and RNA results in phase-separation, facilitated by SMN. Depletion or defects result in failure to assemble transport granules and linked to neurodegeneration. (D) Disassembling of RNA transport granule is vital for the correct delivery of RNA and ribosomes to local sites. Mutations in ALS/FTD related proteins such as FUS and TDP-43 leads to solidification of granules and lack of RNA delivery.

(E) FMRP translationally represses mRNA in RNA granules, creating a spatially timed synthesis of their proteins in the neuronal cell. Loss leads to uncontrolled protein synthesis in inappropriate cellular compartments, decreasing neurite stability and leading to diseases such as Fragile X syndrome. Figure taken from: [113]

1.6 - Charcot-Marie-Tooth disease

Charcot-Marie-Tooth (CMT) disease is a prevalent (1:2500) [114], hereditary neurodegenerative disorder, wherein motor and sensory neurons are predominantly affected. The classical symptoms in patients include such things as progressive loss of function in distal limbs, loss of sensory function, muscle weakness and atrophy, and foot and limb deformities [115], [116]. Generally, onset of the disease is within the second decade of life, and slowly progresses to become more severe as people live with the condition. However, many patients can also develop severe forms with a much earlier onset, even as early as infancy, which can lead to a drastic decrease in quality of life for the patient. Other patients can also have a very late onset, with little or no symptoms until well into adulthood. Consistent with this wide-ranging clinical outcomes of this disease, the disease can be thought of as genetically heterogenous, with a plethora of genetic mutations across a wide range of genes can lead to the development of the disease [117], and accordingly subtypes of CMT have been categorised based on two key factors: The phenotype of the disease, and the genetic mutation that leads to its development. In the first case, two main forms exist: The demyelinating form (CMT1) and the axonal dystrophy form (CMT2) [118]. CMT1 leads to segmental demyelination of motor neurons, causing drastic decreases in nerve conduct velocity (NCV) [119]. Genes involved in maintenance and stabilisation of the myelin sheath covering the neurons, are affected in this CMT form, such as peripheral myelin protein 22 (PMP22), or myelin protein zero (MPZ). Though mutations in other developmental genes are also known to bring about this condition, such as early growth response 2 (EGR2) and neurofilament light (NFL) proteins [120]. The axonal dystrophy (CMT2) form does not disrupt the myelin sheath, which is why NCV is still relatively high in CMT2 (>45m/s NCV) as compared to CMT1(<35m/s NCV), but instead displays a length-dependant degradation of distal synaptic ends [115], [121]. This degradation of synaptic ends of the neurons results in a 'dying back' of the axon, starting at the very tips of motor neurons, with a repeating cycle of degradation, regrowth, degradation, and so on [122]. The genes causing the disease also define the subtype, such as the gene for glycyl-tRNA-synthetase (GARS) leading to CMT2D. Interestingly, six genes that encode for aminoacyl-tRNA-synthetases cause CMT2 (or the intermediate phenotype, DI-CMT): YARS, MARS, HARS, GARS, AARS, and the recently reported WARS [123]. As described above, these enzymes are ubiquitously expressed in all cell types, and are

necessary to carry out esterification of tRNA with their cognate amino acid [20], making them an important bridge between the nucleotide sequence and their translation to peptides. Why mutations in these key translational enzymes seems to have a specific, aberrant effect in motor neurons, is largely unknown.

CMT-related mutations in GARS are the most widely researched, and a number of possible mechanisms have been proposed, among them the most prevalent being: Loss of aminoacylation function, and toxic gain-of-function wherein the mutant GARS can interact and alter the function of specific proteins such as Nrp-1 and HDAC6 [124], [125]. However, in both of these cases not all mutations show the same effect, with aminoacylation activity not correlating with disease phenotype [126]. Mice which contained a deletion in the GARS allele, reducing levels of GARS by more than 50%, showed similar phenotype to control, and measured activity of the P234KY variant showed similar activity to WT GARS [127]. Furthermore, another study concluded that overexpression of WT GARS did not rescue the neuropathy phenotype, and instead suggested a dose-dependent gain-of-function [128]. Also, other studies have not showed a similar interaction with Nrp-1 and HDAC6 [129]. In the latter case, while some mutations did not show the same interaction between mutant GARS and HDAC6, GARS^{P724H} still correlated with disease phenotype, and despite not showing the similar neomorphic interaction, α-tubulin acylation levels still reduced. This indicates that a common mechanism unifying all of the CMT-mutations of GARS leading to development of the disease has yet to be uncovered.

1.7 - C9-orf72-mediated ALS/FTD

Amyotrophic lateral sclerosis (ALS) and frontotemporal dementia (FTD) are devasting neurodegenerative disorders, with different, but sometimes overlapping clinical symptoms. FTD is the second most common cause of pre-senile dementia, wherein the disease causes degeneration of the frontal and temporal lobes of the brain, resulting in progressive changes in behaviour and personality [130]. While ALS - affecting 2 in 100,000 people - is classical defined as a upper and lower motor neuron degenerative disorder leading to muscle weakness and wasting, though frontotemporal defects have also been described for this disease [131].

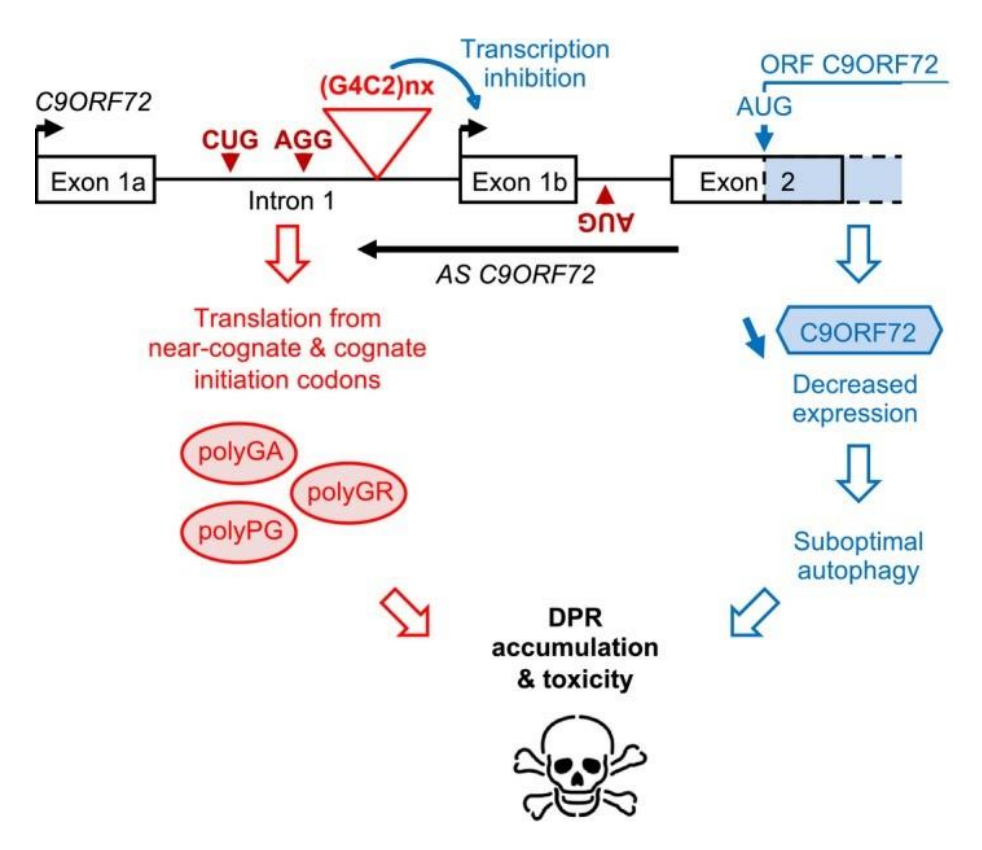


Figure 1.8 – G4C2 repeat expansion leads to translation of Dipeptide repeat proteins (DPRs).

RAN translation occurs at the non-canonical CUG codon upstream of the G4C2 repeat expansion, where PolyGA, Poly GR and PolyPG are translated from each frame of the repeat region. Initiation at the CUG codon also causes epigenetic silencing of the canonical C9orf72 gene. This protein is involved in cellular autophagy which helps clear misfolded or aggregating proteins. A negative feedback loop thus leads to cellular toxicity as DPRs are failed to be broken down and cleared due to decreasing autophagy. Figure taken from: [132].

In 2011, a breakthrough study found that a common inherited cause of both of these diseases is a hexanucleotide repeat GGGCC (G4C2) repeat expansion in the first intron on chromosome 9 of the *C9orf72* gene, with 11.7% of FTD cases and 22.3% of ALS cases related to this expansion [133], [134]. This C9FTD/ALS disorder – the collective term for C9Orf72 expansions leading to either FTD and/or ALS symptoms – has an onset in patients between 27-63 years, and while these repeat expansions in this loci are generally common in healthy individuals, an accumulation above a specific threshold seems to be the leading cause behind the progression [135]. This repeat expansion in the first intron of the gene persists onto the transcribed mRNA [136], and leads to development of the disease through a number of non-exclusive means: Firstly, accumulation and aggregation of mRNA at specific loci leads to

recruitment of RNA-binding proteins, sequestering important proteins necessary for cellular function [137], [138]. Second, the expanded repeat regions on the gDNA can lead to alterations of epigenetic markers, causing decreased expression of C9Orf72 mRNA and protein levels [139], [140]. And third, the expanded C9orf72 mRNA can undergo an unconventional translation, dubbed as RAN (repeat-associated non-AUG) translation, wherein ribosomes can initiate at non-canonical start codons, such as CUG. On the C9orf72 gene, this leads to translation of the repeat region, and synthesis of di-peptide repeat (DPR) proteins [141], [142], and accumulation of these proteins is sufficient to induce neurodegeneration [143], [144]. DPRs impart their toxicity through number of mechanisms, such as: altered ribosome biogenesis, impaired nucleocytoplasmic transport, and shifts in RNA metabolism [144]. Interestingly, translation on these repeat regions can happen in every frame, both on the sense and antisense strand [145], and different combinations of DPRs can illicit different toxicities. The charged DPRs: poly glycine-arginine (PolyGR), and poly prolinearginine (PolyPR), in particular accumulate in membrane-less organelles, such as RNA granules, and can suppress global protein production [146]. Other DPRs, such as Poly glycinealanine (PolyGA) have been shown to aggregate in the axon and dendritic projections of neuronal cells [147], wherein these PolyGA aggregates are mobile, and lead to increased CA²⁺ influx in response to external stimuli, and a reduction production of synaptic vesicleassociated protein 2 (SV2), a necessary protein that forms intrinsic component of synaptic release machinery [148]. The production of these DPRs then is inexorably linked to disrupted neuronal homeostasis and function, leading to selective cell death.

How RAN translation occurs is still not fully understood, but studies have proposed a mechanism where the repeat-region secondary structure can act as an internal ribosome entry (IRES) site [141] – specific RNA elements that can induce cap-independent initiation and translation by internal ribosome entry [149]. Other studies have proposed that the repeat-region can form difficult to scan through structures, such as G-quadruplex that can slow down scanning [150] enough to promote initiation at unfavourable codons [151] then helicases such as DHX36 can then unwind the G-quadruplex to promote DPR translation [152]. Indeed, on the sense strand in the PolyGA frame, 24nt upstream of the hexanucleotide repeat region is a CUG with an optimal kozak sequence [145]. PolyGA is likely translated through a conventional, albeit non-AUG, scanning and initiation mechanism. In contrast, PolyGP, which

exists in frame +2, has a stop codon before the G_4C_2 repeat region, meaning its translation has to be induced directly in the repeat region itself and not at the CUG, or ribosomal frameshifting must occur after initiation in the PolyGA frames. This second mechanism is evidenced by the fact that mutation of the CUG codon 24nt upstream of the G4C2 repeats, prevents translation of all three DPR products from sense strand (Poly-GA/GP/GR) [145], [153]. The induction of the ISR also seems to be pivotal for effective RAN translation on these repeat regions [154]. While under normal circumstances, translation is effectively shut down upon stress induction on the cell, through the eIF2a-phosphorylation mechanism [155], a number of mechanisms exist to still selectively translate genes that could potentially be necessary for cellular response to stress [156]. Upstream open reading frames, as utilised by ATF4, IRES sequences, and Non-AUG initiation codons can bypass this global protein synthesis shutdown [157]–[159]. Thus RAN translation is effectively impervious to the ISR [142]. As DPRs are sufficient to induce the ISR [160], this could potentially lead to a feedback loop of DPRs causing stress response, which shuts down global translation but still allows production of more DPRs.

1.8 - Other neurodegenerative diseases with links to translation

A number of other neurodegenerative diseases also arise, and studies have shown that these are due to dysfunctions of local translation in neurite processes, though through different means, such as changes in transport, localisation, and local translation of axonal mRNA [161]. Also, further emphasising the impact and importance that the polarised cellular structure of the neuronal cell can play on the development of disease, Maday, 2014, highlights a number of transport proteins that are known to give rise to neurodegenerative diseases when mutated [162]. This distinct, compartmentalised structure, maintained by antegrade and retrograde transport, facilitating the local translatome, is seemingly the key for both neuronal cell function [163] and survival, and to also understand how many of these diseases specifically disrupt and lead to degeneration of neuronal cells.

Fragile X Syndrome (FXS)

FXS is an inherited disorder, leading to a plethora of intellectual, behavioural and physical abnormalities and defects [164]. The leading cause of this disease is the loss of the Fragile X

mental retardation protein (FMRP), brought about by excessive (>200) CGG repeat expansions in the promoter-proximal region of the gene loci [165]. This repeat expansion leads to hypermethylation of the promoter region, effectively silencing the FMR1 gene, decreasing functional amount of protein in the cell [166]. FMRP is a ubiquitously expressed protein, though it is found more highly expressed in the neurons [167] and functions primarily in the RNA transport granules in the neuronal cell [168]. FMRP binds both mRNA targets and ribosomes in the granules, effectively causing translational repression of the mRNA inside the granule. This is a vital functionality of the RNA granule, as specifically timing the expression of localised mRNA species — where in the cell and how much — is vital for neuronal development and function [169], [170]. Loss of this protein then not only hinders RNA granule formation, but spatially timed translation in neuronal cells also affected. Loss of this function could lead to axonal growth cone defects [171] and dendritic spine pathology [172], hindering the circuit network of the brain and neurotransmission between neuronal cells.

Huntington's disease

Another neurodegenerative disease that is given rise by nucleotide repeats is Huntingtin's disease (HD). This disease is a dominantly inherited, and slowly progresses over 15-20 years, leading to behavioural disorders, cognitive impairment, and involuntary movements [173]. CAG repeats in exon1 of the sequence of the Huntingtin protein (Htt) cause an expansion of a polyglutamine tract in the N-terminus of the protein [163], [174]. This leads to aggregation of the Htt protein, which can sequester and trap proteins necessary for RNA granule transport in the neuronal cells, a common theme in neurodegenerative disorders [175]. Wild-type Htt itself is also seemingly needed for maintaining the local translatome of the neuronal cell, as Htt has been shown to traffic to dendrites and associate with the 3'UTR regions of neuronal localised mRNAs [163]. While this is the classical view of HD, other studies have also shown that these CAG trinucleotide repeats can undergo RAN translation [176]. As is the case for C9-ALS, the CAG-repeat region can recruit translational factors and allow the expression directly of the DPR proteins through a non-canonical initiation, and which causes expression in all possible frames, leading to cellular toxicity through aggregation of DPR proteins [177].

Vanishing White Matter disease

From the disorders mentioned above, it is clear then the importance of the specific localisation and expressional timing of key mRNA species in distinct compartments of the neuronal cell for general function and development. It is also clear that this lends the neuron a number of vulnerabilities that might only specifically affect neuronal cells, and no other, less structured cells. For example, mutations arising in eIF2B, a key guanine-exchange factor that regenerates GTP on eIF2a-GDP after an initiation cycle [178], gives rise to a fatal leukodystrophy, Vanishing White Matter (VWM), characterised by the loss of the white matter, or the myelin sheath in the brain [179]. Phosphorylated eIF2a under stress conditions, binds to eIF2B with a much higher affinity and represses its activity [155] – this is the typical ISR activation pathway. Under stress conditions, a number of genes are selectively translated through a mechanism of cap-independent initiation. A stress induced transcription factor, ATF4, promotes expression of 4E-BP, which sequesters eIF4E, the methyl-cap binding protein, promoting cap-independent initiation through 5' IRES sequences of stress-response genes [180]. These TFs activate more genes which aid cellular recovery from stress [181]. Mutant eIF2B hyper-suppresses translation during stress, leading to a lack of stress-induced gene expression [182] essentially hindering the cells ability to recover normal translation after stress induction. In VWM pathology, both severe head trauma and neuroinflammation can lead to quickening of the disease progressive, with even the disease lying dormant until such a traumatic event causes sufficient stress on the neuronal cells. Cells in VWM patients thus undergo prolonged states of translational hyper-repression and failure to recover from stress. In neuronal cells, this can lead to complete loss of stability of the cells, and disruption of synaptic function and neurotransmission.

2 - Aims of the thesis

In this thesis, we aimed to address the molecular mechanisms underlying CMT2 associated with pathologic mutations in GlyRS and TyrRS. using deep-sequencing approaches, such as ribosome profiling and RNA-sequencing, coupled with fundamental molecular biology assays. We uncovered a novel mechanism of tRNA sequestration by GlyRS or TyrRS that leads to translational defects in their corresponding codon, i.e. Gly codons and Tyr codons, respectively (Chapter 3 and Chapter 4). Upregulation of the cognate tRNA by administration of in vitro transcribed tRNA alleviates translation defects (Chapter 5).

For another disease, C9Orf72ALS, we utilised ribosome profiling to gauge the level of frameshifting using different disease-relevant contexts (Chapter 5). We detect ribosome-protected fragments during the scanning phase of translation initiation, and possibly determine the frameshifting within the repeat stretch. While we detect enrichment of ribosome-protected reads upstream of the start, the low amount of reads at non-canonical initiation sites does not allow for detecting frameshifting events triggered by queued initiating ribosomes.

3 - tRNA sequestration as an underlying mechanism of CMT2 neuropathy associated with genetic mutations in GARS

This chapter represents part of the publication:

Amila Zuko*, Moushami Mallik*, Robin Thompson, Emily L. Spaulding, Anne R. Wienand, Marije Been, Abigail L. D. Tadenev, Nick van Bakel, Céline Sijlmans, Leonardo A. Santos, Julia Bussmann, Marica Catinozzi, Sarada Das, Divita Kulshrestha, Robert W. Burgess, Zoya Ignatova, Erik Storkebaum., "tRNA overexpression rescues peripheral neuropathy caused by mutations in tRNA synthetase," Science 373, 1161–1166, 2021

This work was executed in collaboration with the group of Prof. Dr. Erik Storkebaum from Radboud Universiteit, Netherlands. Plasmids for GARS expression in E. coli were kindly provided by Prof. Dr. Xiang-Lei Yang, Scribbs Institute, USA. In this study, we have uncovered a mechanism underlying the development of CMT disease, caused by the sequestration of tRNA by CMT-mutant GARS. A short, edited version from the original publication is included here, mainly representing the results from my contribution. My contribution to the paper was producing the data for figure 3.4a, b and figure 3.5b (In the paper as figures 3a, b, and S13, respectively), calculated from kinetic studies carried out using purified protein and in-vitro transcribed tRNA^{Gly} (as seen in figure 3.3). For these experiments, I generated several CMTrelated mutants of GARS through site directed mutagenesis, using the wild-type GARS containing plasmid. All of the different variants of CMT-GARS were expressed in E. coli and purified to homogeneity. A ribosome profiling (or Ribo-seq) was carried out on spinal cord of mice either carrying the WT GARS, or a heterozygous mutant mouse carrying C201R (C157R in humans). My findings with the kinetic studies, substantiated with the Ribo-seq analysis, helped to form the core idea in the paper of the sequestration of tRNA by mutant GARS being an underlying mechanism behind the disease, as seen in the model in figure 3.6. Analysis of ribosome profiling data was carried out by Leonardo Santos. Immunoprecipitation of GARS:tRNA^{Gly} was carried out by Sarada Das. Some results and figures from the paper are included in this section to highlight the main findings of our work, some of which was not carried out by me, though working collaboratively the conclusions and main take-aways of the paper were contributed to by all authors. Where data was not generated by me is

indicated. Some panels not shown but still referred to in the main body of text and figure legends.

3.1 - Introduction

Heterozygous mutations in six genes encoding cytoplasmic aminoacyl-tRNA synthetases (aaRSs) cause axonal and intermediate forms of Charcot-Marie-Tooth (CMT) peripheral neuropathy [125], [183], [184]. aaRSs are ubiquitously expressed enzymes that covalently attach amino acids to their cognate tRNAs (tRNA aminoacylation) [185], [186]. Aminoacylated tRNAs are used by the ribosome for mRNA translation [187]. Interestingly, some CMT aaRS mutations do not affect aminoacylation activity [114], [188]–[191], indicating that loss of aminoacylation activity is not a prerequisite for disease causality. Rather, a gain-of-toxic-function mechanism may underlie CMT associated with glycyl-tRNA synthetase (GARS) mutations [CMT disease type 2D (CMT2D)] [128], [189]. In vivo cell type—specific visualization of newly synthesized proteins in *Drosophila* [192] by fluorescent noncanonical amino acid tagging (FUNCAT) [193] revealed that each of six GARS or tyrosyl-tRNA synthetase (YARS) mutants substantially inhibited global protein synthesis in motor and sensory neurons [189], implicating impaired mRNA translation in CMT2D.

3.2 - Results & Discussion

In this study, we investigated the molecular mechanism by which CMT mutant GARS variants inhibit translation. Manipulation of upstream regulatory pathways or translation initiation did not rescue inhibition of translation, suggesting that CMT mutant GARS may interfere with translation elongation. We thus evaluated the effect of tRNA^{Gly} overexpression by generating *Drosophila* carrying a bacterial artificial chromosome (BAC) transgene containing five tRNA^{Gly} genes with GCC anticodon (tRNA^{Gly-GCC}). Flies with 10 or 20 additional tRNA^{Gly-GCC} gene copies displayed ~13 and ~25% higher tRNA^{Gly-GCC} levels than wild type (WT), respectively. The $10xtRNA^{Gly-GCC}$ transgene partially rescued the translation defect (figure 3.1a), and peripheral neuropathy–like phenotypes induced by three CMT mutant GARS proteins [E71G (Glu⁷¹ \rightarrow Gly), G240R, and G526R], including larval muscle denervation (figure 3.1b), developmental lethality, adult motor deficits, sensory neuron morphology defects, and reduced life span.

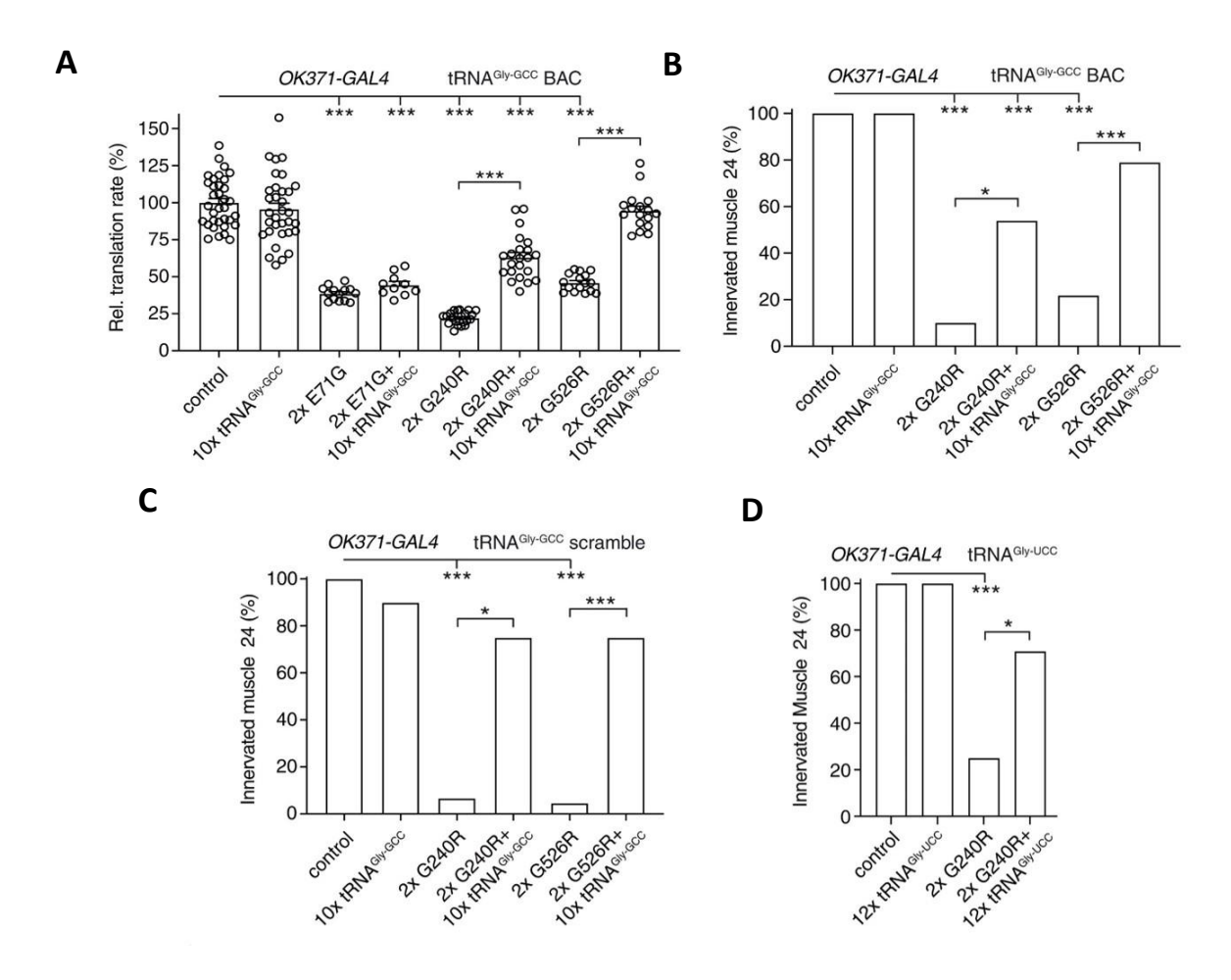


Figure 3.1 - tRNA^{Gly} overexpression rescues inhibition of protein synthesis and peripheral neuropathy phenotypes in Drosophila CMT2D models.

All figures in this panel generated by collaborators. Some panels from paper not shown. (A) Relative translation rate as determined by FUNCAT in motor neurons (OK371-GAL4) of larvae expressing E71G, G240R, or G526R GARS (2x indicates two transgene copies), in the presence or absence of the $tRNA^{Gly-GCC}$ BAC transgene ($10xtRNA^{Gly-GCC}$). n = 10 to 34 animals per genotype; ***P < 0.001 by Kruskal-Wallis test. Single-letter abbreviations for the amino acid residues are as follows: A, Ala; C, Cys; D, Asp; E, Glu; F, Phe; G, Gly; H, His; I, Ile; K, Lys; L, Leu; M, Met; N, Asn; P, Pro; Q, Gln; R, Arg; S, Ser; T, Thr; V, Val; W, Trp; and Y, Tyr. (B, C, and D) Percentage of larvae with innervated muscle 24. GARS transgenes were expressed in motor neurons (OK371-GAL4), in the presence or absence of $10xtRNA^{Gly-GCC}$ BAC (B), $10xtRNA^{Gly-GCC}$ scramble (C), or $12xtRNA^{Gly-UCC}$ (D). n = 19 to 26 (B), 8 to 22 (C), and 12 to 27 (D) animals per genotype; *P < 0.05; ***P < 0.005 by Fisher's exact test with Bonferroni correction. Figure panels taken from figure 1b, c, and g [194].

In general, phenotypic rescue was more pronounced for G240R and G526R than for E71G. tRNA^{Gly-GCC} overexpression did not alter GARS protein levels, nor did it rescue peripheral neuropathy phenotypes induced by CMT mutant YARS, indicating that only the cognate tRNA can rescue. Transgenic lines containing 10 different tRNA^{Gly-GCC} genes ("tRNA^{Gly-GCC} scramble") induced a more pronounced dosage-dependent increase in tRNA^{Gly-GCC} levels than did the BAC transgene (~30% for 10xtRNA^{Gly-GCC}) as well as a more substantial rescue of muscle denervation and motor performance (figure 3.1c). Thus, the degree of rescue correlated with tRNA^{Gly-GCC} overexpression level.

We next generated transgenic lines overexpressing the other tRNA^{Gly} isoacceptor, tRNA^{Gly-UCC}. 12xtRNA^{Gly-UCC} flies displayed ~75% higher tRNA^{Gly-UCC} levels than WT. For E71G and G240R, tRNA^{Gly-UCC} overexpression partially rescued developmental lethality, muscle denervation (figure 3.1d), motor deficits, and life span. For G526R, tRNA^{Gly-UCC} overexpression partially rescued motor performance but aggravated sensory neuron morphology defects and further reduced life span. Thus, for E71G and G240R, both tRNA^{Gly-GCC} and tRNA^{Gly-UCC} partially rescued peripheral neuropathy phenotypes, while for G526R, the rescue was isoacceptor specific. To strengthen the potential relevance for human CMT2D, we evaluated the effect of tRNA^{Gly-GCC} overexpression in CMT2D mouse models. We generated transgenic mice with ~27 (tRNA^{Gly-high}) or two (tRNA^{Gly-low}) copies of a genomic transgene containing two tRNA^{Gly-} GCC genes. In spinal cord (SC), tibialis anterior muscle, and sciatic nerve of tRNA Gly-high mice, tRNA^{Gly-GCC} levels were ~90 to 150% higher compared to WT. Targeted locus amplification (TLA) revealed integration of all transgene copies in Stk38 (serine/threonine kinase 38) on chromosome 17, with an ~7-kb deletion at the integration site, deleting exons 8 through 12 of Stk38. In both male and female Gars^{C201R/+} mice [195] of 3 to 6 weeks of age, tRNA^{Gly-} GCC overexpression fully rescued the reduced body weight and motor deficits. Reduced nerve conduction velocity (NCV) and compound muscle action potential (CMAP) amplitude in *Gars*^{C201R/+} mice were also fully rescued. Thus, increasing tRNA^{Gly-GCC} levels completely prevented peripheral neuropathy in *Gars*^{C201R/+} mice without affecting GARS mRNA and GARS protein levels.

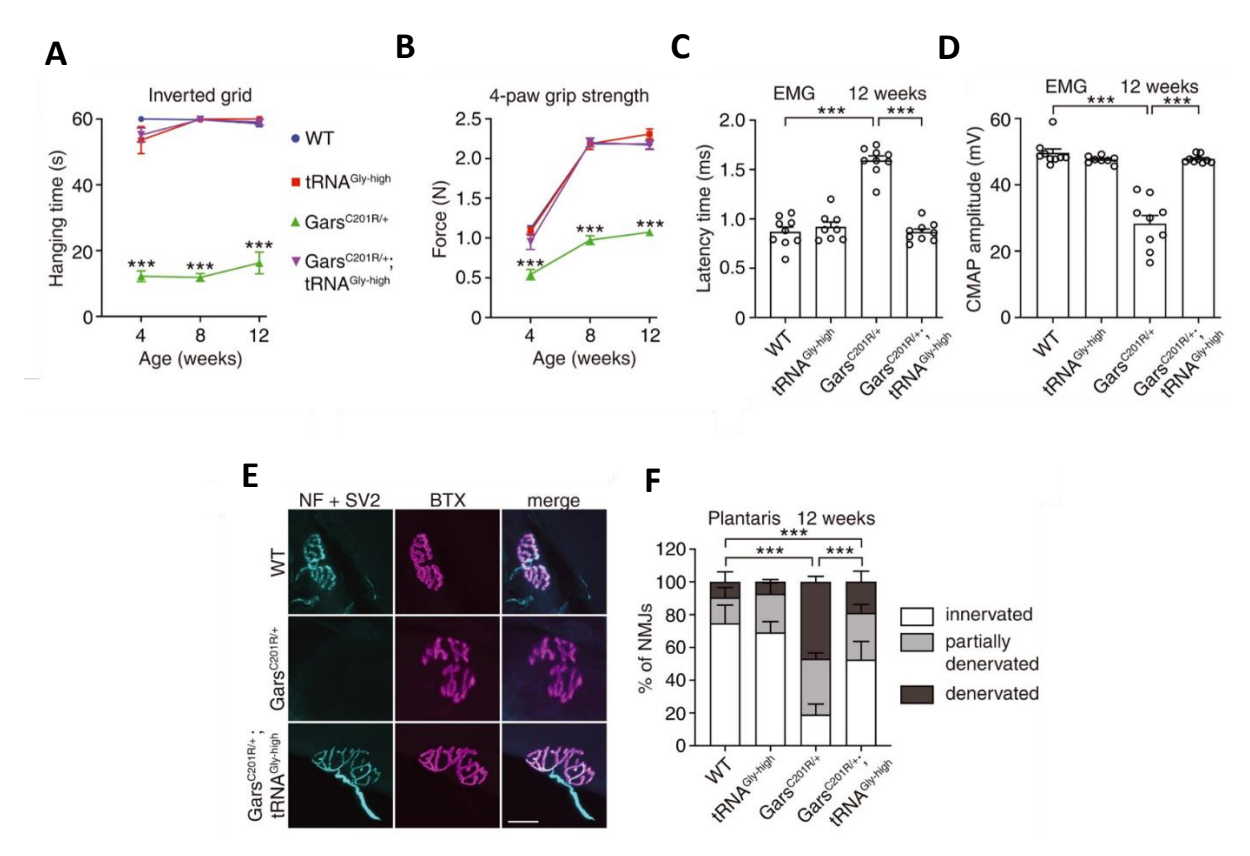


Figure 3.2 - tRNA^{Gly-GCC} overexpression rescues peripheral neuropathy in CMT2D mouse models.

All figures in this panel generated by collaborators. Some panels from paper not shown

(A) Hanging time in the inverted grid test of male $Gars^{C201R/+} \times tRNA^{Gly-high}$ (A) mice. n = 8

or 9 mice per genotype; ***P < 0.0001 by one-sample t test and two-tailed unpaired t test with Bonferroni correction per time point. (B) Four-paw grip strength as measured by dynamometer. n = 8 or 9 mice per genotype; ***P < 0.001 by two-way ANOVA with Tukey's multiple comparisons test per time. (C, D) Electromyography (EMG) at 12 [(C), (D), weeks of age. (C), Latency time between sciatic nerve stimulation at sciatic notch level and detection of a compound muscle action potential (CMAP) in the gastrocnemius muscle. n = 8 or 9 (C) mice per genotype; ***P < 0.0001 by two-way ANOVA with Tukey's multiple comparisons test (C). (D) CMAP amplitude in the gastrocnemius muscle. n = 8 or 9 (D) mice per genotype; ***P < 0.0005 by Brown-Forsythe and Welch ANOVA (D). (E, F) Representative images (E) and quantification (F) of NMJ innervation status in plantaris muscle. In (E), neurofilament (NF) and SV2 label presynaptic nerve endings, while TRITC-conjugated bungarotoxin (BTX) labels postsynaptic acetylcholine receptors. n = 5 mice per

genotype; ***P < 0.005 by Fisher's exact test with Bonferroni correction. Scale bar, 25 μ m. Graphs represent mean \pm SEM. Figure panels taken from figure 2b, c, d, e, g, and h [194].

Follow-up of an independent cohort of *Gars*^{C201R/+} × tRNA^{Gly-high} mice from 4 to 12 weeks of age confirmed full rescue of motor performance (figure 3.2a, b) and neuromuscular transmission (figure 3.2c, d). At 12 weeks of age, tRNA^{Gly-GCC} overexpression fully rescued the reduced gastrocnemius muscle weight and substantially mitigated muscle denervation (figure 3.2e, f). The rescuing effect persisted until 1 year of age in another cohort of *Gars*^{C201R/+} × tRNA^{Gly-high} mice. Body weight and motor performance were fully rescued from 4 to 52 weeks of age, as were NCV, CMAP amplitude, and gastrocnemius muscle weight. Thus, tRNA^{Gly-GCC} overexpression completely prevents peripheral neuropathy in *Gars*^{C201R/+} mice.

Finally, we crossed tRNA^{Gly-high} mice to another CMT2D mouse model carrying a patient mutation (245-248_delETAQ) in the mouse *Gars* gene [196]. At 4, 8, and 12 weeks of age, tRNA^{Gly-GCC} overexpression fully rescued motor deficits, reduced NCV and CMAP amplitude, reduced gastrocnemius weight, and muscle denervation. In tRNA^{Gly-low} mice, the tRNA^{Gly-GCC} level was not altered. *Gars*^{C201R/+};tRNA^{Gly-low} mice were indistinguishable from *Gars*^{C201R/+} mice for all parameters evaluated, showing that tRNA^{Gly-GCC} overexpression, and not the mere presence of the transgene, is responsible for phenotypic rescue.

We next explored the molecular mechanism underlying the rescue of CMT2D phenotypes by $tRNA^{Gly}$ overexpression. We hypothesized that CMT mutant GARS may exhibit altered kinetics of $tRNA^{Gly}$ binding and release. First, size-exclusion chromatography of various purified human GARS variants revealed that WT and E71G migrated predominantly as dimers, whereas L129P, C157R (equivalent to mouse C201R), G240R, E279D, and G526R partitioned between the monomer and dimer forms (figure 3.4a). Next, in vitro kinetic studies were carried out on GARS variants was carried out to with in vitro transcribed $tRNA^{Gly}$ (figure 3.3). All CMT mutant GARS dimers bound $tRNA^{Gly-GCC}$ (K_{on} , association rate constant) with one-half to one-tenth the affinity of WT dimers (figure 3.4b). L129P, C157R, G240R, E279D, and G526R dimers displayed markedly slower $tRNA^{Gly-GCC}$ release (K_{off} , dissociation rate constant), with >80% of traces showing no $tRNA^{Gly-GCC}$ release (figure 3.4b).

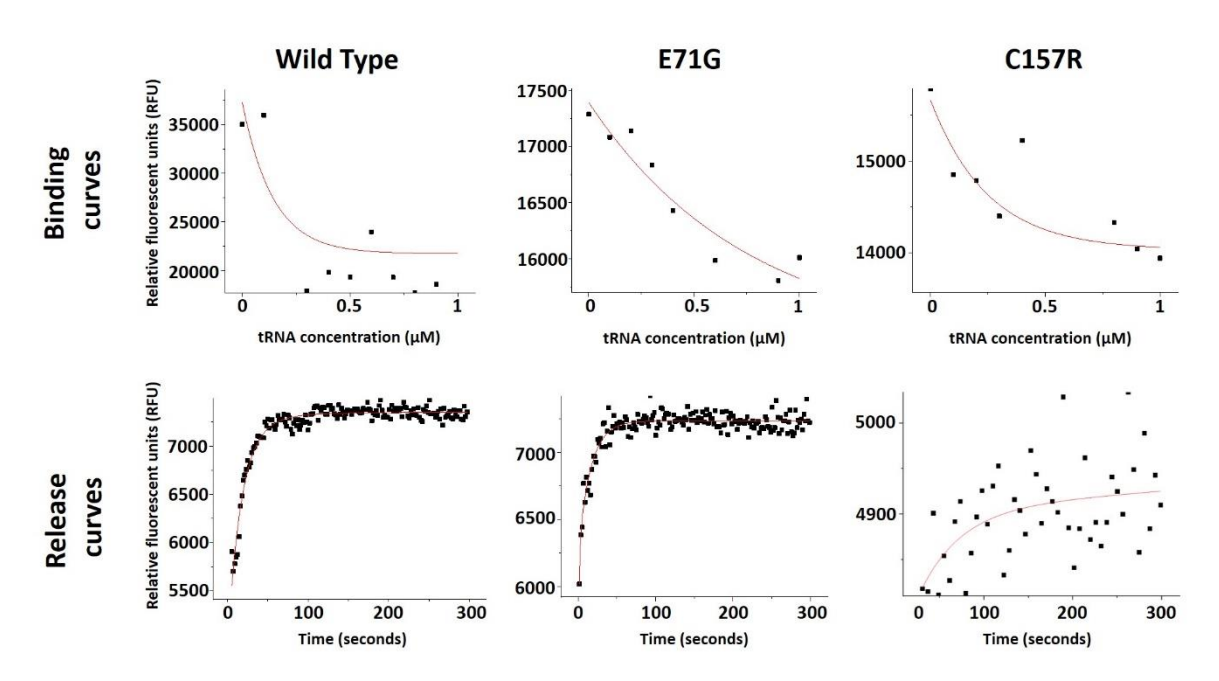


Figure 3.3 – CMT-GARS mutant variants showed slower binding and decreased release kinetics compared to wild type GARS.

in vitro tryptophan quenching curves. Kon data generated from 'binding curves' for each GARS variant used in experiment, and Koff data generated from 'Release curves'. Binding curve readings taken after GARS and tRNA^{Gly} incubated together. Release curve readings taken after addition of ATP and Gly to the same samples, beginning aminoacylation reaction of GARS.

In contrast, E71G dimers displayed tRNA^{Gly-GCC} release kinetics comparable to WT. L129P, C157R, G240R, E279D, and G526R monomers bound tRNA^{Gly-GCC} with very low affinity, but once bound, the tRNA^{Gly-GCC} release was markedly inhibited (figure 3.4b). The tRNA^{Gly-UCC} isoacceptor displayed similar binding and release kinetics to GARS dimers and monomers. The slow tRNA^{Gly} release by CMT mutant GARS dimers and monomers suggests that mutant GARS sequesters a large fraction of cellular tRNA^{Gly} and thus deplete it for translation. To provide in vivo evidence for tRNA^{Gly} sequestration, we immunoprecipitated GARS from brains of *Gars*^{C201R/+} and WT littermate mice and quantified the amount of tRNA^{Gly} bound to GARS. The tRNA^{Gly} amount was ~65% larger in *Gars*^{C201R/+} than in WT (figure 3.4c and figure 3.5a), indicating stronger tRNA^{Gly} association with GARS-C201R.

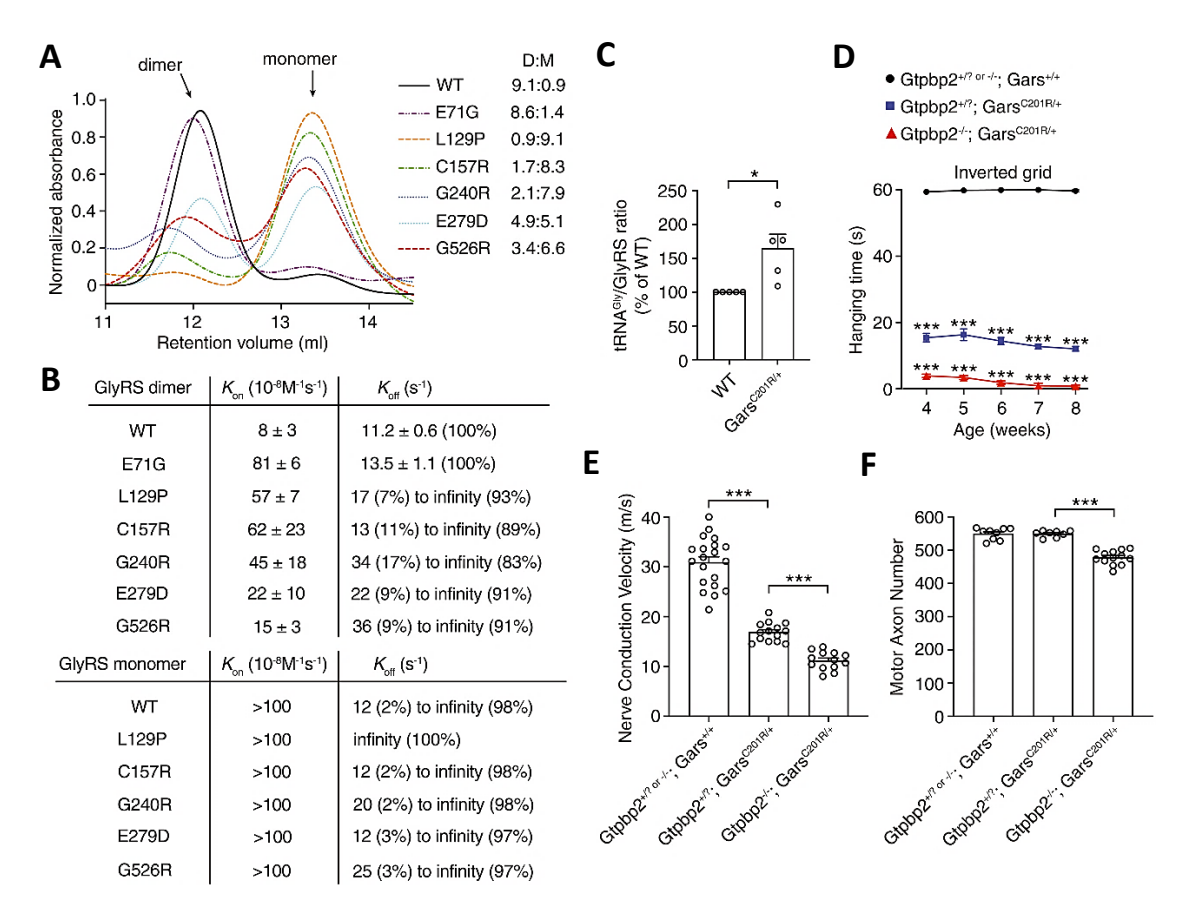


Figure 3.4 – tRNA^{Gly} sequestration by CMT mutant GARS induces ribosome stalling.

(A) Size-exclusion chromatography of purified recombinant human GARS proteins. D:M, dimer-to-monomer ratio. (B) K_{on} and K_{off} values of tRNA^{Gly-GCC} binding and release, respectively, to dimer and monomer forms of the indicated GARS variants. The percentage in parentheses denotes the frequency of a measured value. (C) Quantification of tRNA^{Gly} bound to GARS in tRNA^{Gly}-GARS complexes immunoprecipitated from whole brains of Gars^{C201R/+} and WT littermate control mice. tRNA^{Gly}/GARS ratio of WT is set as 100%; n = 5 independent experiments; *P < 0.05 by one-sample t test. **(D)** Hanging time in the inverted grid test of male Gtpbp2+/? or -/-;Gars+/+ (control), Gtpbp2+/?;Gars^{C201R/+}, and $Gtpbp2^{-/-}$; $Gars^{C201R/+}$ littermate mice at 4, 5, 6, 7, and 8 weeks of age. n = 15 to 28 mice per genotype group; ***P < 0.0005 by one-sample t test and two-tailed unpaired t test with Bonferroni correction per time point. (E) Nerve conduction velocity of the sciatic nerve at 8 weeks of age. n = 13 to 20 mice per genotype group; ***P < 0.0001 by Brown-Forsythe and Welch ANOVA. **(F)** Axon number in the motor branch of the femoral nerve at 8 weeks of age. n = 8 to 13 per genotype group; ***P < 0.0001 by one-way ANOVA with Tukey's multiple comparisons test. Graphs represent mean ± SEM. Figure panels taken from figure 3 [194].

Because tRNA^{Gly} sequestration may lead to ribosome stalling at Gly codons, we performed ribosome profiling on SC extracts of Gars^{C201R/+} and WT littermate mice, revealing that Gly codons are more frequently found in the ribosomal A site in Gars^{C201R/+} SC relative to WT (a cumulative increase of 79%) (figure 3.5b). Prolonged ribosome dwelling at codons is resolved by "ribosome rescue" pathways [197]–[199], and because Gly codons are frequent, ribosome stalling in CMT2D may deplete ribosome rescue factors, and inactivation of a rescue factor may aggravate the phenotype of CMT2D mice. Indeed, inactivation of Gtpbp2, encoding the ribosome rescue factor GTPBP2 (guanosine triphosphate binding protein 2), does not induce peripheral neuropathy by itself [200] but substantially enhanced peripheral neuropathy in Gars^{C201R/+} mice (figure 3.4d, e, f). Thus, ribosome stalling causally contributes to CMT2D pathogenesis. Because stalled ribosomes may activate the integrated stress response (ISR) through general control nonderepressible 2 (GCN2) [201]-[203], and ISR activation was implicated in CMT2D [204], we evaluated ISR induction in CMT2D mice inter-crossed with tRNA^{Gly-high} mice. tRNA^{Gly-GCC} overexpression fully rescued increased phosphorylated eukaryotic initiation factor 2α (eIF2 α) immunostaining intensity (~75% higher than in WT) in spinal motor neurons of Gars METAQ/+ mice as well as the strong induction of activating transcription factor 4 (ATF4) target genes Gdf15, Adm2, B4gaInt2, and Fgf21 in motor neurons of Gars^{C201R/+} mice. Thus, tRNA^{Gly-GCC} overexpression abrogates ISR activation in CMT2D mice, indicating that depletion of the cellular tRNA^{Gly} pool and consequent ribosome stalling is upstream of ISR activation. When Gtpbp2 is inactivated in Gars^{C201R/+} mice, the percentage of motor neurons showing ISR activation does not change, nor do additional cell types show ISR activation, despite widespread Gtpbp2 expression in SC. This suggests that tRNA^{Gly} levels are only below a critical threshold in affected motor and sensory neurons, leading to ribosome stalling selectively in these cell types. This may explain the relatively modest increase in ribosome dwelling at Gly codons in *Gars*^{C201R/+} SC (figure 3.5b).

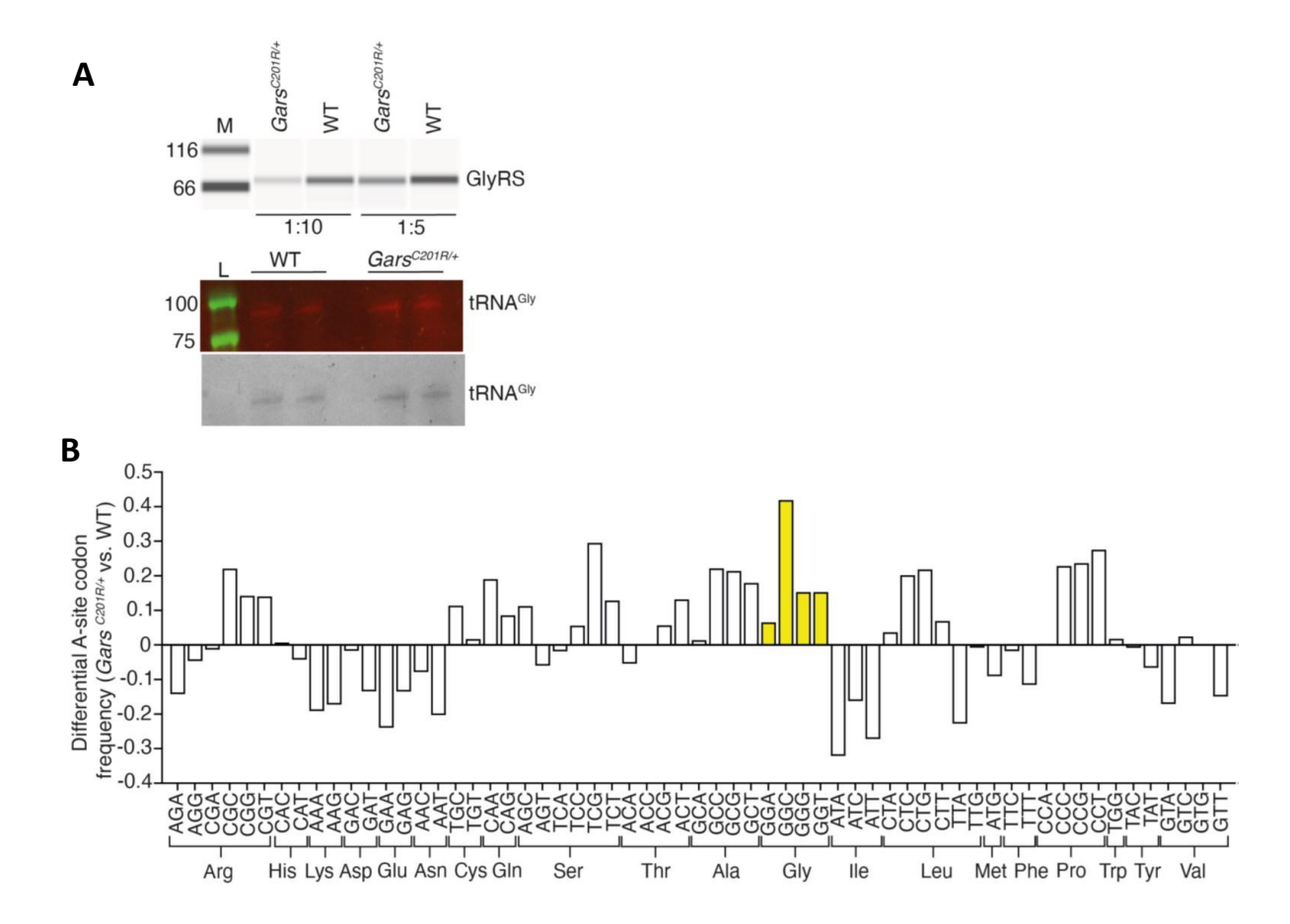


Figure 3.5 - Ribosome stalling on Gly codons contributes to peripheral neuropathy phenotypes in GarsC201R/+ mice. (A) Example of quantification of tRNA^{Gly} bound to GARS in complexes immunoprecipitated from whole brains of Gars^{C201R/+} and WT control mice. The amount of GARS was determined in two dilutions (1:5 and 1:10, upper panel) using a capillary electrophoresis immunoblotting system (Jess, ProteinSimple). GARS-bound tRNA^{Gly} was quantified following ligation with a fluorescent oligonucleotide, loaded onto two lanes and separated on 10% denaturing polyacrylamide gel (middle panel). The quantification was performed in black-white mode (lower panel). M, protein marker; L, prestained DynaMarker for small RNAs (BioDynamics Laboratory Inc, Japan). (B) Relative changes in ribosome dwelling occupancy (frequency) at A-site codons in spinal cord of Gars^{C201R/+} versus WT littermate mice, as determined by ribosome profiling. The A site frequency was separately determined for Gars^{C201R/+} and WT mice, normalized to the transcriptome codon frequencies, and presented as a ratio to visualize the effect of the C201R mutation on A-site codon frequencies. The four Gly codons are highlighted in yellow. Ribosome dwelling occupancy at Gly codons in the A site is elevated in Gars^{C201R/+} spinal cord, most prominently for the GCC codon. Note that among the Gly codons, GGC is the most frequently used. Figure panels taken from figures S13 [194].

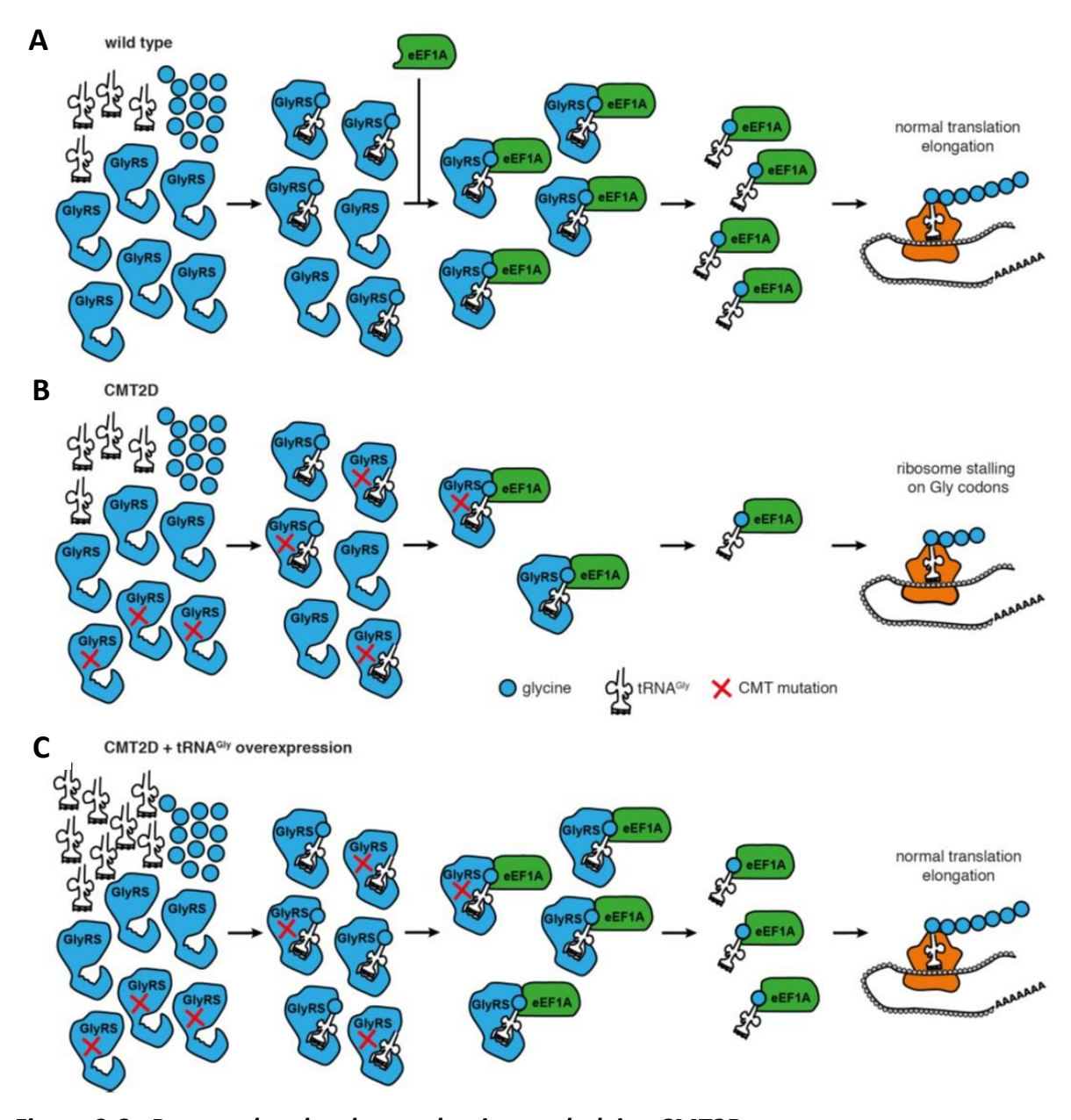


Figure 3.6 - Proposed molecular mechanism underlying CMT2D.

(A) WT GARS binds tRNA^{Gly} and Gly, activates Gly, and aminoacylates tRNA^{Gly}. Glycyl-tRNA^{Gly} is transferred to eEF1A, which delivers glycyl-tRNA^{Gly} to the ribosome for use in translation elongation. (B) In CMT2D, both WT and CMT-mutant (labelled with red cross) GARS proteins are present, derived from the WT and CMT-mutant GARS alleles, respectively. CMT-mutant GARS binds tRNA^{Gly} and possibly Gly, may or may not activate Gly and aminoacylate tRNA^{Gly}, but fails to release tRNA^{Gly} or releases it at a very slow pace. As a consequence, the cellular tRNA^{Gly} pool is depleted below a critical threshold. (C) tRNA^{Gly} overexpression replenishes the cellular tRNA^{Gly} pool, resulting in sufficient tRNA^{Gly} for aminoacylation by WT GARS. Figure panels taken from figure S16 [194].

3.3 - Conclusion

Our data propose a detailed molecular mechanism underlying CMT2D (figure 3.6). Beyond the seven CMT2D mutations studied here, this mechanism may apply to additional CMT mutant GARS proteins, because 14 of 25 reported CMT2D mutations result in net addition of positive charge, which could alter binding and release kinetics of the negatively charged tRNA^{Gly}. Similarly, most CMT-causing mutations in YARS and AARS also result in net addition of positive charge. Finally, our data indicate that increasing tRNA^{Gly} level may constitute a therapeutic approach for CMT2D.

3.4 - Materials and Methods

Expression and purification of recombinant GARS proteins

All GARS variants were cloned into pET28 modified with two expression tags, i.e. 6xHis and SUMO tag, and expressed in the *E. coli* Rosetta strain. Cultures were grown until the exponential phase (OD₆₀₀ = 0.7-0.8) and induced with 0.7mM IPTG for 16h at 22°C. GARS variants were bound to *HisPur Ni-NTA resin* (Thermo) by incubating for 30 minutes at 4 °C, washed multiple times with 20 mM Tris-HCl pH 8.0, 500 mM NaCl, and 10 mM imidazole, followed by twice washing with 20 mM Tris-HCl pH 8.0, 500 mM NaCl, and 20 mM imidazole. The GARS variants were eluted from the resin by cleaving the SUMO tag by incubating the resin with 0.5 mg/mL of ULP overnight at 4°C. The collected supernatant was concentrated using *Vivaspin 20* spin columns, followed by fractionation of dimer and monomer forms via size-exclusion chromatography on *Superdex 200*.

Determination of K_{on} and K_{off} values

 K_{on} values for the cognate tRNA^{Gly-GCC} or tRNA^{Gly-UCC} were determined by monitoring the quenching of intrinsic tryptophan residues. In a 96-well plate format using multiple replicates, 750 nM of each GARS variant was incubated with different tRNA concentrations, ranging from 0-1 μ M, in 25 mM sodium acetate buffer pH 6.0 containing 10 mM MgCl₂, 5 mM DTT, in a final volume of 50 μ L and Trp emission was recorded at 350nm (excitation 280 nm) at 37 °C on a *TECAN Spark* plate-reader. tRNA^{Gly-GCC} and tRNA^{Gly-UCC} were generated via in vitro T7 transcription and purified via 10% polyacrylamide gel electrophoresis. Binding curves were

fitted to exponential decay functions and quantified with *OriginPro*. For determination of $K_{\rm off}$ values, between 0.1-1µM tRNA^{GIV} was added to 750 nM of each GARS variant in 25 mM sodium acetate buffer pH 6.0 containing 10 mM MgCl₂, 5 mM DTT and incubated for 10 min at 37 °C (final volume of 50 µL). To each reaction, Gly and ATP, each 1 mM, were added to the wells. Fluorescence spectra (emission at 350 nm and excitation at 280 nm) were recorded over 5 min, step 1 s. Spectra were fitted in *OriginPro* to an exponential function. For each variant more than 50 traces, in biological replicates setting, were recorded. For the CMT-mutant GARS variants that strongly bind tRNAs^{GIV}, albeit rarely, we detected some events of tRNA release. Those curves were fitted and discrete $K_{\rm off}$ values reported along with the fraction of the cases for which we registered them. The stability of tRNA^{GIV}:GARS complexes depends on both $K_{\rm on}$ and $K_{\rm off}$, i.e. $K_{\rm D}$ value ($K_{\rm D}=K_{\rm on}/K_{\rm off}$) which largely differs among the variants. Along with $K_{\rm D}$, mean life and the half-life of a protein:ligand complex (i.e. $1/K_{\rm off}$ and $1/K_{\rm off}$, respectively) are quantitative predictors on its stability [205]. Together, $K_{\rm D}$ and $1/K_{\rm off}$ of the tRNA^{GIV}-GARS complexes quantitatively recapitulate the tRNA sequestration effect for all CMT-mutant GARS proteins.

Modelling the level of tRNA^{Gly} overexpression needed for rescue

The translation rate of a single codon depends on (i) tRNA aminoacylation by the cognate aaRS; (ii) ternary complex formation with elongation factor eEF1A and its free diffusion to ribosomes; (iii) tRNA recycling mediated by eEF-1B/C [206]. Using the mathematical formalism for describing the translation process [206], the mass balance is described by:

$$\frac{d(f[tRNA])}{dt} = \frac{k_{cat}(1-f)[tRNA]}{K_m + (1-f)[tRNA]} [aaRS] + k_t f[tRNA]m$$

where k_{cat} and $K_{\rm m}$ are the kinetic parameter of the aaRS for tRNA aminoacylation, [tRNA] and [aaRS] are the total concentration of a tRNA species and the cognate aaRS, respectively, f is the fraction of charged tRNA and k_t is the rate constant of translation of a codon which is translated by a fraction of the ribosomes m. The left term in Eq. 1 depends on the aaRS enzymatic properties and the right term, $r_+ = k_+ [{\rm tRNA}] m$, describes the rate of translation of a codon. Taking translation of Gly codons as example, under non-limiting Gly amino acid supply which is the case in balanced fed mammalian cells, $k_{cat} = 0.2$ -0.7 s⁻¹ and $K_{\rm m} = 0.28$ -1.37.10⁻⁶ M for tRNA^{Gly} (the parameters were taken from the enzyme database BRENDA). Since the precise ribosome and total tRNA concentration for the specific tissue is unknown,

we used averaged values for a eukaryotic cell, i.e. 30-100 μ M total tRNA concentration and 1-10 Mio ribosomes/cell (https://bionumbers.hms.harvard.edu). Using the quantitative sets of HeLa and HEK293T tRNAs [207], [208], in a total tRNA concentration of 30-100 μ M, the concentration of tRNA^{Gly} isoacceptors is 0.5-1.7 μ M. The maximal concentration of the ribosomes which could simultaneously request all four Gly codons can be estimated from the cumulative Gly codon usage and is calculated to be 8.3x10⁻⁷ M. At steady state f=0.8, i.e. 80% of the tRNA is charged [209]. The concentration of GARS is estimated from its K_m value to be 0.5-2.4.10⁻⁶ M. Numerically solving Eq. (1) using k_t for wild-type GARS, taking the mean values for all parameters, we obtained that the rate of translation (r_t) and k_t for Gly codons are r_t =0.16x10⁻⁶ mol.l⁻¹.s⁻¹ and k_t =0.22x10⁻⁶ s⁻¹, respectively. The average waiting time for the ribosome for a cognate ternary complex at a codon is determined from:

$$\tau = \frac{1}{k_t f[\text{tRNA}]}$$

Solving Eq (2) for Gly codon results in 4.5 Gly codons/s. This result is consistent with the experimentally measured translation rate in eukaryotic cells (1-7 codons/sec). Since GARS mutations are heterozygous and assuming equal expression from both alleles, the average GARS concentration will be 0.8 μ M wild-type GARS and 0.8 μ M mutated GARS. The markedly slower tRNA^{Gly} release for L129P, C157R, G240R, and G526R GARS (i.e. $K_{off} = \infty$) from the dimers and monomers suggests at steady-state a full saturation of the mutant GARS. As a result, the mutant GARS will sequester 0.8 μ M tRNA^{Gly}. To restore the function of the wildtype GARS counterpart, i.e. to reach the wild-type GARS translation rate of r_t =0.16x10⁻⁶ mol.l⁻¹.s⁻¹, using Eq. 1 we model that the concentration of tRNA should be increased up to 1.9 μ M, i.e. a raise of the total tRNA^{Gly} concentration by 1.7-fold is necessary. For the E279D and E71G, considering the dimer:monomer ratio and that the monomer only sequesters the tRNA, an increase of tRNA by 1.3-fold and 1.1-fold respectively would rescue these mutations.

In vivo quantification of tRNA^{Gly} bound to GARS

Brains from *Gars*^{C201R/+} mice and littermate controls were dissected and snap frozen. Frozen brains were grinded, subjected to UV-crosslinking at 254 nm, 400mJ/cm² (UVP-TL-2000 Translinker) after which lysis buffer (20mM Tris-HCl pH 7.4, 15mM NaCl, 1% NP-40, 0.1% Triton-100,0.5%SDC, 2mM DTT, protease inhibitor) was added. Protein-G-Dynabeads (Invitrogen) were coupled with GARS antibody mixture (rabbit polyclonal; 1:400; Abcam,

ab42905 and rabbit polyclonal; 1:200; Proteintech, 15831-AP) and incubated with the lysed tissue overnight at 4°C. Beads were precipitated by centrifugation and washed with buffer (20mM Tris-HCl pH 7.4, 100mM NaCl, 1% NP-40, 0.1% Triton-100,0.5%SDC,2mM DTT). The tRNA bound to GARS (co-immunoprecipitated with the GARS-antibodies-coated Dynabeads) was extracted with phenol:chloroform (Sigma) and subjected first to tRNA identification, followed by quantification. By this extraction the tRNA is completely deacylated. The identity of tRNAs bound to the immunoprecipitated GARS was determined by Northern blot using Atto565-labeled stoichiometric mixture of degenerated DNA oligonucleotides specifically recognizing the three tRNA^{Gly} isoacceptors with the following sequences: 5′-CCCGGGTCAACTGCTTGGAAGGCAGCTAT-3′, and 5′GYCTCCCGCGTGGSAGGCGAG-3′. For quantification of the GARS-bound tRNA, we used Cy3-labeled fluorescent stem-loop RNA/DNA oligonucleotide that ligates to the unpaired 3′-NCCA

labeled fluorescent stem-loop RNA/DNA oligonucleotide that ligates to the unpaired 3'-NCCA end of the tRNAs^{Gly} (5'pCGCACUGCdTdTXdTdTdGdCdAdGdTdGdCdGdTdGdGdN-3'). The total tRNA extracted from the immunoprecipitated GARS from *Gars*^{C201R/+} and WT mice, in five biological replicates (one wild type and one *Gars*^{C201R/+} brain per replicate), was ligated with the fluorescent oligonucleotide as described [208], loaded on 10% denaturing polyacrylamide gel and the fluorescent signals were quantified using ImageJ. GARS bound to the GARS-antibodies-coated Dynabeads was quantified by the capillary electrophoresis immunoblotting system (Jess, ProteinSimple) using GARS antibody (rabbit polyclonal; 1:200; Proteintech, 15831-AP) as described previously [210]. A standard curve was obtained using purified wild type GARS.

Ribosome profiling of GARS mice

Spinal cord of three *Gars*^{C201R/+} and three WT littermate control mice were flash frozen and immediately lysed by grinding in 10mM Tris-HCL pH 7.4, 5mM MgCl₂, 100mM KCL, 1% NP5, 2% sodium deoxycholate. The lysates from three animals per genotype were pooled. Cycloheximide (100 μg/ml) was added to the sucrose gradient fractions when collecting polysomes to prevent ribosomal dissociation during RNase I digestion. The lysates from three animals per genotype were pooled. Isolation of mRNA-bound ribosome complexes, RNase I digestion-derived ribosome-protected fragments (RPFs) and the cDNA libraries from RPFs were prepared using a protocol for miRNA with direct ligation of the adapters [211]. Sequenced reads were trimmed using *fastx-toolkit* (0.0.13.2; quality threshold: 20), adapters

were cut using *cutadapt* (1.8.3; minimal overlap: 1 nt), and processed reads were uniquely mapped to the mouse genome (GRCm38) using STAR (2.5.4b) [212], allowing a maximum of one mismatch, with parameter settings: --outFilterMismatchNmax 1 --outFilterType BySJout –outFilterMultimapNmax. Uniquely mapped reads were normalised to reads per kilobase per million mapped reads (RPKM). To calibrate the RPFs, i.e. to determine position of the A-site codon within each RPF, the RPFs were binned into groups of equal read length, and each group was aligned via P site positioning over the start codon as described [200], [213], using the calibration tool:

(https://github.com/AlexanderBartholomaeus/MiMB_ribosome_profiling) [214]. Briefly, bins were separately plotted to cover the initiation and early elongation (app. 300 codons). ribosomes spanning the start codon accommodate AUG at their P site, causing a characteristic drop in read density upstream of the start codon. For each bin length, we used this feature to determine the offset between the 5' read end and the P site, and by adding 3nt to the A site. We considered six bins (28-33 nt length) with the highest number of RPFs for calibration. Calibrated reads displayed a 3-nt periodicity indicative of genuine translation. Over all bins, the A-site codon occupancies were summed up on a transcript-specific manner and normalized on the transcript background, i.e. by the mean of randomized reads to consider differences in transcript abundance and codon frequencies across transcripts [200]. To directly compare the differences in the ribosome dwelling occupancy (frequency) at the A-site codon between $Gars^{C201R/+}$ and WT control mice, the summed-up A-site codon occupancies across all transcripts for each species were then divided and presented as differential A-site codon occupancies.

Site-directed mutagenesis

Pet28-SUMO plasmid containing 6xHIS tag and SUMO tag with the wild type GARS, and mutant forms G240R and G526R were supplied by Erik Storkebaum's Lab, Radboud University, Donders institute. Wild type plasmid was mutated to generate plasmids containing a variety of mutant forms the GARS (E71G, C157R, L129P, E279D). Forward and reverse strands were synthesised and ordered from *Microsynth*, with strands carrying mutation in the sequence. PCR mix was made (5x Phusion buffer, 10mM DNTP mix, 10uM forward strand, 10uM reverse strand, 100ng WT plasmid, 0.6uL DMSO, 0.2uL Phusion DNA polymerase), and PCR was carried out to generate mutant plasmids: 95°C - 5min | 95°C

- 30s, 55°C - 30s, 68°C - 10min | x18, 68°C - 3min. Extension time at 68°C depends on the length of plasmid, 1min per kb. PCR products were DPNI digested for 1 hour and 30min at 37°C. Plasmids were sequenced after mutagenesis to confirm correct incorporation of mutation into plasmid sequence.

Generation of tRNA species through in vitro transcription

Sets of DNA primers were designed based on the full length tRNA sequence to be transcribed, with the addition of the T7 promoter site (5'TAATACGACTCACTATA'3) on the 5' end of the forward primer, ensuing primers have an approximate overlap of ~20nt. Primers for tRNAGly^{GCC} and tRNA^{Tyr} were as follows: tRNAGly forward primer – 5'TAATACGACTCACTATAGCATCGGTGGTTCAGTGGTAGAATGCTCGCCTGCCACGCGGGC'3 and reverse primer –

5'TGGTGCATCGGCCGGGAATCGAACCCGGGCCGCCCGCGTGGCAGGCGAGCATTCTA'3.

Primer mix (100µM) was incubated with 0.2M Tris buffer pH 7.5 at 95°C and 5min at room temperature to anneal the overlapping primers. Annealed primers were then incubated with RevertAid H Minus Reverse Transcriptase (Thermo Fischer) with 5x RT buffer and 10mM DNTPs to fill out the annealed primers. cDNA was extracted via Phenol/Chloroform and precipitated from aqueous phase with 100% EtOH. cDNA was then mixed with NTP set (1.25mM final conc per nucleotide), GMP (final conc 10mM), 5X Transcription buffer (Thermo Fischer), and T7 RNA polymerase, and incubated at 37°C for 7hrs. Transcribed tRNA was then ran on a 10% polyacrylamide gel containing urea for 1hr at 20W. tRNA band was visualised by UV shadowing, and was then excised from the gel and eluted overnight in 'crush and soak' buffer (50mM KOAc, 200mM KCl pH 7). Gel pieces were pelleted via centrifugation and tRNA was precipitated with 100% EtOH.

4 - CMT-YARS mutant variants increased ribosome occupancy at Tyr codons

The results from this Chapter are collaborative effort with Prof. Dr. Erik Storkebaum, Radboud Universiteit, Netherlands to disentangle the underlying mechanism of DI-CMT pathology associated with mutations in YARS *Drosophila* larvae for ribosomal sequencing libraries were provided by Dr. Storkebaum's group. My contribution was to produce the sequencing libraries for ribosome profiling along with analysing in vitro kinetics and amount of bound tRNA^{Tyr} to the YARS variants. Deep-sequencing data analysis was carried out by Leonardo Santos, a PhD candidate in our group (figure 4.2, 4.3). Lysates from *Drosophila* also prepared for immunoprecipitation study of YARS:tRNA^{Tyr} complex, which was carried out by myself (figure 4.4).

4.1 - Introduction

CMT related mutations are seen in multiple aaRS enzymes, and all show a similar phenotypic, axonal dystrophy [125]. Each aaRS is specifically tailored to bind to and charge their cognate tRNA with their respective amino acid, and while each aaRS can have specific interactions and activities that alter how it interacts with their ligands, ultimately the end result is the same with every aaRS, in creating the charged-tRNA pool for the cell. As such, it would logically follow that the effects we see in the data above for GARS should also be mimicked in systems that are expressing other CMT-aaRS mutations. Aside from GARS, YARS is the other aaRS that has been extensively studied in regard to CMT, with three prominent mutations characterised in giving rise to CMT in patients: two missense mutations, G41R, E196K, and a four codon deletion, 153-156DelVQKV (Shortened to 153DEL or YARS DEL from hereafter) [215], [216]. As is the case as well for GARS, most of the mutations for YARS are also gain of positive charges, which is the case for the missense mutations, whereas YARS DEL is a gain of a negative charge in the protein. YARS itself is a Class 1 aaRS, and exists as a homo-dimer in the cell, and uniquely among Class 1 aaRS, forms a unique structure where the tRNA binds both dimers, at the active site of one unit and the anticodon binding domain on the other monomer unit forming a bridged architecture [217]. The catalytic domain of YARS carries out the activation of Tyr into the intermediate Tyr-AMP, and for transferring the amino acid onto the

3'CCA end of the cognate tRNA^{Tyr}. The anti-codon binding domain recognises the cognate tRNA and stabilises the tRNA binding to the synthetase, structuring the tRNA into an 'L' shape as it binds both domains [218].

The CMT type given rise by mutations in YARS is classified slightly differently than other CMT2 axonal dystrophies, in that it gives rise to a rarer intermediate type, with both demyelination and axonal dystrophic phenotypes in patients, dubbed as dominant-intermediate type (DI-CMT), so called because it has an NCV between CMT1 and CMT2 [215], [219]. Inherited in the same autosomal dominant manner, the symptoms can range from mild to severe, with similar symptoms as CMT1 or CMT2, such as muscle weakness and wasting, distal limb abnormalities, etc. In another similar fashion to GARS, loss of aminoacylation function is also not common among the described mutations, with E196K showing very little loss of aminoacylation activity, but one of the most severe phenotypes in patients. G41R in contrast is almost enzymatically dead, but shows a milder phenotype in patients [125], [215] compared to E196K, though stronger than the DEL mutation. All tested mutations here all hit directly inside the catalytic domain of YARS [220], yet despite this the impact on the aminoacylation activity ranges wildly between mutations. Again, this firmly demonstrates that the possible loss of function is not the underlying mechanism behind development of CMT, and another gain-oftoxic function effect must be the underlying mechanism involved in the development of this disease. Somewhat contradictory, loss of overall translation and protein synthesis is common in Drosophila models expressing CMT-YARS [189]. If aminoacylation loss is not detectable or unifying between mutants, but there is significant translational reduction, then a different mechanism must come into play that couples together these seemingly contradictory notions. As was shown in the data above for GARS, this tRNA sequestration effect could also be the determining translational defect that may give rise to the CMT development in the cells. To test this, ribosome profiling libraries were generated from whole Drosophila larvae, either expressing WT, or one of the three mutant-YARS. Also, the same set of YARS variants were also expressed in larvae that were overexpressing tRNA^{Tyr} to see if the additional tRNA copies inside the cells could help to alleviate and rescue any possible translational defects caused by the YARS CMT-mutants.

4.2 - Results and Discussion

Initially, tryptophan quenching assay was also carried out for the YARS variants to see if a similar effect is seen with this aaRS, where there is a slow release of tRNA once bound to the synthetase. However, the kinetic assay gave a much more varied result, and did not follow the same expected pattern as before (figure 4.1a). Instead of a decrease in fluorescence with the binding of the tRNA and a reverse of this quenching once the tRNA was added, the opposite trend was seen. In regard to how this assay should work, this result makes little sense. However, Class I aaRS differ greatly compared to Class II aaRSs, as eEF1A binding and forming the complex with the aa-tRNA, is a necessary step to releasing the tRNA from the synthetase once charged. eEF1A (and EF-Tu in yeast) shows a higher affinity to Class I aaRS, and in fact shows low or no binding to Class II, potentially due to the fact that Class II aaRS bind to the major groove of tRNA, which is where eEF1A would typically bind [221]. In the experimental set up here, no eEF1A was added to the reaction, which means the aa-tRNA could not be released from the synthetase. This might explain the trend of the curves, but also means this experiment is unsuitable for this protein. eEF1A could be added, but the protein itself has its own intrinsic fluorescence and would likely interfere with the results. No YARS wild type variant is shown in this experiment, mostly due to problems in expressing and purifying the fully formed YARS protein, further highlighting that this experiment is potentially unsuitable for this protein. To at least try to show that the mutant YARS shows binding activity to the tRNA, an electrophoretic mobility shift assay (EMSA) was carried out using increasing concentrations of E196K and incubating it with tRNA^{Tyr} (figure 4.1b). The decreasing tRNA lower bands into the upper bands clearly shows a shift in the tRNA on the gel and binding of the aaRS to the tRNA. Doublets of upper and lower bands are difficult to explain, though could be due to both monomeric and dimeric structures present in purified protein samples, with different kinetics of binding, as seen for GARS in chapter 3. This would shift tRNA differently on the gel if bound. Despite the quenching assay then not being appropriate for this protein, the EMSA gel shows clearly that the mutant has a binding capability to its cognate tRNA.

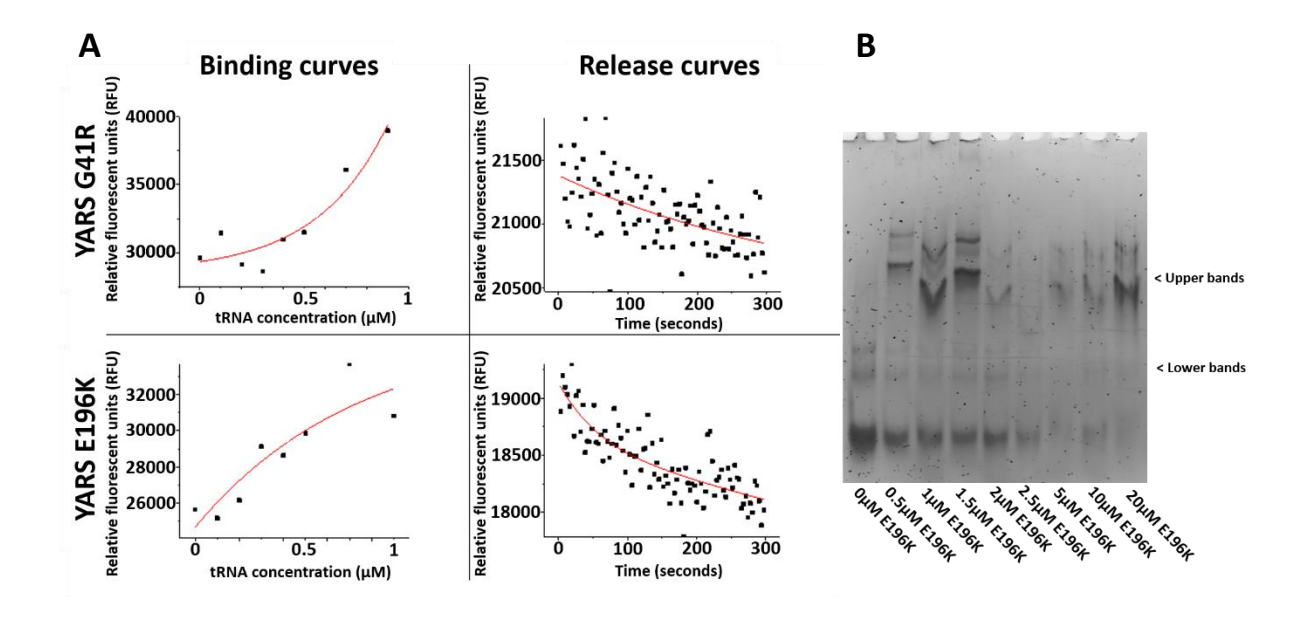


Figure 4.1 – CMT-YARS variants did not show typical binding/release kinetics in in vitro assay, but did show binding.

(A) In vitro tryptophan quenching plots for both the G41R and E196K variants of YARS. 'Binding curves' show the initial reaction between the protein and tRNA^{Tyr}. 'Release curves' generated after addition of ATP and Tyr amino acid to the reaction. Excitation = 295nm. Emission = 350nm. (B) Electrophoretic shift assay (EMSA) gel. Differing concentrations of E196K variant incubated with tRNA and applied onto non-denaturing gel. Shift of the lower band into the upper band with the increasing concentration of YARS indicates binding. Gel stained against nucleic acid with sybr gold.

To continue to investigate the mechanism of CMT-YARS then, ribosome profiling libraries were prepared and analysed to look at the effect of the YARS variants on a codon specific level, as was done with the GARS mice mutant model. Cumulative translational expression in *Drosophila* containing any of the three YARS mutants, showed a decreasing trend (figure 4.2a) when compared with WT, further illustrating that the CMT-relevant mutant forms of the enzyme cause translational defects inside the cell, generally lowering the level of protein synthesis. When further expanding the analysis to look at Ribosomal occupancy on Tyr codons specifically, for the DEL and E196K mutants, we can see an increase in occupancy, which is rescued upon tRNA^{Tyr} overexpression (figure 4.2b, 4.2c). YARS Del showed a ~20% ribosomal speed increase in samples overexpressing tRNA, while E196K showed a more modest increase

of ~10%. Both Del and E196K then worked as originally hypothesised, with both causing decreasing translation and slowdowns at Tyr codons, which can be rescued by tRNA. For G41R however, the opposite trend seems to be happening. While overall translation seems to be slowed down in the G41R condition compared to WT (figure 4.2a), this is not reflected when looking specifically at Tyr codon occupancy, which seems a lower trend then WT, and seemingly exacerbated by tRNA overexpression (figure 4.2c).

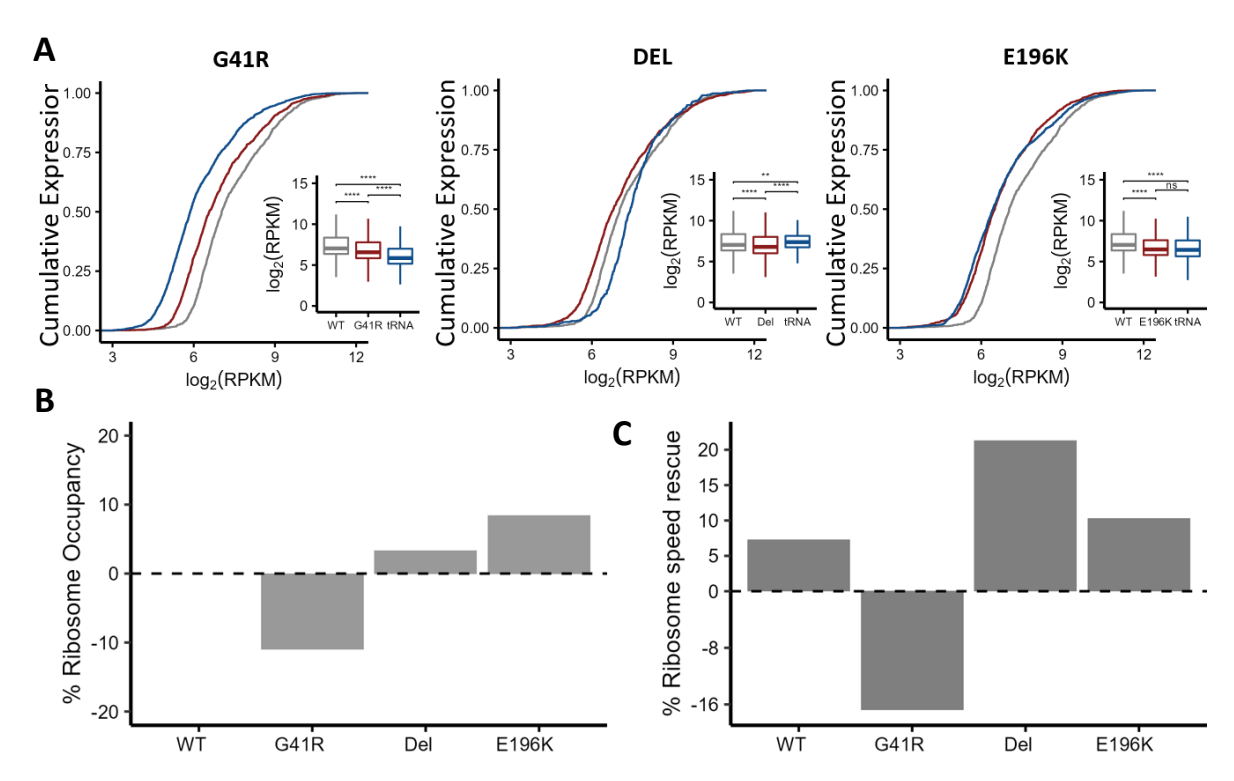


Figure 4.2 – CMT-YARS variants showed increased ribosome occupancy at Tyr codons, except G41R mutant, which was rescued in overexpression models.

(A) Cumulative expression graphs of sequencing reads from Drosophila expressing one of the indicated YARS variants— Insets show Wilcoxon rank-sum test. (B) Relative changes in ribosome occupancy of Tyr codons at the A site when comparing mutant YARS variants to wild type. Mutant YARS increases the frequency of Tyr codons at the ribosomal A site compared to the WT YARS. (C) Ribosomal occupancy rescue by tRNA^{Tyr} overexpression. The overexpression increases the amount of available tRNA^{Tyr}, reducing the frequency of the Tyr codon at the A site causing a decreased occupancy, indicating elongating ribosomes translocate through it faster. We compared the change of each variant overexpressing tRNA^{Tyr} to the non-overexpressing variant pair.

When the reads are positioned specifically on A-site Tyr codons across the entire translatome, and after quantifying frequency of occurrence (figure 4.3) the data sheds light on why this might be the case. In this scenario for G41R, tRNA overexpression only brings the Tyr codon A site frequency to almost exactly WT levels, indicating that overexpression of tRNA^{Tyr} seemingly has no beneficial or detrimental effect for this mutant, as the WT levels with no overexpression of tRNA^{Tyr} should be treated a baseline level of occupancy at unaffected Tyr codons. The lowered A site frequency for G41R on its own though, is harder to explain, but could be due to variability in this specific sample. YARS Del (figure 4.3c) and E196K (figure 4.3d), again, showed the expected trend, with tRNA overexpression reducing A-site Tyr frequency, indicating a speeding up of translation with increasing amounts of available tRNA. For E196K, the tRNA overexpression sample brings the A site frequency back to WT levels. As the E196K mutant sample on its own shows an increased frequency, this returning to 'baseline' levels shows a beneficial effect for this condition then and a rescuing of the detrimental effect of the mutant on its own. For DEL, while the increased A site frequency for the mutant alone is only mild, the tRNA overexpression sample shows a more striking rescuing effect, as the A site frequency even decreases below WT levels, indicating much faster ribosome speeds through Tyr codons due to the increase of tRNA^{Tyr} in the sample.

To further elucidate this increased frequency and increased ribosomal occupancy at Tyr codons, an immunoprecipitation experiment was also carried out here, to see the affinity of the CMT-YARS variants to its cognate tRNA. Despite the varied effects from the previous data, all of the tested YARS mutants showed an increased affinity to tRNA^{Tyr} above WT levels, as seen in an immunoprecipitation pulldown of YARS and tRNA (figure 4.4). In this experiment, E196K showed the highest affinity to tRNA with ~90% increased ratio of bound tRNA to the protein. The E196K samples also showed the highest ribosomal occupancy in our data on Tyr codons, while studies have shown it to not be as enzymatically disturbed compared to other mutants[190], yet this variant shows a strong phenotype in patients. With all of these factors, it follows that E196K binds and sequesters the largest amount of tRNA, correlating to the stronger phenotype and largest decrease in translation in the cells.

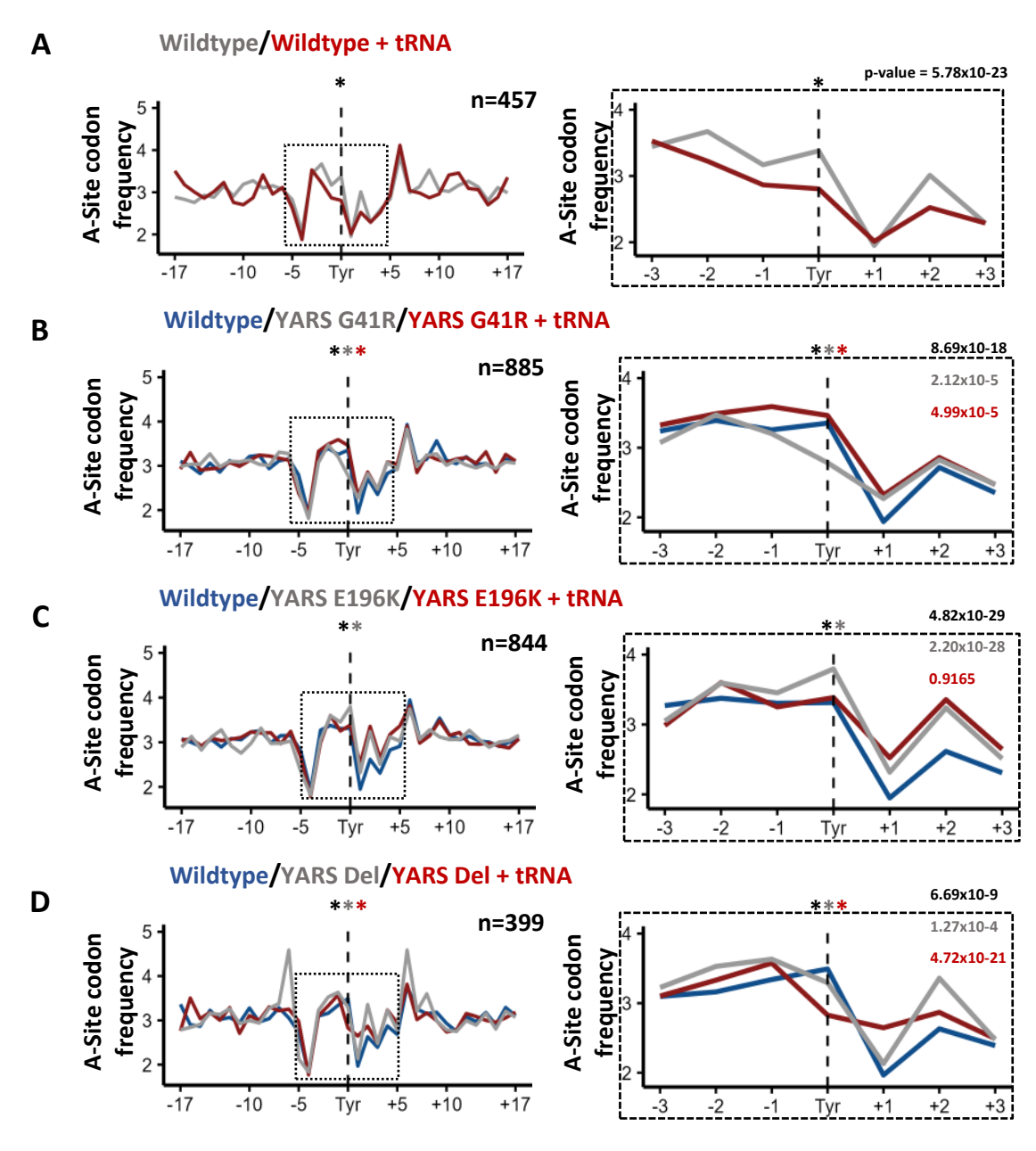


Figure 4.3 – Cumulative plots of sequencing reads showing the ribosome dwelling frequency at and surrounding the Tyr codon across the entire translatome.

Over expression of $tRNA^{Tyr}$ (red line on each graph) reduces the ribosomal frequency at the Tyr codons, compared to the non-overexpression of $tRNA^{Tyr}$ (grey line). This indicate a faster translation of Tyr codons when $tRNA^{Tyr}$ has a higher abundance. Comparison of each of the human YARS variants to its respective overexpression of $tRNA^{Tyr}$ sample and to the WT (blue line) was also carried out, as shown for WT (A) as well as for G41R (B), Del (C) and E196K (D) variants. The n values denotates the number of overlapping genes used for each comparison. This was to ensure equal translation context for each compassion surrounding the Tyr codon. P-values are calculated using the Mann-Whitney test.

Overexpression of tRNA then helped to alleviate the effects caused by this mutant. Tyr codons are one of the rarest in the human genome (Table 1.1), though surprisingly is a fairly abundant tRNA species, more abundant than tRNAs that have more frequently used codons [222]. Therefore, it is possible that for a stronger effect to be felt in the cells, the enzyme must show a much higher affinity to the tRNA. To then be able to effectively relieve the stalling effect, more tRNA must be used to buffer against the sequestration effect. In this way, it can be seen that the cell has a specific threshold it can withstand before an effect is properly acquired on the cell.

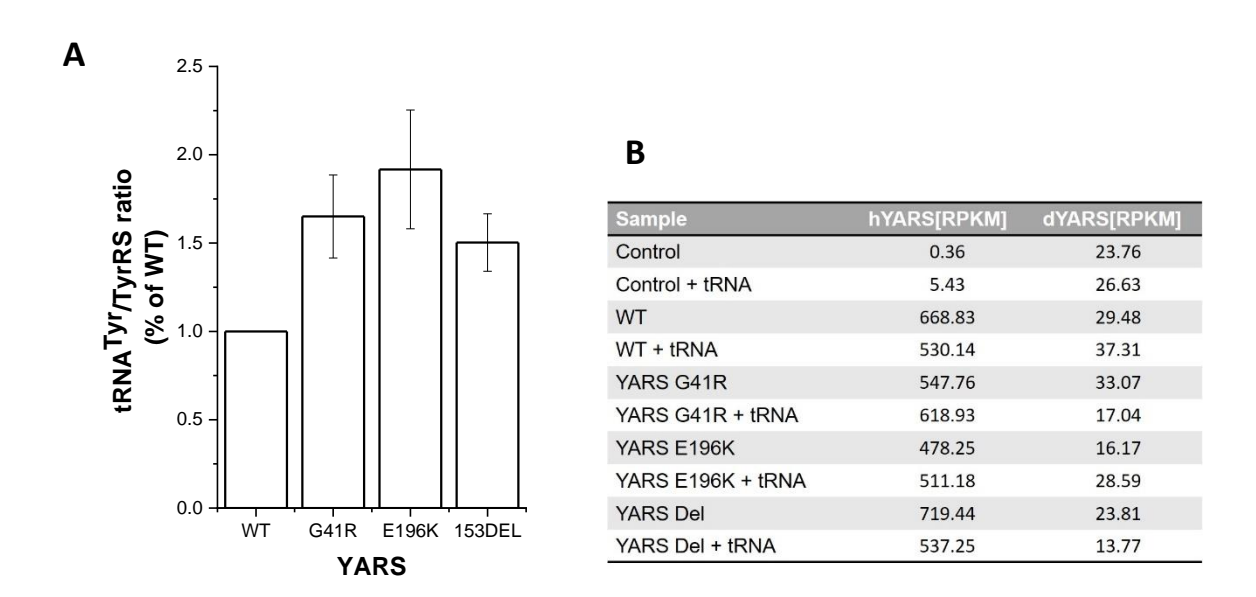


Figure 4.4 – CMT-YARS variants had an increased binding affinity to its cognate tRNA^{Tyr}.

(A) Immunoprecipitation of YARS showed higher ratio of tRNATyr bound to CMT-YARS. $tRNA^{Tyr}$ bound to YARS in YARS: $tRNA^{Tyr}$ complexes quantified after immunoprecipitation from Drosophila larvae expressing WT YARS or indicated CMT-YARS variant. Data shown as ratio of tRNA bound to protein in each sample. WT ratio of $tRNA^{Tyr}$ /YARS complexes set to 100% for comparison. Error bars indicate SEM of n=5 independent experiments. P value calculated from one-tailed t-test. **(B)** Expression levels of the endogenous Drosophila and human TyrosyltRNA synthetase genes (YARS), dYARS and hYARS respectively, for each YARS variant.

For G41R, the protein's enzymatic activity is drastically reduced[190]. Therefore it would require a much larger amount of tRNA to be able to effectively relieve any potential translational defects caused by the mutant YARS, as even though the equilibrium of the aaRS:tRNA can be shifted to better favour released tRNA, with no ability to charge the tRNA,

the cell is reliant on the endogenous, non-mutant YARS to keep up with demand of the cell to supply enough charged Tyr-tRNA^{Tyr}. It is possible then that under certain situations, such as stress, periods of cell growth or repair where the translational and metabolic demand of the cell is perturbed, this reliance on the single non-mutant YARS may not be able to meet the cellular demands, leading to increased instability of the cell.

4.3 - Conclusion

CMT-related YARS mutants showed a very similar trend that was observed in the case of GARS. All tested YARS mutants showed a higher affinity to its cognate tRNA^{Tyr}, and on a global level in a Drosophila model, all mutants reduced levels of translation occurring when compared to a wild type expressing sample. This follows previous data that shows the global protein synthesis is reduced in a CMT-aaRS context. tRNA overexpression also helped to alleviate this translation reduction, especially in regard to the E196K and 153DEL mutants. tRNA helped to speed up the ribosomes on Tyr codons, as would be expected if the sequestration effect is reducing the available tRNA pool in the cell. The effect here is milder than with GARS, and that could be for multiple reasons. Gly codons are more abundant, with a higher codon usage bias in humans. This is especially true for the GGC codon, which is also the codon showing the highest slowdown in our earlier mouse ribosome profiling data. In contrast to Tyr codons which are rarer. Also, YARS is a Class I aaRS where the release step of the aa-tRNA is already a limiting factor of the aminoacylation activity, and requires eEF1 to bind and pull the tRNA off of the synthetase [223]. Slowing this down by increasing the affinity of the tRNA to the synthetase might not have as dramatic an effect if this step is already slow as compared to other aaRSs. Either way, both E196K and 153DEL showed that increasing the tRNA amounts can help rescue the effect, even if more tRNA is required to overcome this buffered threshold. For G41R, as this variant is enzymatically inactive, it might simply be the case that additional tRNA might not be able to overcome the sequestration effect, as even if the protein releases the tRNA, it would not be charged, which means the endogenous WT form would need to overcompensate for this, which may be limited itself in its activity. It is also worth noting that this ribosome profiling experiment was carried in whole Drosophila larvae. As CMT disease specifically affects peripheral neurons and no other tissue, using whole organism lysates might mask any specific deleterious effect that the CMT-mutations have on

one specific tissue type, and also any beneficial effect that the tRNA overexpression might be causing. Moving forward, a model would need to be established to better test the CMT-YARS mutants, where the specific tissue type can be isolated and examined.

4.4 - Materials and Methods

Immunoprecipitation of YARS:tRNATyr complexes

Immunoprecipitation of the YARS:tRNA^{Tyr} complexes and their subsequent quantification and analysis, was carried out as previously described in Chapter 2. Each independent experiment was carried out with 8 snap-frozen larvae, either expressing WT human YARS or a CMT-YARS variant. Protein-G Dynabeads (Invitrogen) were coupled with two anti-YARS antibodies; 2µg each: Mouse monoclonal (Abcam, ab50961) and rabbit polyclonal (Bethyl Labs, # A305-064A) for the pulldown of the complexes. The sequence of the Cy3-labelled RNA/DNA oligonucleotide used for tRNA^{Tyr} quantification is as follows: 5'pCGCACUGCdTdTXdTdTdGdCdAdGdTdGdCdGdTdGdGdN-3'. For the YARS protein quantification by the capillary electrophoresis immunoblotting system (Jess, ProteinSimple), mouse monoclonal antibody (Abcam, ab50961); 1:25 dilution, was used.

Ribosome profiling

Collection of Ribosomal protected fragments (RPFs) was carried out as previously described in chapter 3 [194]. Eight *Drosophila* larvae overexpressing each indicated YARS variant, were lysed together and pooled for each individual sample. Sequenced reads were depleted from adapter sequences and uniquely mapped to the *Drosophila melanogaster* (BDGP6.32) as previously described in [194]. Thereafter, the sequencing data were analysed as described in chapter 3. The direct comparison of the codon frequency at the ribosomal A site between each variant and the overexpression of the tRNA^{Tyr}, was carried out by summing the codon occupancy of all transcripts for each species individually and presented as differential A-site codon occupancies. Cumulative plots were generated by selecting the intersection of stably translated genes between the samples in each comparison to ensure the same codon context. We centered the Tyr codons and expanded the selection 17 codons up and downstream of each Tyr codon. We excluded Tyr codons surrounded by additional Tyr, within the 36-codon

window, to avoid Tyr overrepresentation. P-values were calculated using the Mann-Whitney test calculated in R. The ribosome speed rescuing was calculated by comparing the increase or decrease of each variant with overexpression of tRNA^{Tyr} to their respective pair without tRNA^{Tyr} overexpression.

YARS purification and Tryptophan quenching assay

Purification of YARS variants and quenching assay were carried out as described in chapter 2. Pet-SUMO vector cloned to overexpress YARS WT, G41R, and E196K variants, and purified via affinity chromatography with Ni-NTA resin, followed by size exclusion chromatography on a *Superdex 200* column. Quenching assay was carried out as before with the same concentrations of YARS and in vitro tRNA^{Tyr}.

Generation of tRNA species through in vitro transcription

Generation of tRNA was carried out as previously described in Chapter 2. Primers used to in vitro synthesise tRNA^{Tyr} were as follows:

forward primer -

5'TAATACGACTCACTATACCTTCGATAGCTCAGTTGGTAGAGCGGTGGACTGTAGATCCAT'3 and reverse primer –

5'TGGTCCTTCGAGCCGGATTTGAACCAGCGACCTATGGATCTACAGTCCACCGCTC'3.

Electrophoretic shift assay

EMSA gel was carried out using in vitro transcribed tRNA^{Tyr} and purified YARS variants. tRNA was first folded by incubating tRNA in 450mM Tris-HCl(pH 7.5) buffer at 85°C for 3min. MgCl2 was added to final concentration of 200mM and incubated at 37°C for 30min. Protein(concentration indicated per sample) was incubated alongside 1μM tRNA in 250mM sodium acetate buffer (pH 5.2, 5mM MgCl2), 5mM DTT for 30min at 37°c. Samples were ran on 6% non-denaturing PAA gel initially for 30min at 350v, then overnight at 120v, 4°C. Gel stained with Sybr gold nucleic acid dye (ThermoFisher).

5 – Length dependent decrease of translation along neurites is exacerbated in cells expressing CMT-GARS variants

The smNPC cells used in this chapter were supplied by Andreas Hermann, Universität Rostock, Germany. He and the postdoc in the lab, Dr. Hannes Glaß, introduced me to the culturing and differentiation of the smNPCs into motor neuron cells.

5.1 - Introduction

Local translation at the distal ends of neurites, such as at the pre and post-synaptic ends in dendrites and axons respectively, is becoming increasingly understood to be vital in the maintenance and function of these specialised comparts of the neuronal cell [100], [101]. Importantly, the translation occurring in these distinct poles of the cell is measurably distinct from the translatome in the cell body, or somata of the neuronal cell. Distinct sets of genes are translated in these areas necessary for function, development, plasticity, transport, and more [224]. Even sets of ribosomal proteins are translated at the distal ends of neurites, to maintain dynamic exchange and repair of ribosomes situated at distinct sites of the neuronal cell [225]. As the neuron is a highly specialised cell with a unique structure that facilitates its function of passing along signals to other cells, this compartmentalised translation enhances the cells adaptability, and help overcomes logistical burdens of having to synthesis and then transport proteins down long stretches of the cell to get to sites where they are needed. Despite this necessary localised translation in the cell, the levels of translation happening in the distal ends of the neuron away from the somata, is not at a magnitude similar to the somata [226]. This seems to be due to the evidence that suggests that as you move distally away from the somata in the cell down to the distal regions, there exists a 'gradient' of translational machinery, with less ribosomes [101], translation factors [227], and even tRNA as the length of the neuron increases [228]. For the ribosomes, recent studies have shown that the neuropil compartment of mice hippocampal - the area of the hippocampus enriched in neurites – shown a significant lower quantifiable amount of 18S and 28S rRNA and ribosomal proteins in the neuropil, as well as fewer ribosomal proteins being actively translated [101], [225]. Neuronal cells have shown to have elongation and initiation factors

at dendrites as well as at post and pre-synapses, and typically these exists at a lower basal level than that of the somata, as would be logical for areas with lower amounts of relative translation [227], [229]. Though the neuron can adapt based on specific stimuli, with increased activity, or needs for growth, allowing the neuronal cell a degree of plasticity.

In regards to our findings with CMT in that GARS and YARS seem to sequester their cognate tRNA, reducing the available pools of tRNA in the cell; it could be possible that this is causing an aberrant effect on the local translation happening in the neuronal cells. The axonal dystrophy forms of CMT progresses in a length dependent manner, with the distal ends of neurons, such as at the neuromuscular junctions, dying first. This leads to a 'dying back' phenotype, with a continuous cycle of distal end death, and regrowth, with the neurons becoming progressively smaller, leading to loss of motor and sensory function in patients [230]. Why mutations in ubiquitously expressed enzymes, such as the aaRSs, would only target and cause defects in neuronal cells is not well understood, especially with no unifying mechanism found between all of the different disease-associated mutant forms of these enzymes. This length dependency then, seems critical in the progression and development of CMT in the neuronal cell, as no other cell type in the body would experience this extreme amount of polarisation. If this structure of the cell is the weak point that is targeted in the CMT context, then it could be that disruptions in local translation play a pivotal role in the development of this disease. tRNA sequestration by the CMT-aaRS then may cause specific aberrant effects in the local translation happening at the distal ends of the neuron, specifically by this sequestration having a disproportionate effect on the already limited tRNA pool in the distal neuron. To test this, SH-SY5Y cells - a neuroblastoma cell line - were differentiated into a neuron-like, branched phenotype [231]. The levels of translation occurring at different parts of the cell can be measured by a puromycin-integrated assay, an antibiotic that integrates into the peptidyl-transfer centre of the ribosome can becomes bound to the nascent chain peptide. This can be stained against with antibodies and relative translational activity can be measured [228].

5.2 - Results & Discussion

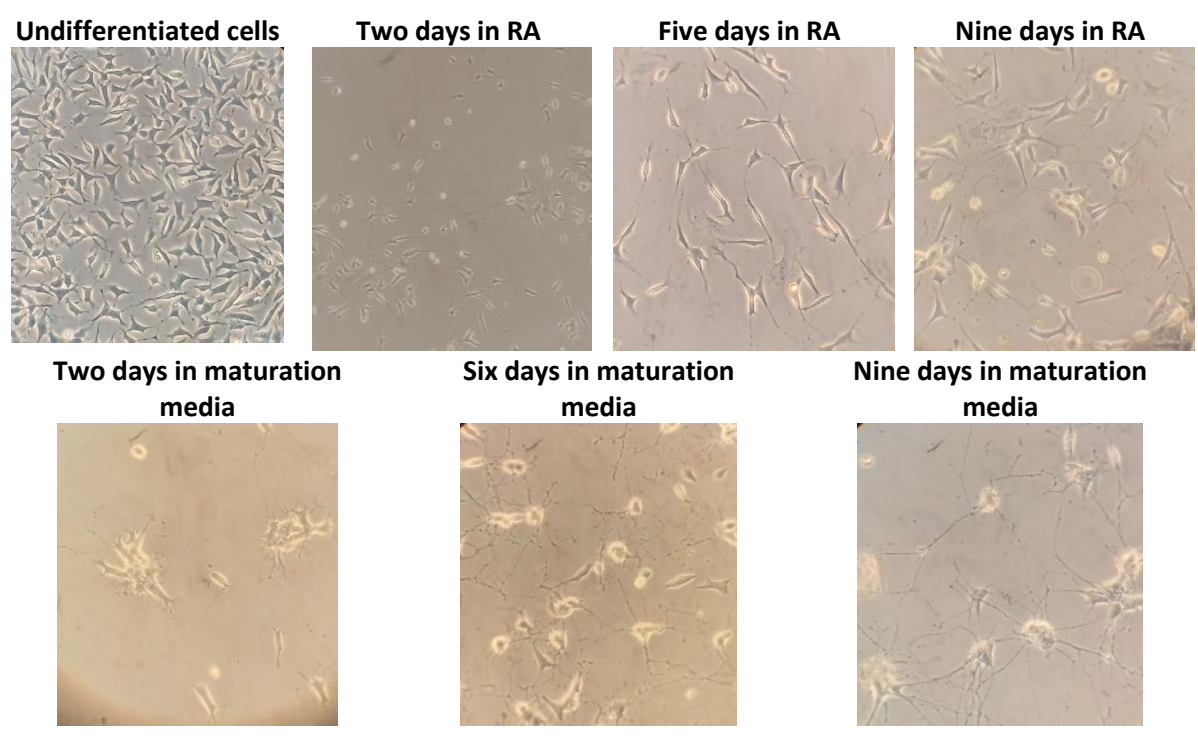


Figure 5.1 – Differentiation of SH-SY5Y cells into a branched, neuronal-like phenotype.

Utilising retinoic acid, and mild media starvation to prevent neuroblastoma cells from continually growing, the cells were differentiated and matured into a neuronal-like cell after 18 days. This procedure allows cells times to properly mature. Images acquired from a light microscope taken at 10x magnification. No scale bars shown.

SH-SY5Y cells were successfully differentiated into a distinct, branched phenotype resembling a mature neuronal cell (figure 5.1). The differentiated cells were transfected with either GARS wild type, or one of the CMT-GARS mutants and treated and stained against the integrated puromycin (figure 5.2a). Neurite tracing of the images after staining showed a decreasing trend of relative translation happening as the length of the neurite increases (figure 5.2b) consistent with our understanding that while local translation is indeed occurring at the distal ends, it is in a much lower quantity than the level of protein synthesis happening at the somata.

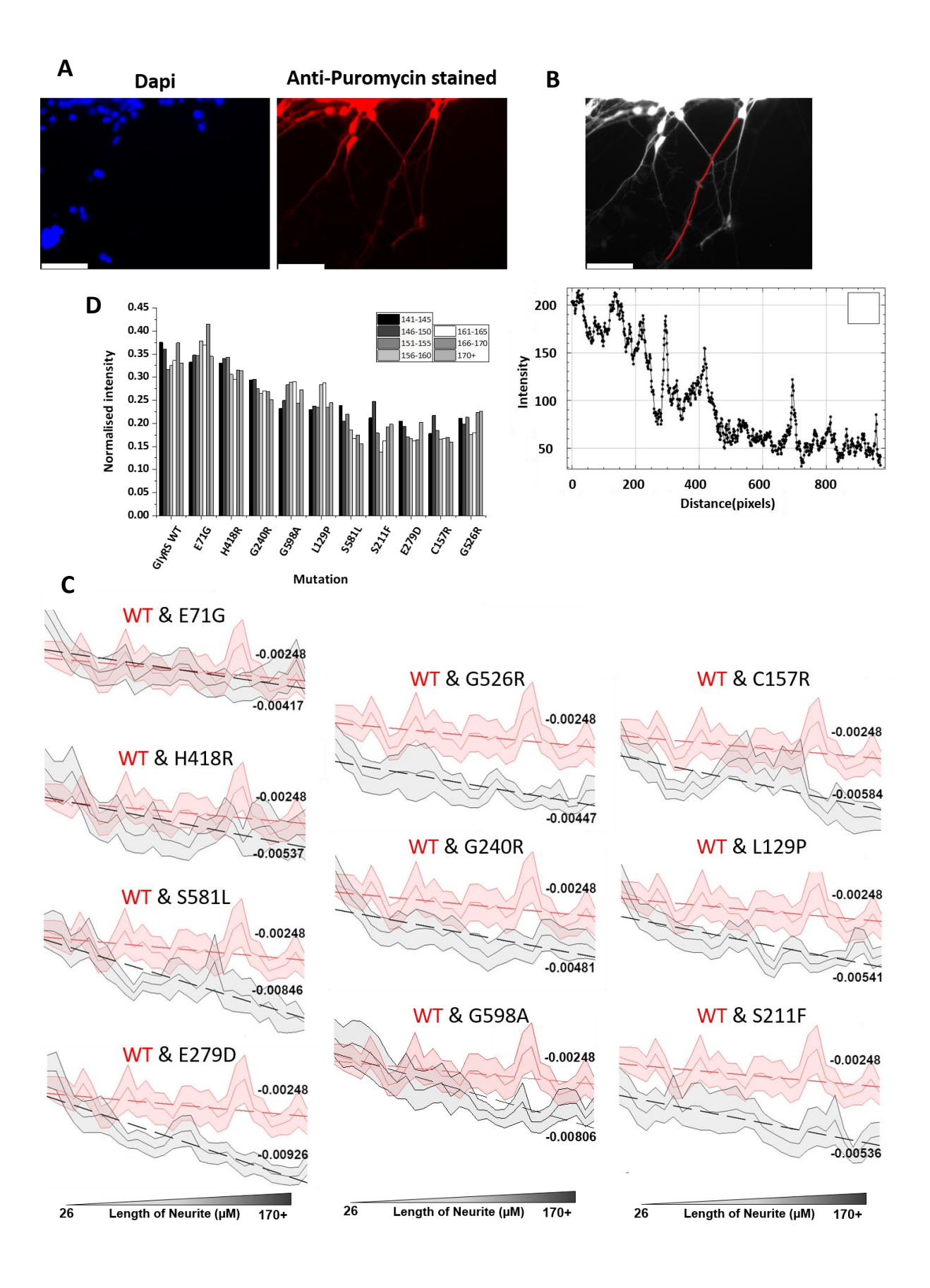


Figure 5.2 – Cells transfected with CMT-GARS variants showed a length-dependant decrease of translation.

(A) SH-SY5Y cells were differentiated, transfected with different GARS variants, treated with puromycin, and then stained with both Dapi for imaging the nucleus, and an anti-puromycin antibody. Images taken at a magnification of 40x. Scale bar = $44.1\mu m$. (B) Neurite tracing plugin for ImageJ was used to acquire intensity profiles. Images were selected based on a number of criteria: Clear beginning point, with the neurite extending from the somata of the cell, a low amount of other neurites crossing the measured neurite as this might obscure data and prevents knowing which direction measured neurite keeps extending towards. Finally, path of the neurites must not be crossing or overlaid with background fluorescence given off by either cell debris, or antibody that was not adequately washed away from plate. Neurites of a distance of 170μm+ were only chosen. Distance calculated by pixel length given from scale bar. (C) Averaged intensity profiles from n=10 images for each condition. Plots show SEM at each data point on graph. Intensity of each profile was background subtracted from three independent points taken, and then normalised against the first point of each profile, to give a relative fluorescence normalised against intensity given from somata of the cell. Linear regression plotted on each point, with slope of the line indicated on each plot. (D) Bar plot showing only the intensities from $141\mu M$ to $170\mu M+$, essentially showing only the distal ends of each plot.

When comparing all the CMT-GARS conditions against the GARS WT transfected, almost all variants showed a steeper decreasing trend of translation at the distal ends, with the slope of the curve showing a downward trend as the length of the neurite increases, all of which is more pronounced than wild type (figure 5.2c, d). The exception being E71G and H418R variants. E71G, as seen previously in our other experiments with GARS, consistently shows a more 'wild type-like' phenotype, consistent with its milder clinical outcome and slow progression in patients, which is also the case for H418R. This results then show a clear relation between the CMT-GARS and a disruption of the local translation happening at the distal end, possibly caused by the sequestration of tRNA^{Gly}. To see if this is happening in the cell body or the neurite itself, the distribution of the GARS variants was also tested by staining for the endogenous GARS or the transfected GARS variant via a 6xHis tag (figure 5.3). The WT

GARS seems to be fairly well distributed in the cell, with most if not all of the neurites stained with both the endogenous (anti-GARS) and the transfected (Anti-His). The mutant variants seem to show slightly different distribution patterns. E71G for example seems mostly localised at the cell body, while other mutants seem to be equally distributed, such as S211F and E279D. Interestingly, E71G and H418R show the greater tendency to localise to the cell body rather than the neurites; both variants which cause the least amount of translation defects in the distal end (figure 5.2d). As there is more protein synthesis happening in the cell bodies, and by extension more tRNA and other translational machinery, sequestration of tRNA in this compartment of the cell would not engender the strongest effect caused by a perturbation in the tRNA pool. However, if the CMT-GARS is distributed more evenly across the cell and towards the distal end, then the enzyme is free to bind and sequester tRNA in areas of the cell which would be more susceptible to decreasing quantities of tRNA available for local translation. This may explain the decreasing trend of translation happening in the distal ends as seen in figure 5.2c, d, a trend that depicts what could be a leading cause behind the development and progression of the disease in the neurons.

As has already been established in the previous chapters, addition of excess tRNA can help to reverse some of the phenotypes and severity of CMT in models. This is likely due to the reversal of translational defects caused by mutant forms of the aaRS. To this end, smNPC (small molecule neural progenitor cells), an iPSC derived neuronal stem cell [232], were differentiated into a motor neuron like phenotype, transfected with GARS variants, and then also transfected with equimolar concentrations of all tRNA^{Gly} species (CCC, GCC, TCC). smNPCs have the advantage over SH-SY5Y cells, as they are more similar to a primary cell, expressing the correct neuronal markers and phenotypes that a primary cell tissue type would also express, whereas SH-SY5Y cells spark controversy on whether proper dopaminergic markers are appropriately increased upon differentiation [233]. A sequencing experiment was also carried out on differentiated SH-SY5Y cells, grown on a transwell, cell plate inserts to allow separation between the somata and neurite compartment. While the cells do indeed differentiate into a branched phenotype, they don't seem to properly express motor neuronal markers, or properly localise well known axonal mRNA species such as Camklla (figure 5.4a, b).

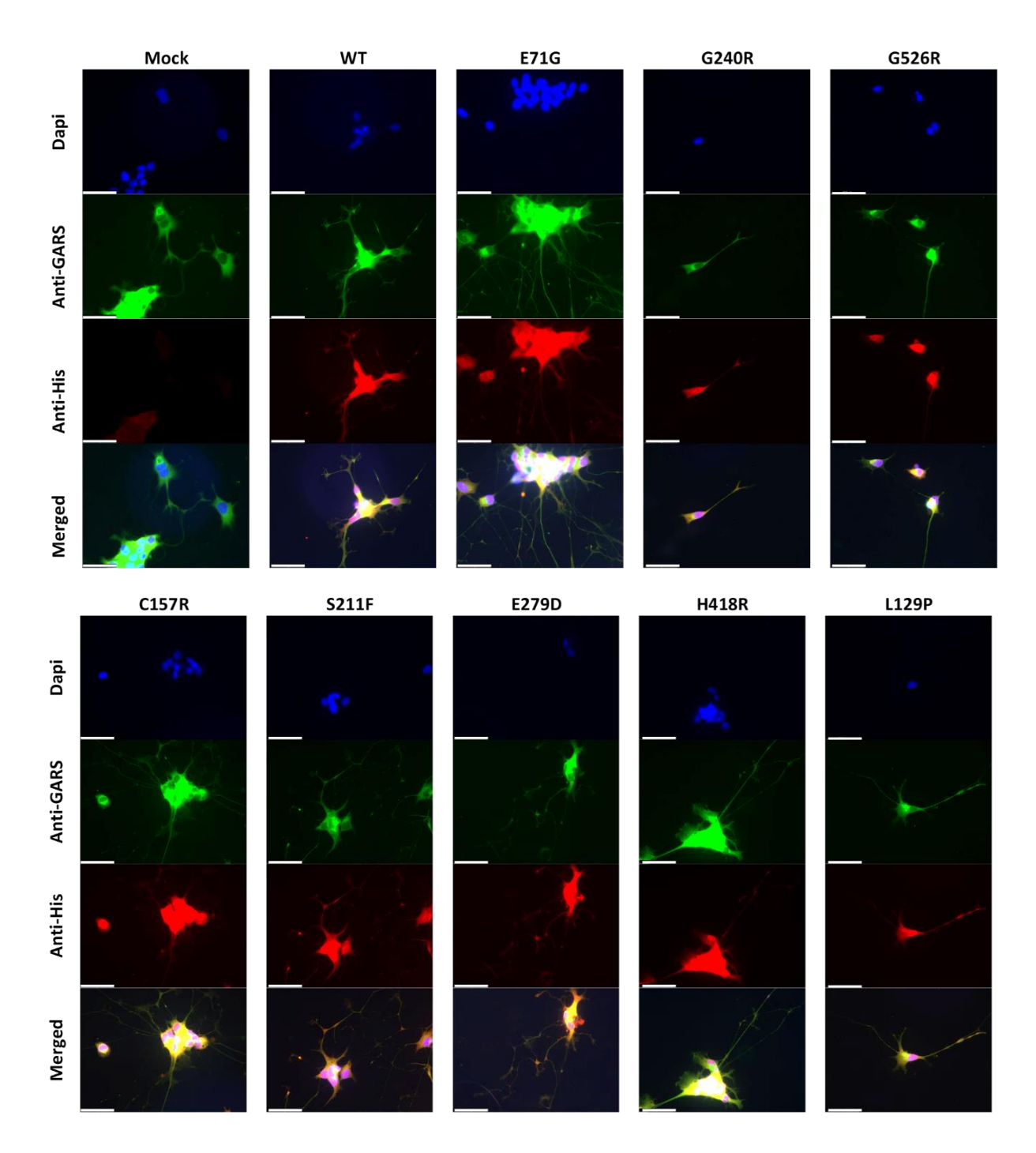


Figure 5.3 – CMT-GARS variants show different distribution pattern to WT GARS.

SH-SY5Y cells were differentiated and transfected with various constructs expressing different variants of GARS (indicated above images). After 48hr of expression, cells were stained with: anti-puromycin and anti-GARS antibody, as well as Dapi stain for nucleus imaging. Magnification set at 40x. Scale bar = 44.1μ m.

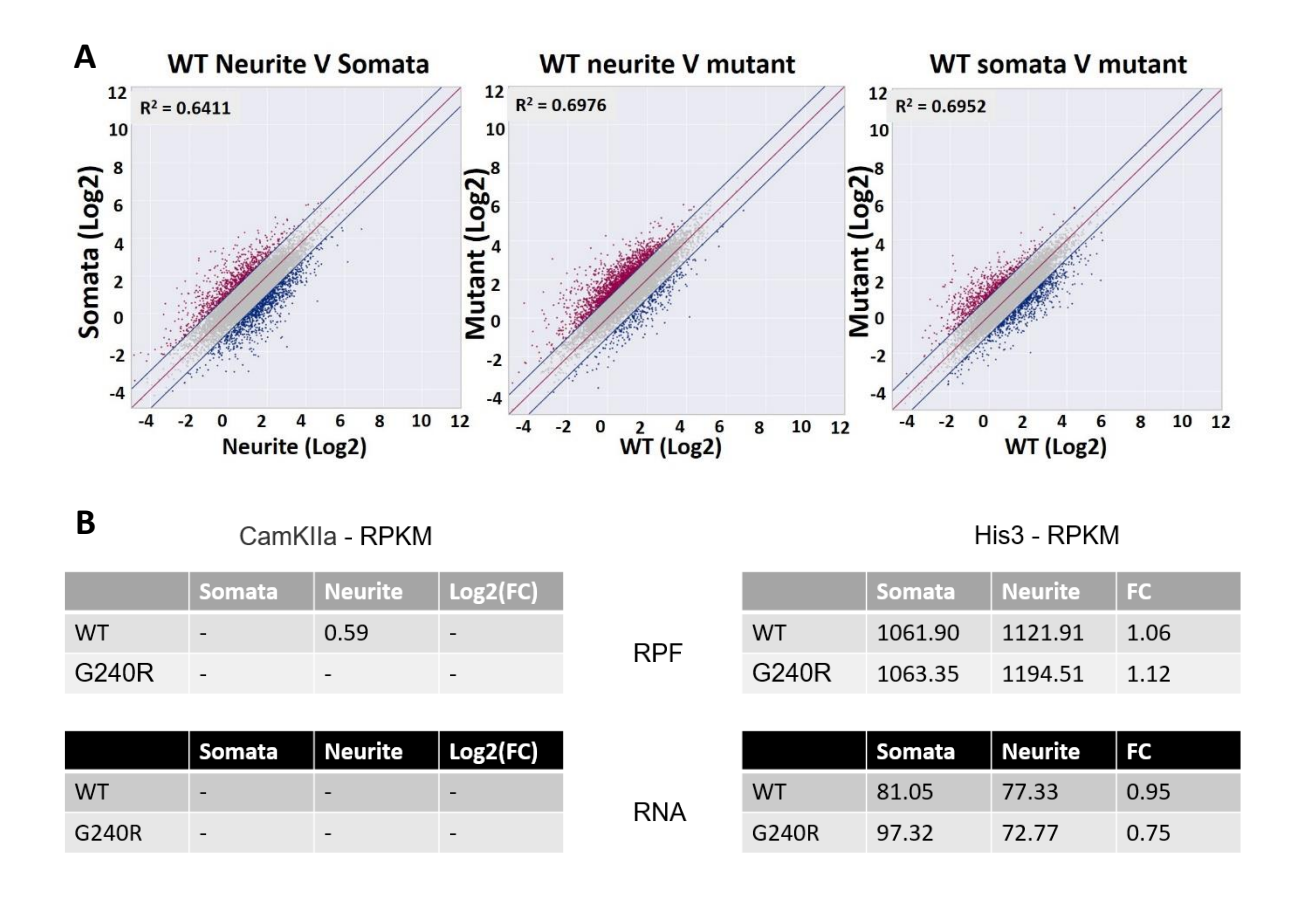


Figure 5.4 – Differentiated SH-SY5Y cells did not show a clear separation between somata and neurite compartments, or specific neuronal markers.

Sequencing data of differentiated SH-SY5Y cells, grown on a Transwell permeable cell membrane to allow for separation of somata and neurite fraction. Library preparation carried out as previously described in chapter 2. Two conditions were laid out, wild-type GARS transfected, and one transfected with a CMT-GARS variant. (A) Correlation graphs between different conditions and different compartments. Threshold set at value of 1 (blue line). Above (dark red) or below (dark blue) the line indicates overexpressing genes in either condition as donated by the axis. R² value shown in top left of graphs. (B) RPKM values for His3 and CamkIla in both samples, and in either RNA-seq or ribosome profiling data. Analysis carried out by Leonardo Santos.

Taken together then, the decision was made to swap to these smNPC cell lines to have a better representative model to test our hypothesis. After differentiation, smNPCs displayed a similar branched phenotype (figure 5.5a). Puromycin integration assay carried out on matured neurons also showed that in smNPCs a similar trend is seen in the cells not transfected with tRNA as seen in the SH-SY5Y (figure 5.5c, d), with decreasing translation

towards the distal end of the neuron. WT and E71G are still roughly equal as well, further showing the recapitulation of the trend. The effect is somewhat subtler in smNPCs, though this could simply be due to the fact that smNPCs, being a terminally differentiated motor neuronal cell, might be generally metabolically slower than that of SH-SY5Y cells. Cells with higher proliferation rates generally need to maintain higher levels of protein synthesis to meet demand [234], which a neuroblastoma cell-line such as SH-SY5Y would certainly meet that criteria. smNPC cells were also co-transfected with tRNA^{Gly}, though initially a trial transfection was carried out with fluorescently labelled tRNA to ensure tRNA can be efficiently transfected into the matured smNPC cells (figure 5.5b). With confirmation of tRNA transfectability into these cells, tRNAGly was then transfected into mature smNPCs, of all three codons (GCC, CCC, TCC). With the addition of the tRNA, overall translation in the cells was vastly improved (figure 5.5d), with some mutant conditions showing an almost doubling of relative translation levels. While many mutants show an increased translation levels with the addition of excess tRNA^{Gly}, the levels of improvement varied. L129P and E71G showed the greatest increase amount the mutant variants, along the lines of the increase seen in the WT. However, G240R showed only a limited increase, while E279D showed no improvement. Of the mutants tested here, L129P and G240R have been shown to suffer aminoacylation loss in vitro [188], however for G240R this is not recapitulated completely in a Drosophila model [189] with G240R only showing a reduction as compared to WT, and I have seen no evidence that L129P has yet been tested in a proper in vivo model [235]. E279D has also yet to be tested in either an in vitro, or *In vivo* model. In could be possible that E279D has a complete loss of aminoacylation activity, since as we have seen in our data, this mutant consistently performs among the worst of the CMT-GARS variants, with higher amounts of translation reduction at the distal neurons, and increased holding rates of tRNA in our kinetic assays. While enzymatic activity is not a good indicator for disease onset, it could potentially be a limiting factor in how effective tRNA is in rescuing the effects the mutant incurs on the cell. The G41R mutant in our YARS data also behaves similar to this, where in that scenario the enzyme is enzymatically inactive, so it would require a much greater amount of tRNA to overcome the effect. Here it could be the same, as if E279D is inactive, it would require a larger amount of tRNA to compensate for the sequestration effect, allowing the endogenous, unmutated GARS to charge more tRNA to increase the available amount in the tRNA pool.

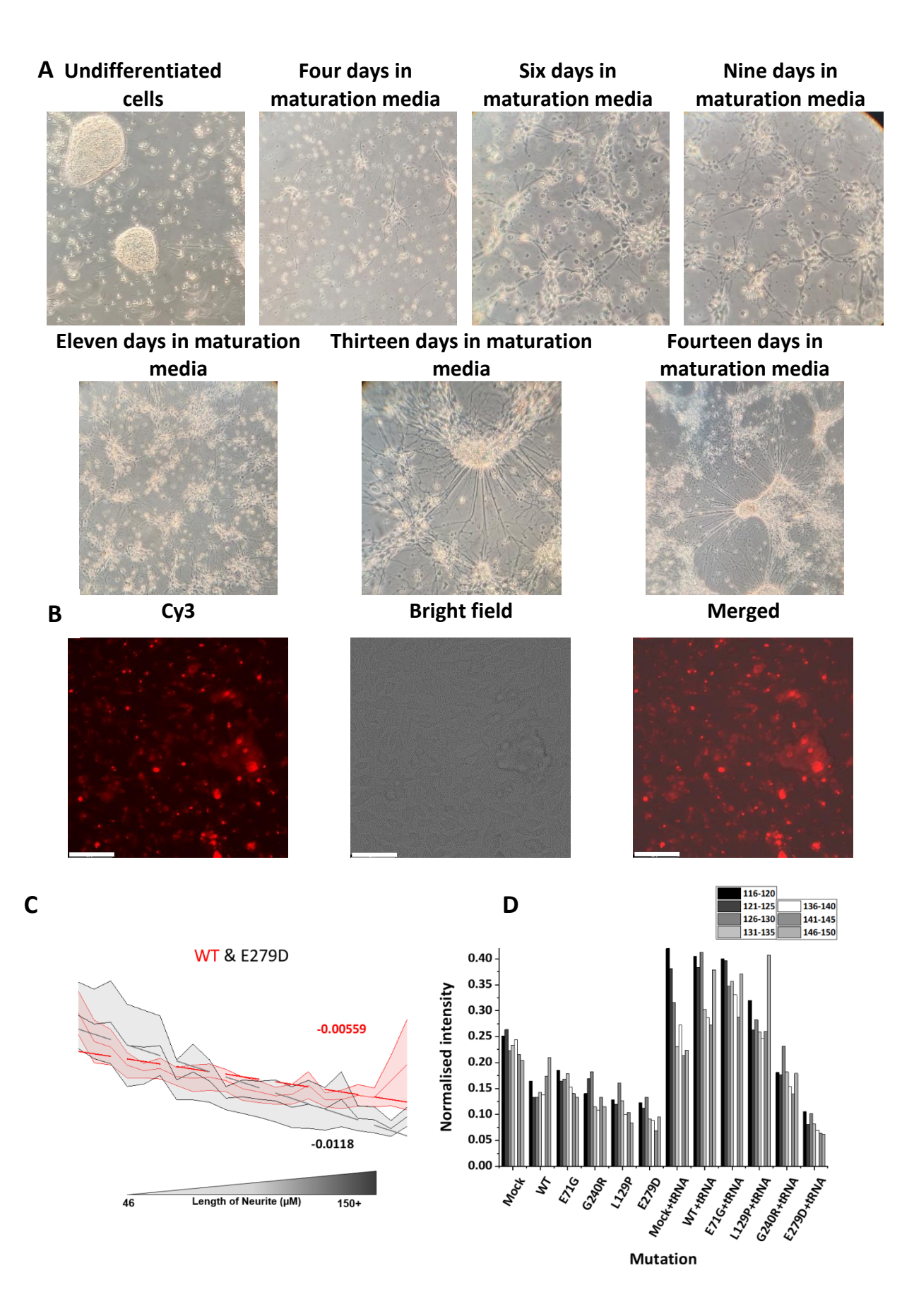


Figure 5.5 – smNPCs were successfully differentiated into a branched phenotype, and showed a length-dependant decrease of translation in neurites, rescued by tRNA.

(A) Differentiation of smNPC into peripheral motor neurons. Downstream experiments carried out on cells after fourteen days in maturation media, once the cells have formed a dense, neuronal network. Images acquired from a light microscope at different magnifications. No scale bar shown. (B) Transfection of SH-SY5Y cells with Fuse-It-mRNA (see materials and methods) kit with fluorescently labelled tRNA with Cy3 bound oligo. Magnification set at 20x. Scale bar = 66.4µm. (C, D) smNPC cells were differentiated into motor neuronal cells. Puromycin integration assay carried out as described previously for SH-SY5Y cells. Cells were stained against puromycin, and neurite tracing was carried out as before. Independent samples were also co-transfected with equimolar concentrations of tRNA-Gly for all three anticodons (GCC, TCC, CCC) at concentration of 250nM each. Cells were treated with puromycin 48hr post-transfection. Neurite profiles were analysed as described above.

5.3 - Conclusion

Length dependent degradation of motor and sensory neurons begins at the distal end of the neurons, causing a slow 'dying back' and receding from neuromuscular junctions [230]. Here, I show that there is a reduction of transitional rate in a neuronal cell, in a length-dependent manner. In other words, translation is lower in the neuronal cell the further you move away from the somata. While this is to be somewhat expected, as there is a 'gradient' of translational machinery down the neurite track, the effect is more pronounced in cells expressing CMT-GARS variants. The sequestration of tRNA by the mutant GARS could then be having an aberrant effect on the distal translation. While there currently is little evidence for how tRNA is transported around the neuronal cell, tRNA can move bi-directionally in both antegrade and retrograde directions [228], with demonstratable slower motility inside the dendritic and neurite processes. This slower motility may make it more difficult to maintain adequate levels in areas of high translational load, and when perturbed, could have a drastic effect on translational levels in the cell. GARS also seems to be distributed throughout the entire neuron as well (fig 5.3). Together, this could mean that CMT-GARS can bind and sequester tRNA at the distal ends of neurons for longer stretches of time. This perturbation of an already low number of tRNA could have a more pronounced effect on translation in the

distal areas, which is exactly what my data shows. Some of the GARS variants showed a much more pronounced reduction than others, with some of the most severe forms of the diseases showing the strongest trend downwards, and vice versa with the milder forms also being closer to the wild type, such as E71G. Both age of onset for CMT2D and disease severity correlate fairly well with our data and how the earliest onset and more severe forms of the disease show the lowest levels of translation at the distal end [125], [236], demonstrating fairly clearly that this length dependent aberrant translation, seems to play a large role in the disease development.

5.4 - Materials and Methods

<u>Differentiation of neuroblastoma cell line, SH-SY5Y into branched neuronal-like phenotype</u>

Differentiation: Protocol used from Shipley et al, 2016, with minor alterations [237]. SH-SY5Y cells (passage number between 10-15) were split onto fresh plates in differentiation media #1 [EMEM media, 2.5% heat-inactivated FBS (ThermoFisher), 2mM L-glutamine, 1% Pen/Strep, 5μM all-trans RA (Sigma)]. Cells grown for seven days, changing media to fresh diff media #1 every other day. On seventh day, cells were split 1:1 with 0.025% trypsin-EDTA onto new plate. A day later, media was changed to differentiation media #2 [EMEM, 1% heat-inactivated FBS, 1% Pen/Strep, 2mM L-glutamine, 5μM RA] and cultured for 3 days.

Plate coating: ECM coated plates were prepared by incubating coating media [F12 media, human fibronectin (Sigma, 1:1000 dilution), 0.3mg/mL collagen (Corning), 1% BSA, 1% Pen/Strep] on plates at 37°C overnight (For microscopy studies, glass slide was added into the plate and also coated. For separation of somata and neurite fractions, 75 mm Transwell permeable support (Corning) was coated). Media was aspirated off in the morning and left to dry for ~30min before adding cells.

Maturation: Cells were split again in trypsin-EDTA 1:1 onto coated plates in diff media #2. The next day, media was changed to differentiation media #3 [Neurobasal plus media (ThermoFisher), 1% B-27 supplement (ThermoFisher), 20mM KCl, 2mM GlutaMax (ThermoFisher), 50ng/mL BDNF (BioZol), 10ng/mL NGF- β (ProspecBio), 1mM Db-cAMP (Santa Cruz Bio Technology), and 5μM RA]. Cells were cultured for 8 days, changing the media for fresh diff media #3 every other day. Cells then ready for downstream experiments. For

transfection of cells with pcDNA construct containing GARS variants, Lipofectamine 2000 (ThermoFisher) was used, following manufacturers protocol with no changes.

Puromycin integration and immunocytochemical staining of cells

Protocol used from Koltun, et al, 2020 with minor alterations [228]. After cells were fully differentiated, they were incubated with $1\mu g/mL$ puromycin (StemCell Technologies) for 10min at 37°C. Cells washed with 1x PBS and then fixed in a 4% paraformaldehyde solution in PBS for 10min at room temperature. PFA aspirated and cells washed once in PBS and stored in PBS until subsequent ICC staining.

Cells were first permeabilised with 1% Triton X-100 in PBS (PBS-T) for 5 mins shaking. This was repeated three times. Blocking buffer [10% FBS, 0.3% BSA, 1% Triton X-100, in PBS] added to cells and incubated shaking for 1hr at room temperature. Primary antibodies in fresh blocking buffer was added to the cells and incubated overnight at 4° C, shaking. Cells were washed three times in PBS-T, and incubated with secondary antibody in PBS-T for 1hr at room temperature. Cells washed three more times in PBS-T, twice in only PBS. DAPI stain at a concentration of 1µg/mL in PBS was added to the cells and incubated for 1min. Cells washed twice more with PBS and mounted onto glass slides for microscopy.

Antibodies used in this study were:

Primary: Anti-puromycin 1:10000 (Merck, MABE343), Anti-GARS 1:1000 (Abcam, ab42905), Anti-His 1:1000 (Abcam, ab18184).

Secondary: Donkey anti-mouse alexa fluor 568 IgG 1:500 (ThermoFisher), Goat Anti-Rabbit alexa fluor 488 IgG 1:500 (ThermoFisher).

The plasmids used to transfect the cells used in this chapter were provided by Prof. Dr. E Storkebaum, Radboud Universiteit. All GARS variants used in this section were mutated from this original plasmid, as previously described (Chapter 3).

Imaging of neuronal cells and single neurite tracing

Images were acquired on a *Leica fluorescent microscope*, at 40x magnification or 20x, depending on the experiment (detailed in figure legend). At 40x magnification, 1 pixel = 167.7nm.

After image acquisition, for measurement of translation in neuron, the *ImageJ* plugin 'Simple Neurite Trace' was used. Images were first grey-scaled, and intensity profile of anti-puromycin

channel was taken by tracing the neurite from the beginning of the neurite (where it pinches off from the somata) to the distal end. Measurements given in pixel colour intensity at individual pixel distance along neurite. Blank measurements were also taken for each image and subtracted from the total intensity of the neurite profile. Distance bins were made (e.g, 141-150µm) for ease of comparison by averaging intensity between these regions of the profile data. Averaged intensity was normalised to very first reading of the neurite for each individual image, indicating the maximum fluorescence of the cell closest to the somata. Intensities across all images of a single condition were averaged between the distance bins and SEM was also calculated.

<u>Differentiation of small molecule neural progenitor cells into mature neurons</u>

smNPC cells were supplied by Prof. Dr. Andreas Hermann, Universität Rostock, Germany. Cells were differentiated following the protocol from Reinhardt, *et al*, 2013 [232] with minor alterations.

Expansion: Cells were expanded and maintained in expansion media [50% DMEM/F12, 50% Neurobasal plus, 1:200 N2 supplement (ThermoFisher), 1:100 B27 supplement without vitamin A (ThermoFisher), 1% Pen/Strep, 1% L-glutamine, 150μM ascorbic acid (AA), 0.5μM purmorphamine (PMA, StemCell), 3μM CHIR99021 (CHIR, StemCell)] changing media every other day with fresh expansion media. Cells always cultured on poly-laminin coated plates. Cells were split 1:2 or 1:3 every ten days. Cells were split with pre-warmed Accutase (ThermoFisher) for 15min at 37°C. Cells were pelleted at 300g for 5min.

Plate coating: Poly-laminin coating [5g/mL laminin (Sigma), 10μg/mL poly-l-ornithine (Thermofisher), 1% Pen-Strep]. Was made up in PBS. Coating mix was added to plates at a concentration of 0.2-0.5μg laminin per cm². Plates were sealed with parafilm and left overnight at 4°C. The next day, coating was aspirated from the plate and dried for 15min before plating cells.

Differentiation and maturation into motor neurons: Cells split onto freshly coated plates. Three days later, media was changed to differentiation media [50% DMEM/F12, 50% Neurobasal plus, 1:200 N2 supplement (ThermoFisher), 1:100 B27 supplement without vitamin A (ThermoFisher), 1% Pen/Strep, 1% L-glutamine, 1 μ M PMA]. Two days later, fresh differentiation media was added to the cells, supplemented with 1 μ M RA. Media changed every other day for eight days, with freshly supplemented RA. On the ninth day, media

changed to maturation media [50% DMEM/F12, 50% Neurobasal plus, 1:200 N2 supplement (ThermoFisher), 1:100 B27 supplement without vitamin A (ThermoFisher), 1% Pen/Strep, 1% L-glutamine, 10ng/mL BDNF (BioZol), 10ng/mL GDNF (PeproTech), 10ng/mL NGF- β (ProspecBio), 500 μ M Db-cAMP (Santa Cruz Bio Technology)]. Following one day in maturation media, cells were split, counted, and split onto final plate. For imaging analysis, 6-well plates were coated with a glass slide in each well, with 250,000 cells per well. Cells were cultured in maturation media for fourteen more days, changing the media every other day.

Fuse-It-mRNA and DNA transfections

For transfecting smNPCs with pcDNA carrying GARS variants and different species of tRNA^{Gly}, Fuse-It-DNA and Fuse-It-mRNA kits were used (Beniag) following manufacturers protocol. For transfecting plasmids into the cell, 5µg was used per well of a 6-well plate. For tRNA transfection, 750ng of tRNA^{Gly} was used which consisted of a mix of three tRNAs in equimolar concentrations: tRNA^{Gly-GCC}, tRNA^{Gly-TCC}, tRNA^{Gly-CCC}. Cells that were transfected with both DNA and tRNA, the DNA transfection was carried out first. The cells left to recover for 4 hours after transfection, and then tRNA was transfected in. Downstream experiments carried out 48hr post-transfection.

Generation of tRNA species through in vitro transcription

Generation of tRNA was carried out as previously described in Chapter 2. Primers used in generation of tRNA^{Gly} species were as follows:

GCC:

Forward: 5' TAATACGACTCACTATAGCATGGGTGATTCAGTGGTAGAATTTTCACCTGCCATG '3

Reverse: 5' TGGTGCATAGGCCAGGAAATGAACCTGGACCTCCTGCATGGCAGGTGAAAATTCTA '3

TCC

Forward: 5' TAATACGACTCACTATAGCGTTGGTGGTATAGTGGTTAGCATAGCTGCCCTC '3

Reverse: 5' TGGTGCGTTGGCCGGGAATCGAACCCGGGTCAACTGCTTGGAAGGCAGCTATGC '3

CCC

Forward: 5' TAATACGACTCACTATAGCATTGGTGGTTCAGTGGTAGAATTCTCGCC '3

Reverse. 5' TGGTGCATTGGCCGGGAATTGAACCCGGGTCTCCCGCGTGGGAGGCGAGAATTCTAC

'3

6 – C9*Orf72*ALS-associated G₄C₂ repeat regions caused ribosomal queuing behind start codon

This work was carried out in collaboration with Prof. Dr. Ya-Ming Hou and members of her group at the Thomas Jefferson University, USA. I preformed ribosome profiling with different constructs provided as plasmids by the group of Dr How. After transformation of the plasmids in SH-SY5Y cells I performed ribosome profiling (or Ribo-seq). Data analysis of the Ribo-seq were performed by Leonardo Santos, a PhD candidate in our group.

6.1 - Introduction

Repeat-associated non-AUG (RAN) translation occurs on the C9orf72 gene, leading to the translation of dipeptide repeat proteins (DRPs) [145]. Translation occurs in all three frames when the ribosome initiates at the non-canonical start codon on this repeat region, leading to the translation of Poly-Glycine-Alanine (PolyGA), Poly-Glycine-Proline (polyGP), and Poly-Glycine-Arginine (PolyGR) leading to cytotoxicity inside cells [132]. For this to occur, the ribosome must shift its frame of translation beginning at the non-canonical start. Highlighting this, recent data has heavily implicated the ribosomal protein RPS25 in the mechanism of IRES entry and initiation for RAN translation to occur, and knocking down this protein drastically reduced Poly-GA and Poly-GR protein production in other frames of repeats [238]. Showing quite specifically that RAN translation is indeed what leads to the production of DPRs from multiple frames on the C9Orf72 mRNA. How this frameshifting occurs in the context of the C9Orf72 gene is not understood. One potential possibility could be that collisions are occurring on the transcript between the Pre-initiation complexes (PiCs) and allowing the ribosome to be 'pushed' into different frames. Ribosomal collisions have been reported to induce frameshifting on the ribosome, if the quality control pathway has not been properly engaged to deal with the aberrant stalls [239]. Also, initiation at these non-canonical codons (CUG) has also been shown to be much more inefficient and slower than at the canonical AUG [240], taking longer for the ribosome to be fully engaged and shifted into its elongation phase. As there is evidence that the repeat region also acts as an IRES [141], there could potentially be a scenario then that the 40S ribosome is recruited directly to the RAN site, wherein it slowly begins initiation to translate the repeat region, producing DPRs. At the same time, a more

'canonical' cap-dependent initiation event could have occurred, sending a PiC scanning along the mRNA. These two ribosomes could collide, or lead to 'queuing' of the ribosomes, and force the ribosomes into different frames on the transcript, allowing production of the multiple DPRs from different reading frames on the repeat region. Either way, the production of these DPRs is heavily implicated in cellular toxicity and the progression of neurodegenerative diseases, and has even been implicated in the development of other types of neurodegenerative diseases, such as Huntington's diseases [174]. This demonstrates that understanding how these DPRs are produced, and how frameshifting occurs to produce the whole array of DPRs available, is necessary to fully understand the mechanism of this disease. To test for this frameshifting, SH-SY5Y cells were transfected with different constructs, either with a canonical AUG start codon, or in its place a RAN associated CUG codon, or AGG. On the endogenous C9Orf72 mRNA transcript, a CUG non-canonical codon is within an ideal kozak sequence in position -24nt relative to the repeat and seems to be the major factor in triggering RAN translation [145], whereas the AGG is at position -15nt and not in a kozak sequence. This AGG, while playing some role in RAN translation of the repeats as a nearcognate initiation codon [241], [242], does not seem to play as important a role as the CUG [154] allowing it to be used as an ideal negative control. Ribosome profiling libraries can be used in this scenario to see exactly where the ribosomes are translating, where the frame of translation can also be determined. This will inform us whether the frame of translation is being altered more acutely on the constructs with the non-canonical start codons, and if we can detect queuing or collisions of PiCs behind the start codon. Two other conditions were also used: the addition of extra Met-tRNAi^{Met} to the cells, and also treating the cells with harringtonine. Addition of excess, charged Met-tRNAi^{Met} to the cells may increase the formation of PiCs as it is needed in the formation of the ternary complex at the beginning of initiation [9]. Harringtonine is widely used to stall ribosomes in initiation at the start codon, preventing the ribosome from transitioning into the elongation phase [243]. Both of these conditions should increase the ribosome coverage at the start codon and upstream of it, allowing us to get a better understanding of how the scanning and initiation ribosomes are behaving in the context of C90rf72ALS.

6.2 - Results and Discussion

Single-ended, ribosome profiling libraries from all conditions were generated. Harringtonine treatment successfully resulted in stalling of ribosomes at the start codon across the entire coding sequence in all samples (figure 6.1b, 6.1c), seen by accumulation of reads at start codon, depletion of reads across the coding sequence, and primarily a shortened read length. Reads were mapped to the construct and then calibrated to their 5' most nucleotide on each individual read (figure 6.1d) providing a clearer visualisation of accumulation of reads at individual points on the construct, such as at or upstream of the start codon, or at and near the G_4C_2 repeat region. For the AUG -tRNA-Harr condition (AUG denoting start codon identity; "-tRNA" for whether tRNAi^{Met} was co-transfected into the cells, and "-harr" for whether harringtonine was used), we see a good coverage of the plasmid, with reads mapping to the entire length of the sequence, both upstream and downstream of the start codon. This was to be expected, as AUG is the canonical start codon and should allow for proper initiation and elongation to occur on the sequence. However, when the constructs contain either a CUG or AGG start codon at the same position, the amount of reads across the construct decreases. Both CUG and AGG, while they can be used for RAN translation, are both inefficient initiation sites for the ribosome in comparison to AUG. This may reduce the number of mappable reads to the construct as the majority of ribosomes simply scan past the CUG/AGG codon, fail to initiate, and then fall off the construct, preventing us from capturing it on the sequence when carrying out ribosome profiling.

Reads on the construct were also calibrated to the 5' most nucleotide and mapped to the upstream region of each construct (figure 6.2). In this analysis, we can see whether there are clusters of reads occurring in the upstream region of the start codon. Different clusters would indicate different things, such as reads immediately upstream of the start codon - from the start to -30 nucleotide position - would indicate reads associated with ribosomes initiating at the start codon.

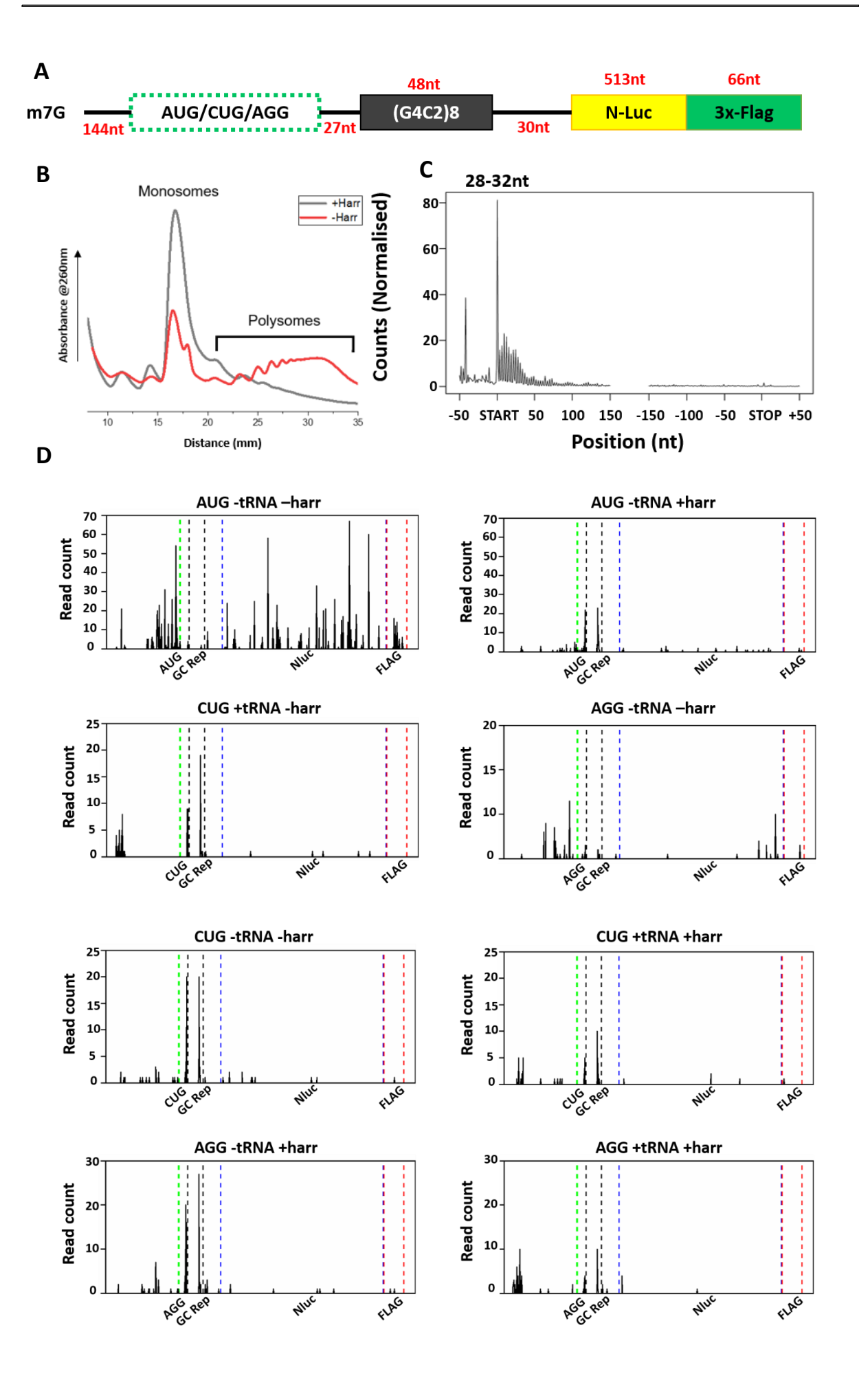


Figure 6.1 – Reads from ribosome profiling were successfully mapped to constructs, with notable accumulation at G_4C_2 repeat regions.

(A) Plasmid construct with the alternate start codon position highlighted, as well as the length of G_4C_2 repeat region. (B) Polysome profile of sample treated with or without harringtonine, showing the effect harringtonine has on reducing polysomes and enriching monosome fraction. (C) Coverage plot from sequencing reads from sample treated with harringtonine. Start codon and stop codon positions shown. (D) Reads from sequencing libraries were mapped to the transfected construct, then calibrated to their 5' most nucleotide. Read count was plotted across the entire sequence of the construct. Green dotted line indicates the start codon of the plasmid, and the black dotted line is the GC-repeat region just downstream of the start codon.

Reads between positions -90 and -60 may indicate PiCs that are scanning towards the start codon and possibly queued, or stalled behind the initiating ribosome. And reads at the beginning of the sequence, around position -170, are PiCs that have just touched down on the sequence and are, or will begin to scan along the transcript. Noticeable clusters of reads upstream of the start codon are seen in some constructs (figure 6.2). Sequences which were co-transfected with additional Met-tRNA^{Met} (CUG +tRNA -harr, CUG +tRNA +harr, and AGG +tRNA +harr) all show an increased clustering at the furthest upstream position, around -170 nucleotides from the start codon. This shows that the addition of excess initiation-tRNA does help to enhance formation of PiCs, though this increased number of scanning complexes does not seem to translate into an increased quantity of initiating ribosomes, further highlighting the inefficient initiation of the CUG and AGG codons. The addition of harringtonine was effective in enriching ribosomes at the start sites while depleting elongating ribosomes across the entire transcriptome of the cells (figure 6.1c and figure 6.3a, b), but it did not lead to an enrichment of initiating ribosomes at the start site on this construct at either CUG, AGG, or even AUG.

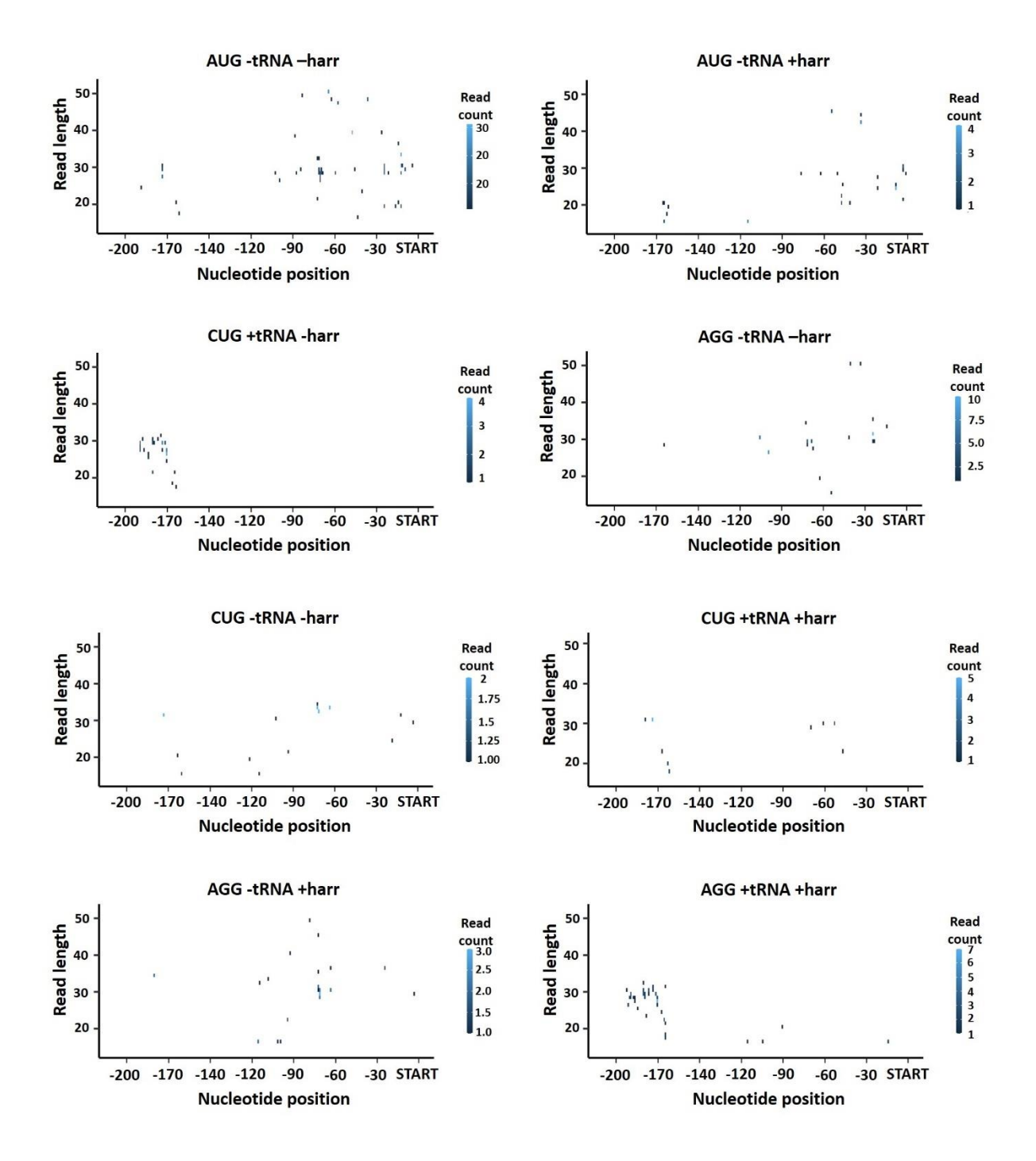


Figure 6.2 – Read clusters show possible accumulation of ribosomes behind the start codon, and at the beginning of the transcript.

Reads from all samples were plotted upstream of the alternate start codon on each plasmid (designated on each graph). Positions are shown as -nt relative to the start codon, and read lengths of each individual mapped reads are also indicated. Nucleotide positions around -30nt would indicate a ribosome initiating at the start codon if read length is between 20-30nt. Increased read lengths further upstream of the start codon might be an indicator for queued or collided ribosomes on sequence.

In a number of the samples there are peaks of the read counts at the beginning and end of the GC-repeat regions. This may be indicative of stalling at the GC region, as these repeat regions are prone to forming G-quadruplex structures that will stall ribosomes as they are unable to bypass the highly structured region. However, sequencing of highly repetitive regions is difficult, as reads that map to multiple sequences, be them on the transcript of interest or elsewhere, are generally discounted as it is impossible to know exactly where the read originally comes from. The fact that these read peaks are only at the beginning and end of the GC-repeat region is a cause of this, as the flanking regions around the GC-repeat will give unique reads that won't multimap to multiple sites in the genome. This makes it difficult to ascertain whether these are indicative of stalling ribosomes, or simply an artefact in the sequencing data. DPR products also activate the ISR response in cells through their aggregation of necessary factors. It could also simply be a limitation of these procedure that the cells become stressed once DPR production is increased, which shuts down the level of protein synthesis and the number of ribosomes on mRNA transcripts [242]. This build-up of DPRs, which in turn misfold and cause ISR activation, could be a general feature of C9-ALS phenotypic development in neuronal cells.

Reads in each library were also positioned to the P site - possible due to the fact that libraries were generated from ribosomal protected fragments (RPFs) — and then mapped to both the entire transcriptome as well as the construct in each condition (figure 6.4). The positioning can then inform us of which frame each individual read was in, allowing comparison between different genes inside the same condition. Comparing the transcriptome to the construct frames can inform us on whether there is a deviation of the frames on the construct as compared to the entire transcriptome inside the same sample, as the frame distribution inside the transcriptome would be what the cells endogenously exist and express. As seen in the data here, most of the conditions had a similar distribution of frames between the construct and the transcriptome.

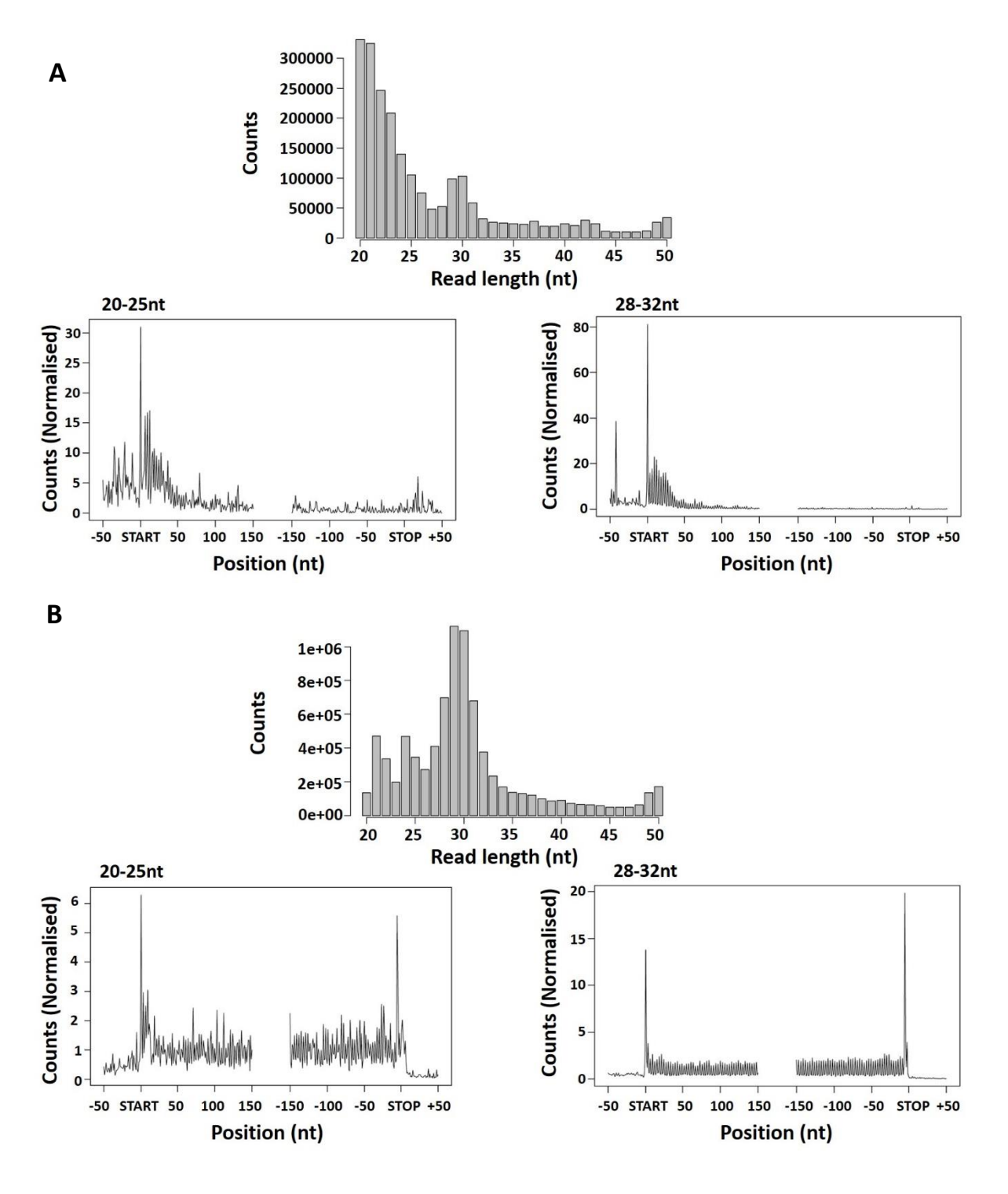


Figure 6.3 – Harringtonine treatment successfully depleted elongation ribosomes and accumulated reads at start codons across transcriptome.

(A) Reads mapped to the entire human transcriptome and calibrated to the P site (20-25nt and 28-32nt) for AUG -tRNA +harringtonine. (B) Reads mapped to the entire human transcriptome and calibrated to the P site (20-25nt and 28-32nt) for AUG -tRNA – harringtonine.

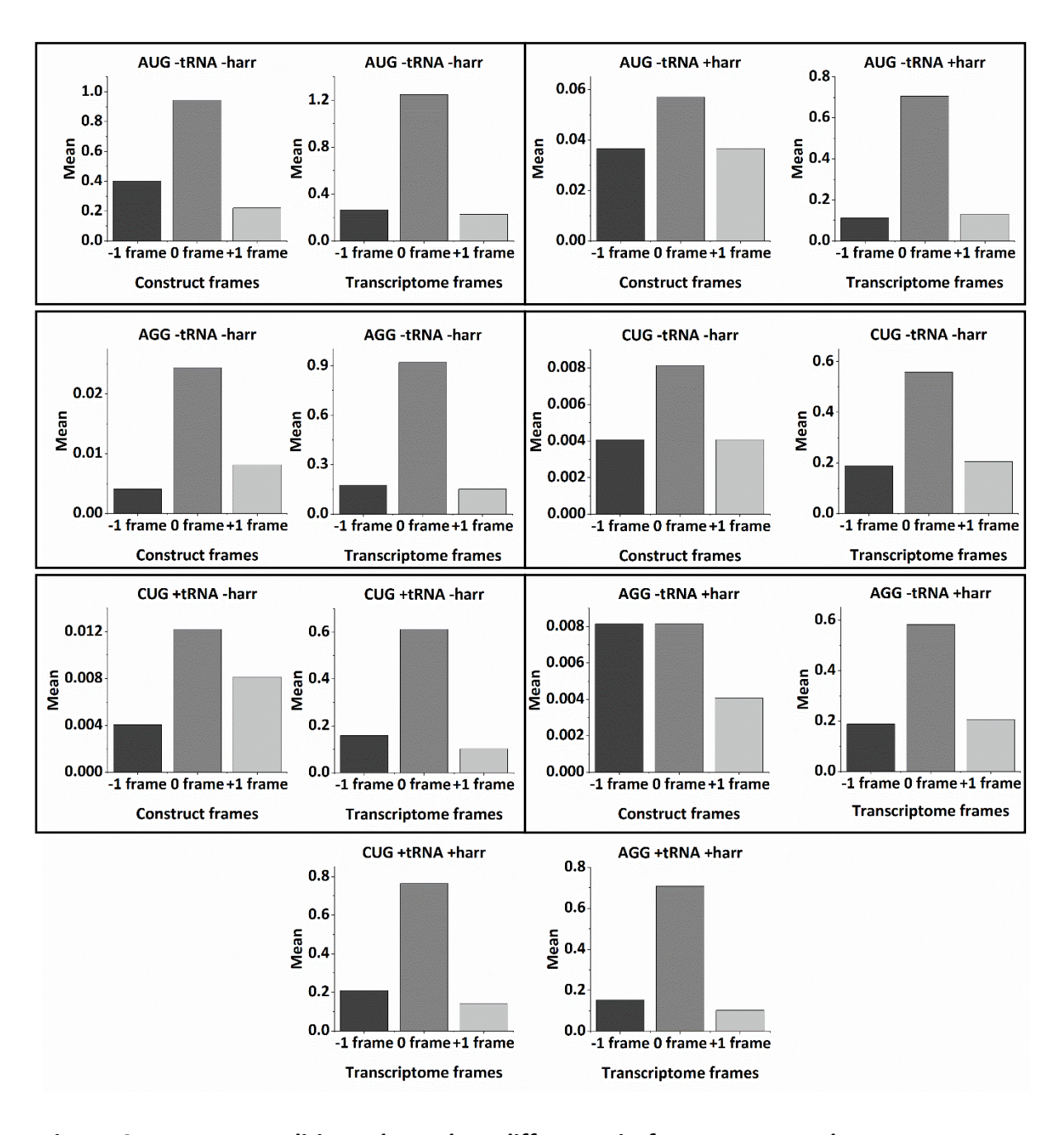


Figure 6.4 – Most conditions showed no difference in frame coverage between construct and transcriptome in samples.

Frameshift analysis of all conditions. Reads were computed to the P site, and then the abundance of reads in each frame (-1, 0, and +1) on either the entire transcriptome or specifically on the construct were taken. For the transcriptome frames, the mean of frames across all genes from the sequencing libraries was taken, generating a much more extensive list of data for each individual frame in the cell. For the conditions 'CUG +tRNA +harr' and 'AGG +tRNA +harr' no construct frame data was available as read depth on the construct was too low.

This indicates that no significant frameshifting is occurring in the sample, as the frames are distributed in a similar fashion across the endogenous transcriptome. The notable exceptions are the 'CUG +tRNA -harr' and the 'AGG -tRNA +harr' conditions. In the former, there is a sizeable shift in the reading frame into the +1 frame. This would align with our hypothesis of ribosomes queuing up and 'pushing' the leading ribosome into a different frame. Though when looking at the plots from figure 6.1 and 6.2, there does not seem to be a queuing up of ribosomes directly behind the start codon, and instead a build-up right at the beginning of the transcript, most likely the position where the ribosome 'touches down' on the mRNA. It could be that in this position the ribosomes are still queuing up and forcing frameshifts, but this specific clustering is only seen in samples with excess met-tRNAi^{Met} which means this does not entirely match with the endogenous activity inside the cell. Also, as seen in all data, coverage on the construct was low, especially when attempting frame analysis. This discrepancy between the construct read coverage and the transcriptome, may go to explain some of the deviations between the construct and transcriptome frame data.

6.3 – Conclusion

While we can detect clustering of reads upstream of the start site, we cannot distinguish whether they originate from scanning, queuing, or initiating ribosomes, making drawing solid conclusions from the current data difficult. And while we can see possible accumulation of reads around the G4C2 repeat region flanks on the construct, a number of factors limit how much we can conclusively take away, as reads cannot be assigned in the main body of the G4C2 repeat region due to the limitations of ribosome profiling in this context. Coverage across the constructs with a CUG or AGG start codon was decidedly low, especially in comparison to the construct initiating with the canonical AUG codon. This limits our ability to firmly state whether PiCs are queuing or stalling behind the initiating Ribosome. The harringtonine treatment, despite enriching Ribosomes at the start sites across the entire transcriptome, failed to do so on our constructs, which would have helped confirm the accumulation of colliding or queuing PiCs. Also, as the coverage was low, frameshift analysis was not conclusive enough to see whether the Ribosomes, after initiating, were in fact being pushed into different frames of translation.

6.4 - Materials and Methods

In vitro charging of tRNAi^{Met} with MARS

Charging of Met-tRNAi^{Met} was carried out as follows: First 20µg of tRNAi^{Met} was denatured by incubating at 85°C for 3 minutes. 10X AA buffer [200mM Tris-HCl pH 7.5, 2ßßmM KCL, 200mM MgCl2, 100mM DTT] was added. The reaction was then cooled at room temperature for 5 minutes and the following were added to the indicated final concentrations: 0.625mM ATP, 0.2mg/mL BSA, 0.5mM methionine, 160pmoles MARS. Final reaction volume brought up 100µL in H2O. Incubated at 37°C for 15 minutes to charge the tRNAi^{Met}.

Ribosome profiling of SH-SY5Y cells

Ribosome profiling of SH-SY5Y cells carried out as previously described in chapter 2. Undifferentiated cells were grown to 70-80% confluence on 15cm cell culture plates before lysing and subsequent RNasel digestion and RPF isolation. Cells transfected utilising lipofectamine 2000 reagent (ThermoFisher) following manufacturers protocol with 20 μ g of plasmid containing construct containing one of the start codons (figure 6.1). 20 μ g of charged Met-tRNAi^{Met} was co-transfected alongside plasmid. Harringtonine treatment was carried out 48hrs post-transfection by adding harringtonine directly to cell plate to a final concentration of 2 μ g/mL and incubated at 37°C for 10mins. Reads mapped to the construct and the entire transcriptome for each individual condition. Reads were calibrated to the P site or the 5' most nucleotide, depending the experiment.

7 - Discussion

In this work, we set out to uncover and understand the molecular mechanisms underlying the neurodegenerative disease Charcot-Marie-Tooth disease, and investigate the frameshifting mechanism occurring in the C9Orf72ALS context. Both of these are debilitating, progressive diseases of which, especially for CMT, the molecular mechanisms underpinning the disease is still poorly understood. By utilising deep-sequencing approaches and a raft of molecular biological assays, we could come at these topics from a unique angle that help further our understanding of how these diseases initially manifest and progress. For CMT, our work provides evidence for a unique, gain-of-function effect for two CMT-related proteins, GARS (Chapter 3, and Chapter 5) and YARS (Chapter 4). Both of these proteins show a very similar effect in different models and conditions, providing strong evidence for our tRNA sequestration hypothesis. And for our work with C9-ALS (Chapter 6), while there was a number of limitations in our work, we have developed a strong starting point for further investigation, and have devised an analytical method for observing how ribosomes and the pre-initiation complex acts upstream of the start codon in regards to queuing of ribosomes before initiation at the canonical or non-canonical start codon. These two diseases were chosen as they both have a unique translational link: CMT specifically has an interesting translational link in that specific subtypes of the diseases are caused by mutations in translational necessary enzymes: the tRNA-aminoacyl-synthetases [244]. And for C9-ALS, the translational link is clear, as there is a necessity for di-peptide repeat proteins to be translated in a specific, non-canonical way and in multiple frames for the disease to develop [132]. Our approach then shows great promise in providing clear evidence of the development causes of these diseases, especially for CMT. Other neurodegenerative diseases, such as Huntington's disease, Fragile X syndrome, Vanishing white matter, and many others [161] could all benefit from this approach as all have demonstrable translational links [168], [176], [182]. Neurodegenerative diseases provide a unique problem in regard to how they affect neuronal cells specifically, especially when disease-related mutations are in genes which are ubiquitously expressed and necessary for general cell function, such as is the case for aaRSs in CMT. Trying to understand how the unique structure and function of neuronal cells are

specifically affected by these disorders, is key to understanding their development and progression.

7.1 - Charcot-Marie-Tooth disease

The length dependent degradation of motor and sensory neurons is the classical physiological symptom of CMT2 development in patients [230], with the neurons slowly dying and receding starting from the distal ends, such as the neuromuscular junctions. In the above data, I attempt to reconcile this phenotypic symptom with a possible molecular mechanism, causative of this disease. From the evidence gathered, we can see the mutant forms of GARS and YARS - both clinically relevant proteins for the development of CMT in patients – display a higher affinity to their cognate tRNA. As a consequence, this leads to a slowing of the ribosome at Gly and Tyr codons, respectively, as the ribosome sits ideally waiting for a tRNA to enter the A site so it can continue elongating. This sequestration effect thus leads to translational slowdowns at the respective codon. This could potentially be the leading cause of this disease progression. As previously discussed, CMT seems to target lower motor and sensory neurons specifically [115], which are the longest neurons in the body. Local translation at the distal sites of these neurons needs to be strictly maintained in order to properly maintain function and homeostasis at these sites [97]. Perturbance of this would lead to neuronal instability, and lead to the progressive dying back phenotype. The translational effects we see in our data, however, is fairly subtle, with no indications of outright protein synthesis shutdown or ribosomal stalling occurring. This is perhaps not surprising, given the disease context. CMT is a slowly progressing disease, where patients can live with it for a long time, even decades, depending on the mutation. If this sequestration effect caused a complete shutdown of protein synthesis, then the disease would be outright lethal, with cells being unable to develop and function from the outset. This is perhaps underscored by the fact that the majority of patients are Heterozygous for this disease [120], and homozygous models are difficult if not impossible to produce in mice depending on the mutation. P278KY homozygous mice are non-function at birth, and C157R homozygous mice, while could be born, died soon after [195], [245]. Generally homozygous mutants produced more severe phenotypes, such as central nervous system dysfunctions. Therefore, the effect must be subtle, but deleterious enough in the long term to cause gradual instability. While

specific genes would still need to be looked at and observed to see exactly the identity or types of genes that are mostly affected, any short-term study that doesn't look at this effect in a longer timeframe, allowing for the progressive disease to build up and cause more noticeably effects, would likely see no strong change. Either way, the benefits of seeing what genes are mostly disrupted would again lead to further understanding the development of this disease. More specifically, isolating the distal neuronal compartments form the somata to then analyse the local translatome and transcriptome of the distal neurons as compared to the somata, and in the context of CMT, would be invaluable. An analysis of codon occupancy or ribosomal stalling in the distal neurite compared to somata would also provide further evidence to this hypothesis of tRNA sequestration having an aberrant effect on local translation.

The benefit of this sequestration hypothesis is that it is a unifying mechanism that can better explain why this disease progresses, more so than other ideas in the current literature that try to explain a universal cause of this disease. Some of the major hypotheses currently being proposed involve: Neomorphic binding functions via interactions with HDAC6, mitochondrial dysfunctions, or disrupted noncanonical functions of the CMT-aaRS. Mutant GARS in particular has been shown in studies to have a number of aberrant binding partners, possible due to the changed binding sites from altered open conformation states [246]. One of these interactions is the reported interaction with HDAC6, the α -tubulin deacetylase enzyme [129]. While acetylated tubulin is found scattered across the microtubule network and leads to stability, deacetylated α -tubulin is necessary for the dynamic function of the transport network, especially in places of growth such as growth cones [247]. Interruption of this function by GARS could disrupt the transport network in the neuronal cell. Another current hypothesis is that mitochondrial dysfunction could be an underlying cause or marker for CMT development with patient samples carrying GARS mutations showing disrupted mitochondrial function [248]. Mitochondrial dysfunctions have been shown related to other forms of CMT, such as with GDAP1 mutants [249], and mitochondrial distribution, density, and function inside axons and dendrites is coupled directly to neuronal health [250]. However, mutations linked to CMT in YARS and GARS are not tied directly to mitochondrial function. YARS has separate genes for the mitochondrial form and the cytoplasmic form, and none of the CMT-related mutations hit the mitochondrial gene. Also, while GARS is unique in that a single gene codes for the mitochondrial and cytoplasmic form, none of the CMT-

mutants also hit in the N-terminal mitochondrial targeting sequence [251]. While this means that the mitochondrial form might still harbour some of the mutants, the fact is this feature cannot be shared across both aaRS related to CMT.

Some aaRSs have acquired noncanonical functions, such as angiogenesis, post-translational modifications, or the ability to be secreted from the cell to carry out extracellular functions, for example activating immune cells to release inflammatory cytokines in the antiviral response [252], [253]. GARS itself can be secreted from macrophages and exhibits antitumorigenic activity [254]. Separate studies have shown that both AARS and GARS have an aberrant binding to Neuropilin1 (Nrp1) – a receptor protein that typically binds to its ligand partner, vascular endothelial growth factor (VEGF) – and outcompetes VEGF for the binding. Nrp1 is needed for axon guidance and cell body growth and migration of neuronal cells, and disruption could lead to many defects in neuronal cell, and VEGF signalling is thought to protect neuronal cells from damage [246], [255]. While the tRNA sequestration hypothesis does not directly contradict these other models, the major issue with these hypotheses so far, is that not all of these interactions occur for all CMT-related mutants, and some of these are specific to one CMT-aaRS or another, leading to a still lack of a unifying mechanism to adequately explain the disease progression. For example, YARS also has its own Neomorphic binding partners in TRIM28, which can lead to sequestration of TRIM28 and activation of DNA damage repair genes, but this seems unique to YARS [256]. Of course, in this work sequestration of tRNA still needs to be seen for other proteins, such as HARS and AARS, but there is compelling evidence for it occurring in two contexts across many mutant variants of the proteins. One interesting line of enquiry that has yet to be explored fully, is the involvement - or lack thereof - of the Multi-synthetase complex (MSC). This is a protein complex with multiple aaRS bound together, supported by a number of accessory proteins, that form a structure that helps to channel charged aa-tRNA to the ribosome, thereby increasing translation efficiency [257], [258]. Interestingly, none of the CMT relevant aaRSs are known to associate to the MSC, instead being free to travel independently in the cytoplasm [20]. This has a number of interesting connotations when taking the sequestration of tRNA into account. Does the MSC help to prevent any sequestration effect by channelling elongation factors to bind to and associate with the Class I aaRS inside the MSC in higher affinity to better remove charged tRNA from the aaRSs? [259], [260]. Also, does the fact that the CMT-aaRSs are free to travel in the cell, mean they are more able to travel to distal areas

of the neuronal cell and sequester tRNA at these sensitive sites? All could be relevant paths to better understanding how this molecular mechanism develops. Specifically, trying to disrupt the MSC, or disrupting the association of one specific aaRS to the MSC and instead making it free in the cytoplasm, consequently seeing if this could lead to development of CMTlike symptoms, might be strongly indicative of the importance of this complex. Finally, we also showed here that tRNA overexpression rescues the deleterious effects of the mutant forms of both GARS and YARS, with a rescuing effect on Ribosomal occupancy, and reversing some of the phenotypic effects of the disease as seen in mouse and Drosophila models. Importantly, we have shown that addition of excess tRNA^{Gly} caused an increase in the amount of relative translation at the distal end of the neurites, highlighting that tRNA could potentially be a therapeutic agent for treating this disease. Similar in that works need to be done to see what gene sets expression is being mostly disrupted due to the sequestration of tRNA, works also needs to be done to see on a translational level, what specific effect the additional tRNA is having to counter the CMT phenotype. As we are treating with only one type of tRNA species, such as tRNA^{Tyr} or tRNA^{Gly}, then it follows that genes containing mostly that specific codon would benefit the most from addition of tRNA to decode that specific species.

7.2 - C9Orf72 mediated ALS/FTD

The translation of the di-peptide repeat proteins from all of the frames in the C9orf72 gene are a precursor to disease development [143], with each DPR having specific toxic effects on the cell [147]. As had been shown in studies and discussed above, frameshifting of the ribosome at or near the repeat region is the cause behind the translation of all of these DPRs from different frames. How this occurs is then vital to fully understand the mechanism of this disease. In the work here, we wanted to investigate whether ribosomes 'queuing' at initiation on non-canonical codons is facilitating the frameshifting to occur, through an as of yet not well understood mechanism of the queuing or stalled ribosomes, being able to 'push' the leading ribosome into different frames. While ribosomes can have difficulties translating repeat heavy regions [261], as discussed above, evidence of C9Orf72 suggests that the frameshifting must be occurring before the ribosome encounters the repeat region. Studies have also shown that ribosomal collisions can alter frames of the leading ribosome in bacterial

models [262] and in eukaryotic cells [239], [263], though this is only for two elongating ribosomes, and little has been shown in regard to pre-initiation complexes, or initiating ribosomes. Thus, while there is ample evidence to suggest frameshifting can occur due to colliding ribosomes, whether it is occurring in the specific context of RAN translation on non-canonical initiation codons is largely unknown.

The results from the sequencing analysis from the different C9 conditions revealed some interesting information, though limitations in this are apparent. First, from the coverage data, we can see indications that the addition of the excess tRNAi^{Met} enhances the formation of PiCs on the transcript, as seen by the greater amount of reads at the 5' most end of the construct. This would be expected, since charged tRNAi^{Met} is necessary for the formation of the ternary complex, which precedes the assembly of the rest of the pre-initiation complex. Excess amounts can thus lead to more PiCs forming and attaching to mRNA transcripts. However, despite this, on the CUG and AGG constructs, the read coverage of the transcripts was fairly low, especially as compared to the construct carrying the AUG start codon. Initiation at the non-canonical start codons is known to be more inefficient than AUG [240], which is logical as the cell would generally not favour random and uncontrollable initiation to keep occurring. This has the consequence though of depleting our analysis of usable reads. Scanning is a faster process than elongation as elongation involves more complicated steps, such as translocation of the ribosome, tRNA selection, and decoding which in itself involves the movement and interactions of eEF1, and peptide bond formation. Whereas PiC scanning is merely a process of inspection by tRNAi^{Met} on the mRNA. Estimates for scanning speeds vary, from 8-9nt/s [264] to upwards of 60-100nt/s, depending on whether you are referring to 'net' scanning rate, or single codon triplets [265]. Elongation rate on the other hand lies somewhere between 3aa/s to 5.6aa/s [266], [267] in eukaryotic cells with an initiation time of around ~25s on the AUG start codons. Meaning that if the PiCs are not initiating properly on the non-canonical start codons, then it simply scans through and falls off the sequence and doesn't allow their coverage to be properly captured in our setup. This inefficient initiation is seen in the +harringtonine samples which should force ribosomes to stall at initiation [268], but instead sees no major increase of stalled ribosomes at the non-canonical start codons. This lack of read depth on our construct unfortunately limits how much we can conclusively draw from the data, and how much we can deduce about any possible frameshifting occurring. Interestingly though, we see in our data that there is an accumulation of reads at the G₄C₂ repeat regions. These regions could form rigid secondary structures, akin to a Gquadruplex structure, a four stranded structure that is notoriously difficult for the ribosome to scan through [269], [270]. Surprisingly, the accumulation of reads at these regions does not disappear after harringtonine treatment, which should be the case if these are elongating ribosomes, unless some of the ribosomes scanning through this section are dramatically slowed down enough that they persist even after pulsing the cells with the antibiotic. Since previous studies have indicated that frameshifting is occurring before the repeat region in a C9Orf72 context, this would indicate that these reads are from elongating ribosomes that have effectively stalled in the repeat regions. This might be supportive of the repeat region acting as an IRES sequences with the ability to recruit ribosomes directly, and the scanning/initiating ribosomes coming from upstream of the repeat region could then collide and force the ribosome into a different frame. However, one issue with this is that, mapping reads from repetitive regions is difficult, since generally when mapping reads you remove reads that multi-map to multiple regions. Repeat regions, by nature are of course repetitive, meaning many of the reads in this region may be lost due to multi-mapping to other GC rich regions. This is an unfortunate limitation that is difficult to overcome, outside of increasing the fragment lengths used in the sequencing library generation.

Overall, our data indicates that excess tRNAi^{Met} aids in the formation of PiC formation on transcripts, and that this analysis we have set out is adequate to properly investigate the queueing of ribosomes at the start codon, and whether this can lead to the frameshifting of ribosomes on the transcript. To move forward, the experimental setup would need to change to better accommodate the retrieval of mRNA fragments protected by the PiC. Recently studies have shown that chemical crosslinking of the scanning complex to the mRNA using formaldehyde can be used effectively in this manner, and would be a good approach to move forward with this work [271]. Also, for a molecular assay to test for the frameshifting in different conditions, a triple-reporter construct can be generated, that expressions one of three fluorescent reporters in each frame. This would be a good way to see if excess PiC formation can force the ribosome to undergo more frameshifting, evidencing the 'pushing' hypothesis further.

7.3 - Conclusion

The work carried out during this project, especially in regard to our worked carried out for the Charcot-Marie-Tooth disease, has uncovered a novel mechanism underlying the development of this disease. We have utilised and shown the effectiveness and versatility of tRNA as both a potential therapeutic agent in the rescuing of CMT phenotype. And importantly, shown that investigating the translational landscape of the cell in regard to neurodegenerative disease, is both vital, and a useful pool of information in uncovering the exact mechanism behind their development. While questions are still unanswered in both disease contexts, we have built a strong foundation on to which more experiments and investigative paths can be taken. One other necessary point for the continuation of this work, is that in regard to neurodegenerative diseases, the importance of the unique structure and organisation of the neuronal cell cannot be understated. When it comes to diseases that specifically hit a certain cell type with mutations in proteins that are seemingly necessary for general cellular function, then the question must be asked about what makes that cell type unique amongst all the others. In the case for CMT here in this study, we can begin to build a case that the structure and the length, both corroborating with the disease phenotype, plays a major role in the disease mechanism. This idea can be further extended when looking at other diseases. Huntington's is another disease that toxicity from DPRs produced via RAN translational plays a role in its development [177]. Perhaps an approach to understanding how these DPR aggregates affect local translation at specific points in the neuronal cell could be a bountiful line of inquiry. Fragile X syndrome could also make use of this approach, looking specifically where on the neurites that sequestered RNA or dysregulated expression is causing the greatest instability. While the work here for C9-ALS unfortunately ran into some unforeseen limitations, we have set a solid basis of understanding for how to approach this question of frameshifting of the ribosome. We have also uncovered a unique molecular mechanism underlying Charcot-Marie-Tooth disease by looking and considering the direct effect the protein has on a translational level, both generally and in a site-specific manner in the compartmentalised neuronal cell. We have also shown that tRNA could act as a therapeutic agent for the potential treatment of this disease.

8 - Bibliography

- [1] D. N. Wilson and J. H. D. Cate, "The structure and function of the eukaryotic ribosome," *Cold Spring Harb. Perspect. Biol.*, vol. 4, no. 5, p. 5, May 2012.
- [2] R. Green and H. F. Noller, "Ribosomes and translation," *Annu. Rev. Biochem.*, vol. 66, no. 1, pp. 679–716, Jun. 1997.
- [3] C. E. Aitken, A. Petrov, and J. D. Puglisi, "Single ribosome dynamics and the mechanism of translation," *Annu. Rev. Biophys.*, vol. 39, no. 1, pp. 491–513, Apr. 2010.
- [4] M. V. Rodnina and W. Wintermeyer, "The ribosome as a molecular machine: The mechanism of tRNA-mRNA movement in translocation," *Biochem. Soc. Trans.*, vol. 39, no. 2, pp. 658–662, Apr. 2011.
- [5] X. Agirrezabala and J. Frank, "Elongation in translation as a dynamic interaction among the ribosome, tRNA, and elongation factors EF-G and EF-Tu," *Q. Rev. Biophys.*, vol. 42, no. 3, pp. 159–200, Aug. 2009.
- [6] S. C. Blanchard, H. D. Kim, R. L. Gonzalez, J. D. Puglisi, and S. Chu, "tRNA dynamics on the ribosome during translation," *Proc. Natl. Acad. Sci. U. S. A.*, vol. 101, no. 35, pp. 12893–12898, Aug. 2004.
- [7] M. Gamarra, A. de la Cruz, M. Blanco-Urrejola, and J. Baleriola, "Local Translation in Nervous System Pathologies," *Front. Integr. Neurosci.*, vol. 15, Jun. 2021.
- [8] A. G. Hinnebusch, "Structural Insights into the Mechanism of Scanning and Start Codon Recognition in Eukaryotic Translation Initiation," *Trends Biochem. Sci.*, vol. 42, no. 8, pp. 589–611, 2017.
- [9] B. Eliseev *et al.*, "Structure of a human cap-dependent 48S translation pre-initiation complex," *Nucleic Acids Res.*, vol. 46, no. 5, pp. 2678–2689, 2018.
- [10] M. A. Algire, D. Maag, and J. R. Lorsch, "Pi release from eIF2, not GTP hydrolysis, is the step controlled by start-site selection during eukaryotic translation initiation," *Mol. Cell*, vol. 20, no. 2, pp. 251–262, 2005.
- [11] J. L. Llácer *et al.*, "Conformational Differences between Open and Closed States of the Eukaryotic Translation Initiation Complex," *Mol. Cell*, vol. 59, no. 3, pp. 399–412, 2015.
- [12] L. Shivaya Valasek, "'Ribozoomin' Translation Initiation from the Perspective of the Ribosome-bound Eukaryotic Initiation Factors (eIFs)," *Curr. Protein Pept. Sci.*, vol. 13, no. 4, pp. 305–330, 2012.
- [13] S. Wagner, A. Herrmannová, R. Malík, L. Peclinovská, and L. S. Valášek, "Functional and Biochemical Characterization of Human Eukaryotic Translation Initiation Factor 3 in Living Cells," *Mol. Cell. Biol.*, vol. 34, no. 16, pp. 3041–3052, 2014.
- [14] V. G. Kolupaeva, T. V. Pestova, and C. U. T. Hellen, "Ribosomal binding to the internal ribosomal entry site of classical swine fever virus," *Rna*, vol. 6, no. 12, pp. 1791–1807, 2000.
- [15] K. H. Nielsen *et al.*, "Synergistic activation of eIF4A by eIF4B and eIF4G," *Nucleic Acids Res.*, vol. 39, no. 7, pp. 2678–2689, 2011.
- [16] A. Marintchev *et al.*, "Topology and Regulation of the Human eIF4A/4G/4H Helicase Complex in Translation Initiation," *Cell*, vol. 136, no. 3, pp. 447–460, Feb. 2009.
- [17] R. J. Jackson, C. U. T. Hellen, and T. V. Pestova, "The mechanism of eukaryotic translation initiation and

- principles of its regulation," Nat. Rev. Mol. Cell Biol., vol. 11, no. 2, pp. 113-127, 2010.
- [18] F. Martin *et al.*, "Ribosomal 18S rRNA base pairs with mRNA during eukaryotic translation initiation," *Nat. Commun.*, vol. 7, p. 12622, Aug. 2016.
- [19] H. Khatter, A. G. Myasnikov, S. K. Natchiar, and B. P. Klaholz, "Structure of the human 80S ribosome," *Nature*, vol. 520, no. 7549, pp. 640–645, Apr. 2015.
- [20] M. Angel, R. Gomez, and M. Ibba, "Aminoacyl-tRNA synthetases," 2020.
- [21] H. Ramu *et al.*, "Nascent Peptide in the Ribosome Exit Tunnel Affects Functional Properties of the A-Site of the Peptidyl Transferase Center," *Mol. Cell*, vol. 41, no. 3, pp. 321–330, Feb. 2011.
- [22] Y. Chadani, N. Sugata, T. Niwa, Y. Ito, S. Iwasaki, and H. Taguchi, "Nascent polypeptide within the exit tunnel stabilizes the ribosome to counteract risky translation," *EMBO J.*, vol. 40, no. 23, Dec. 2021.
- [23] P. V. Sergiev *et al.*, "Function of the ribosomal E-site: A mutagenesis study," *Nucleic Acids Res.*, vol. 33, no. 18, pp. 6048–6056, Oct. 2005.
- [24] A. Brown, S. Shao, J. Murray, R. S. Hegde, and V. Ramakrishnan, "Structural basis for stop codon recognition in eukaryotes," *Nature*, vol. 524, no. 7566, pp. 493–496, Aug. 2015.
- [25] C. U. T. Hellen, "Translation termination and ribosome recycling in eukaryotes," *Cold Spring Harb. Perspect. Biol.*, vol. 10, no. 10, Oct. 2018.
- [26] S. E. Kolitz and J. R. Lorsch, "Eukaryotic initiator tRNA: Finely tuned and ready for action," *FEBS Lett.*, vol. 584, no. 2, pp. 396–404, Jan. 2010.
- [27] A. Bastide and A. David, "Interaction of rRNA with mRNA and tRNA in translating mammalian ribosome: Functional implications in health and disease," *Biomolecules*, vol. 8, no. 4, Sep. 2018.
- [28] S. Shao, J. Murray, A. Brown, J. Taunton, V. Ramakrishnan, and R. S. Hegde, "Decoding Mammalian Ribosome-mRNA States by Translational GTPase Complexes," *Cell*, vol. 167, no. 5, pp. 1229-1240.e15, Nov. 2016.
- [29] A. Rozov, N. Demeshkina, I. Khusainov, E. Westhof, M. Yusupov, and G. Yusupova, "Novel base-pairing interactions at the tRNA wobble position crucial for accurate reading of the genetic code," *Nat. Commun.*, vol. 7, no. 1, p. 10457, Jan. 2016.
- [30] M. F. Juette *et al.*, "Didemnin B and ternatin-4 differentially inhibit conformational changes in eEF1A required for aminoacyl-tRNA accommodation into mammalian ribosomes," *Elife*, vol. 11, Oct. 2022.
- [31] J. Pan, L. B. Ruest, S. Xu, and E. Wang, "Immuno-characterization of the switch of peptide elongation factors eEF1A-1/EF-1 α and eEF1A-2/S1 in the central nervous system during mouse development," *Dev. Brain Res.*, vol. 149, no. 1, pp. 1–8, Mar. 2004.
- [32] M. Valle *et al.*, "Cryo-EM reveals an active role for aminoacyl-tRNA in the accommodation process," *EMBO J.*, vol. 21, no. 13, pp. 3557–3567, Jul. 2002.
- [33] R. M. Voorhees, T. M. Schmeing, A. C. Kelley, and V. Ramakrishnan, "The mechanism for activation of GTP hydrolysis on the ribosome," *Science* (80-.)., vol. 330, no. 6005, pp. 835–838, Nov. 2010.
- [34] A. Ferguson *et al.*, "Functional Dynamics within the Human Ribosome Regulate the Rate of Active Protein Synthesis," *Mol. Cell*, vol. 60, no. 3, pp. 475–486, Nov. 2015.
- [35] P. C. Whitford, P. Geggier, R. B. Altman, S. C. Blanchard, J. N. Onuchic, and K. Y. Sanbonmatsu,

- "Accommodation of aminoacyl-tRNA into the ribosome involves reversible excursions along multiple pathways," *Rna*, vol. 16, no. 6, pp. 1196–1204, Jun. 2010.
- [36] J. Frank, H. Gao, J. Sengupta, N. Gao, and D. J. Taylor, "The process of mRNA-tRNA translocation," *Proc. Natl. Acad. Sci. U. S. A.*, vol. 104, no. 50, pp. 19671–19678, Dec. 2007.
- [37] A. H. Ratje *et al.*, "Head swivel on the ribosome facilitates translocation by means of intra-subunit tRNA hybrid sites," *Nature*, vol. 468, no. 7324, pp. 713–716, Dec. 2010.
- [38] D. Susorov *et al.*, "Eukaryotic translation elongation factor 2 (eEF2) catalyzes reverse translocation of the eukaryotic ribosome," *J. Biol. Chem.*, vol. 293, no. 14, pp. 5220–5229, Apr. 2018.
- [39] L. F. Lareau, D. H. Hite, G. J. Hogan, and P. O. Brown, "Distinct stages of the translation elongation cycle revealed by sequencing ribosome-protected mRNA fragments," *Elife*, vol. 2014, no. 3, May 2014.
- [40] L. Y. Frolova *et al.*, "Mutations in the highly conserved GGQ motif of class I polypeptide release factors abolish ability of human eRF1 to trigger peptidyl-tRNA hydrolysis," *Rna*, vol. 5, no. 8, pp. 1014–1020, 1999.
- [41] J. Sund, M. Andér, and J. Åqvist, "Principles of stop-codon reading on the ribosome," *Nature*, vol. 465, no. 7300, pp. 947–950, Jun. 2010.
- [42] A. V. Pisarev *et al.*, "The Role of ABCE1 in Eukaryotic Posttermination Ribosomal Recycling," *Mol. Cell*, vol. 37, no. 2, pp. 196–210, Jan. 2010.
- [43] X. Ou, J. Cao, A. Cheng, M. P. Peppelenbosch, and Q. Pan, "Errors in translational decoding: TRNA wobbling or misincorporation?," *PLoS Genet.*, vol. 15, no. 3, p. e1008017, Mar. 2019.
- [44] G. Hanson and J. Coller, "Translation and Protein Quality Control: Codon optimality, bias and usage in translation and mRNA decay," *Nat. Rev. Mol. Cell Biol.*, vol. 19, no. 1, pp. 20–30, Jan. 2018.
- [45] S. Juszkiewicz, V. Chandrasekaran, Z. Lin, S. Kraatz, V. Ramakrishnan, and R. S. Hegde, "ZNF598 Is a Quality Control Sensor of Collided Ribosomes," *Mol. Cell*, vol. 72, no. 3, pp. 469-481.e7, Nov. 2018.
- [46] Y. Matsuo *et al.*, "Ubiquitination of stalled ribosome triggers ribosome-associated quality control," *Nat. Commun.*, vol. 8, no. 1, p. 159, Jul. 2017.
- [47] S. Hashimoto, T. Sugiyama, R. Yamazaki, R. Nobuta, and T. Inada, "Identification of a novel trigger complex that facilitates ribosome-associated quality control in mammalian cells," *Sci. Rep.*, vol. 10, no. 1, p. 3422, Feb. 2020.
- [48] Y. Nakamura, T. Gojobori, and T. Ikemura, "Codon usage tabulated from international DNA sequence databases: Status for the year 2000," *Nucleic Acids Res.*, vol. 28, no. 1, p. 292, Jan. 2000.
- [49] J. R. Iben and R. J. Maraia, "tRNA gene copy number variation in humans," *Gene*, vol. 536, no. 2, pp. 376–384, Feb. 2014.
- [50] J. M. Goodenbour and T. Pan, "Diversity of tRNA genes in eukaryotes," *Nucleic Acids Res.*, vol. 34, no. 21, pp. 6137–6146, 2006.
- [51] S. Renana and T. Tamir, "Modelling the efficiency of codon-tRNA interactions based on codon usage bias," *DNA Res.*, vol. 21, no. 5, pp. 511–525, Oct. 2014.
- [52] A. Riba, N. Di Nanni, N. Mittal, E. Arhné, A. Schmidt, and M. Zavolan, "Protein synthesis rates and ribosome occupancies reveal determinants of translation elongation rates," *Proc. Natl. Acad. Sci. U. S.*

- A., vol. 116, no. 30, pp. 15023–15032, Jul. 2019.
- [53] T. A. Thanaraj and P. Argos, "Ribosome-mediated translational pause and protein domain organization," *Protein Sci.*, vol. 5, no. 8, pp. 1594–1612, Aug. 1996.
- [54] C. J. Tsai, Z. E. Sauna, C. Kimchi-Sarfaty, S. V. Ambudkar, M. M. Gottesman, and R. Nussinov, "Synonymous Mutations and Ribosome Stalling Can Lead to Altered Folding Pathways and Distinct Minima," *J. Mol. Biol.*, vol. 383, no. 2, pp. 281–291, Nov. 2008.
- [55] D. Pak, Y. Kim, and Z. F. Burton, "Aminoacyl-tRNA synthetase evolution and sectoring of the genetic code," *Transcription*, vol. 9, no. 4, pp. 205–224, May 2018.
- [56] G. Eriani, M. Delarue, O. Poch, J. Gangloff, and D. Moras, "Partition of tRNA synthetases into two classes based on mutually exclusive sets of sequence motifs," *Nature*, vol. 347, no. 6289, pp. 203–206, Sep. 1990.
- [57] S. Cusack, C. Berthet-Colominas, M. Härtlein, N. Nassar, and R. Leberman, "A second class of synthetase structure revealed by X-ray analysis of Escherichia coli seryl-tRNA synthetase at 2.5 Å," *Nature*, vol. 347, no. 6290, pp. 249–255, Sep. 1990.
- [58] X. L. Zhou *et al.*, "Role of tRNA amino acid-accepting end in aminoacylation and its quality control," *Nucleic Acids Res.*, vol. 39, no. 20, pp. 8857–8868, Nov. 2011.
- [59] M. Sprinzl and F. Cramer, "Site of aminoacylation of tRNAs from Escherichia coli with respect to the 2' or 3' hydroxyl group of the terminal adenosine," *Proc. Natl. Acad. Sci. U. S. A.*, vol. 72, no. 8, pp. 3049–3053, Aug. 1975.
- [60] R. Giegé, M. Sissler, and C. Florentz, "Universal rules and idiosyncratic features in tRNA identity," *Nucleic Acids Res.*, vol. 26, no. 22, pp. 5017–5035, Nov. 1998.
- [61] R. Sankaranarayanan *et al.*, "Zinc ion mediated amino acid discrimination by threonyl-tRNA synthetase," *Nat. Struct. Biol.*, vol. 7, no. 6, pp. 461–465, Jun. 2000.
- [62] S. Fukai *et al.*, "Structural basis for double-sieve discrimination of L-valine from L-isoleucine and L-threonine by the complex of tRNA(Val) and valyl-tRNA synthetase," *Cell*, vol. 103, no. 5, pp. 793–803, Nov. 2000.
- [63] D. Tworowski, A. V. Feldman, and M. G. Safro, "Electrostatic potential of aminoacyl-tRNA synthetase navigates tRNA on its pathway to the binding site," *J. Mol. Biol.*, vol. 350, no. 5, pp. 866–882, Jul. 2005.
- [64] S. Tamaki, M. Tomita, H. Suzuki, and A. Kanai, "Systematic analysis of the binding surfaces between tRNAs and their respective aminoacyl tRNA synthetase based on structural and evolutionary data," *Front. Genet.*, vol. 8, no. JAN, Jan. 2018.
- [65] A. Kumar, J. Åqvist, and P. Satpati, "Principles of tRNAAla Selection by Alanyl-tRNA Synthetase Based on the Critical G3·U70 Base Pair," *ACS Omega*, vol. 4, no. 13, pp. 15539–15548, Sep. 2019.
- [66] K. Breitschopf and H. J. Gross, "The discriminator bases G 73 in human tRNAser and A73 in tRNALeu have significantly different roles in the recognition of aminoacyl-tRNA synthetases," *Nucleic Acids Res.*, vol. 24, no. 3, pp. 405–410, Feb. 1996.
- [67] G. Eriani and J. Gangloff, "Yeast aspartyl-tRNA synthetase residues interacting with tRNA(Asp) identity bases connectively contribute to tRNA(Asp) binding in the ground and transition-state complex and

- discriminate against non-cognate tRNAs," J. Mol. Biol., vol. 291, no. 4, pp. 761-773, Aug. 1999.
- [68] I. Finarov, N. Moor, N. Kessler, L. Klipcan, and M. G. Safro, "Structure of Human Cytosolic Phenylalanyl-tRNA Synthetase: Evidence for Kingdom-Specific Design of the Active Sites and tRNA Binding Patterns," *Structure*, vol. 18, no. 3, pp. 343–353, Mar. 2010.
- [69] X. Deng *et al.*, "Large conformational changes of insertion 3 in human glycyl-tRNA synthetase (hGlyRS) during catalysis," *J. Biol. Chem.*, vol. 291, no. 11, pp. 5740–5752, Mar. 2016.
- [70] R. Sankaranarayanan *et al.*, "The structure of threonyl-tRNA synthetase-tRNAThr complex enlightens its repressor activity and reveals an essential zinc ion in the active site," *Cell*, vol. 97, no. 3, pp. 371–381, Apr. 1999.
- [71] M. I. Valencia-Sánchez *et al.*, "Structural insights into the polyphyletic origins of glycyl tRNA synthetases," *J. Biol. Chem.*, vol. 291, no. 28, pp. 14430–14446, 2016.
- [72] N. M. Reynolds *et al.*, "Cell-specific differences in the requirements for translation quality control," *Proc. Natl. Acad. Sci. U. S. A.*, vol. 107, no. 9, pp. 4063–4068, Mar. 2010.
- [73] T. Bullwinkle, B. Lazazzera, and M. Ibba, "Quality control and infiltration of translation by amino acids outside of the genetic code," *Annu. Rev. Genet.*, vol. 48, no. 1, pp. 149–166, Nov. 2014.
- [74] M. T. Boniecki, M. T. Vu, A. K. Betha, and S. A. Martinis, "CP1-dependent partitioning of pretransfer and posttransfer editing in leucyl-tRNA synthetase," *Proc. Natl. Acad. Sci. U. S. A.*, vol. 105, no. 49, pp. 19223–19228, Dec. 2008.
- [75] Z. Liu *et al.*, "Homologous trans-editing factors with broad tRNA specificity prevent mistranslation caused by serine/threonine misactivation," *Proc. Natl. Acad. Sci. U. S. A.*, vol. 112, no. 19, pp. 6027–6032, 2015.
- [76] J. W. Lee *et al.*, "Editing-defective tRNA synthetase causes protein misfolding and neurodegeneration," *Nature*, vol. 443, no. 7107, pp. 50–55, Sep. 2006.
- [77] H. Roy, J. Ling, M. Irnov, and M. Ibba, "Post-transfer editing in vitro and in vivo by the β subunit of phenylalanyl-tRNA synthetase," *EMBO J.*, vol. 23, no. 23, pp. 4639–4648, Nov. 2004.
- [78] J. Ling *et al.*, "Resampling and Editing of Mischarged tRNA Prior to Translation Elongation," *Mol. Cell*, vol. 33, no. 5, pp. 654–660, Mar. 2009.
- [79] D. Boinagrov, S. Pangratz-Fuehrer, B. Suh, K. Mathieson, N. Naik, and D. Palanker, "Upper threshold of extracellular neural stimulation," *J. Neurophysiol.*, vol. 108, no. 12, pp. 3233–3238, Dec. 2012.
- [80] V. E. Abraira and D. D. Ginty, "The sensory neurons of touch," *Neuron*, vol. 79, no. 4, pp. 618–639, Aug. 2013.
- [81] T. Taylor-Clark and B. J. Undem, "Transduction mechanisms in airway sensory nerves," *J. Appl. Physiol.*, vol. 101, no. 3, pp. 950–959, Sep. 2006.
- [82] N. Stifani, "Motor neurons and the generation of spinal motor neuron diversity," *Front. Cell. Neurosci.*, vol. 8, no. OCT, Oct. 2014.
- [83] M. E. Calcagnotto, "Interneurons: Role in maintaining and restoring synaptic plasticity," *Front. Psychiatry*, vol. 7, no. MAY, p. 86, 2016.
- [84] L. Li et al., "The functional organization of cutaneous low-threshold mechanosensory neurons," Cell, vol.

- 147, no. 7, pp. 1615–1627, Dec. 2011.
- [85] M. De Lera Ruiz and R. L. Kraus, "Voltage-Gated Sodium Channels: Structure, Function, Pharmacology, and Clinical Indications," *J. Med. Chem.*, vol. 58, no. 18, pp. 7093–7118, Sep. 2015.
- [86] J. E. Lisman, S. Raghavachari, and R. W. Tsien, "The sequence of events that underlie quantal transmission at central glutamatergic synapses," *Nat. Rev. Neurosci.*, vol. 8, no. 8, pp. 597–609, Aug. 2007.
- [87] C. E. Holt, K. C. Martin, and E. M. Schuman, "Local translation in neurons: visualization and function," *Nat. Struct. Mol. Biol.*, vol. 26, no. 7, pp. 557–566, 2019.
- [88] B. G. Hiester, M. I. Becker, A. B. Bowen, S. L. Schwartz, and M. J. Kennedy, "Mechanisms and role of dendritic membrane trafficking for long-term potentiation," *Front. Cell. Neurosci.*, vol. 12, Oct. 2018.
- [89] R. V. Haberberger, C. Barry, N. Dominguez, and D. Matusica, "Human dorsal root ganglia," *Front. Cell. Neurosci.*, vol. 13, no. June, pp. 1–17, 2019.
- [90] C. Sun *et al.*, "The prevalence and specificity of local protein synthesis during neuronal synaptic plasticity," *Science Advances*, vol. 7, no. 38. pp. 790–807, 2021.
- [91] J. Nijssen, J. Aguila, R. Hoogstraaten, N. Kee, and E. Hedlund, "Axon-Seq Decodes the Motor Axon Transcriptome and Its Modulation in Response to ALS," *Stem Cell Reports*, vol. 11, no. 6, pp. 1565–1578, 2018.
- [92] S. G. Dastidar and D. Nair, "A Ribosomal Perspective on Neuronal Local Protein Synthesis," *Front. Mol. Neurosci.*, vol. 15, p. 18, 2022.
- [93] O. Steward and C. E. Ribak, "Polyribosomes associated with synaptic specializations on axon initial segments: Localization of protein-synthetic machinery at inhibitory synapses," *J. Neurosci.*, vol. 6, no. 10, pp. 3079–3085, Oct. 1986.
- [94] C. C. Garner and A. Matus, "Different forms of microtubule-associated protein 2 are encoded by separate mRNA transcripts," *J. Cell Biol.*, vol. 106, no. 3, pp. 779–783, Mar. 1988.
- [95] K. E. Burgin, M. Neal Waxham, S. Rickling, S. A. Westgate, W. C. Mobley, and P. T. Kelly, "In situ hybridization histochemistry of Ca2+/calmodulin-dependent protein kinase in developing rat brain," *J. Neurosci.*, vol. 10, no. 6, pp. 1788–1798, Jun. 1990.
- [96] I. J. Cajigas, G. Tushev, T. J. Will, S. Tom Dieck, N. Fuerst, and E. M. Schuman, "The Local Transcriptome in the Synaptic Neuropil Revealed by Deep Sequencing and High-Resolution Imaging," *Neuron*, vol. 74, no. 3, pp. 453–466, May 2012.
- [97] E. L. Spaulding and R. W. Burgess, "Accumulating evidence for axonal translation in neuronal homeostasis," *Front. Neurosci.*, vol. 11, no. MAY, May 2017.
- [98] D. S. Campbell and C. E. Holt, "Chemotropic responses of retinal growth cones mediated by rapid local protein synthesis and degradation," *Neuron*, vol. 32, no. 6, pp. 1013–1026, 2001.
- [99] J. Tcherkezian, P. A. Brittis, F. Thomas, P. P. Roux, and J. G. Flanagan, "Transmembrane Receptor DCC Associates with Protein Synthesis Machinery and Regulates Translation," *Cell*, vol. 141, no. 4, pp. 632–644, May 2010.
- [100] N. Mazaré et al., "Local Translation in Perisynaptic Astrocytic Processes Is Specific and Changes after Fear

- Conditioning," Cell Rep., vol. 32, no. 8, p. 108076, Aug. 2020.
- [101] A. Biever *et al.*, "Monosomes actively translate synaptic mRNAs in neuronal processes," *Science* (80-.)., vol. 367, no. 6477, 2020.
- [102] M. S. Fernandopulle, J. Lippincott-Schwartz, and M. E. Ward, "RNA transport and local translation in neurodevelopmental and neurodegenerative disease," *Nat. Neurosci.*, vol. 24, no. 5, pp. 622–632, 2021.
- [103] S. C. Weber and C. P. Brangwynne, "Getting RNA and protein in phase," *Cell*, vol. 149, no. 6. Elsevier Inc., pp. 1188–1191, 2012.
- [104] S. E. Encalada, L. Szpankowski, C. H. Xia, and L. S. B. Goldstein, "Stable kinesin and dynein assemblies drive the axonal transport of mammalian prion protein vesicles," *Cell*, vol. 144, no. 4, pp. 551–565, Feb. 2011.
- [105] Y. C. Liao *et al.*, "RNA Granules Hitchhike on Lysosomes for Long-Distance Transport, Using Annexin A11 as a Molecular Tether," *Cell*, vol. 179, no. 1, pp. 147-164.e20, Sep. 2019.
- [106] K. Kipper, A. Mansour, and A. Pulk, "Neuronal RNA granules are ribosome complexes stalled at the pretranslocation state: Neuronal RNA granules as ribosome containing complexes," J. Mol. Biol., vol. 434, no. 20, p. 167801, Oct. 2022.
- [107] J. López-Erauskin *et al.*, "ALS/FTD-Linked Mutation in FUS Suppresses Intra-axonal Protein Synthesis and Drives Disease Without Nuclear Loss-of-Function of FUS," *Neuron*, vol. 100, no. 4, pp. 816-830.e7, Nov. 2018.
- [108] C. Lagier-Tourenne, M. Polymenidou, and D. W. Cleveland, "TDP-43 and FUS/TLS: Emerging roles in RNA processing and neurodegeneration," *Hum. Mol. Genet.*, vol. 19, no. R1, pp. R46–R64, Apr. 2010.
- [109] K. Yasuda, H. Zhang, D. Loiselle, T. Haystead, I. G. Macara, and S. Mili, "The RNA-binding protein Fus directs translation of localized mrnas in APC-RNP granules," J. Cell Biol., vol. 203, no. 5, pp. 737–746, Dec. 2013.
- [110] K. Yasuda, S. F. Clatterbuck-Soper, M. E. Jackrel, J. Shorter, and S. Mili, "FUS inclusions disrupt RNA localization by sequestering kinesin-1 and inhibiting microtubule detyrosination," *J. Cell Biol.*, vol. 216, no. 4, pp. 1015–1034, Apr. 2017.
- [111] C. Fallini *et al.*, "The Survival of Motor Neuron (SMN) protein interacts with the mRNA-binding protein HuD and regulates localization of poly(A) mRNA in primary motor neuron axons," *J. Neurosci.*, vol. 31, no. 10, pp. 3914–3925, Mar. 2011.
- [112] C. Fallini, P. G. Donlin-Asp, J. P. Rouanet, G. J. Bassell, and W. Rossoll, "Deficiency of the survival of motor neuron protein impairs mrna localization and local translation in the growth cone of motor neurons," *J. Neurosci.*, vol. 36, no. 13, pp. 3811–3820, Mar. 2016.
- [113] M. S. Fernandopulle, J. Lippincott-Schwartz, and M. E. Ward, "RNA transport and local translation in neurodevelopmental and neurodegenerative disease," *Nat. Neurosci.*, vol. 24, no. 5, pp. 622–632, May 2021.
- [114] A. Antonellis *et al.*, "Functional analyses of glycyl-tRNA synthetase mutations suggest a key role for tRNA-charging enzymes in peripheral axons," *J. Neurosci.*, vol. 26, no. 41, pp. 10397–10406, 2006.
- [115] H. M. E. Bienfait et al., "Phenotype of Charcot-Marie-Tooth disease Type 2," Neurology, vol. 68, no. 20,

- pp. 1658–1667, 2007.
- [116] A. S. D. Saporta, S. L. Sottile, L. J. Miller, S. M. E. Feely, C. E. Siskind, and M. E. Shy, "Charcot-marie-tooth disease subtypes and genetic testing strategies," *Ann. Neurol.*, vol. 69, no. 1, pp. 22–33, Jan. 2011.
- [117] J. Chad Hoyle, M. C. Isfort, J. Roggenbuck, and W. David Arnold, "The genetics of Charcot–Marie–Tooth disease: Current trends and future implications for diagnosis and management," *Appl. Clin. Genet.*, vol. 8, pp. 235–243, 2015.
- [118] K. Misu *et al.*, "An axonal form of Charcot-Marie-Tooth disease showing distinctive features in association with mutations in the peripheral myelin protein zero gene (Thr124Met or Asp75Val)," *J. Neurol. Neurosurg. Psychiatry*, vol. 69, no. 6, pp. 806–811, 2000.
- [119] N. Hattori *et al.*, "Demyelinating and axonal features of Charcot-Marie-Tooth disease with mutations of myelin-related proteins (PMP22, MPZ and Cx32): A clinicopathological study of 205 Japanese patients," *Brain*, vol. 126, no. 1, pp. 134–151, 2003.
- [120] S. H. Nam and B.-O. Choi, "Clinical and genetic aspects of Charcot-Marie-Tooth disease subtypes," *Precis. Futur. Med.*, vol. 3, no. 2, pp. 43–68, Jun. 2019.
- [121] D. Pareyson, V. Scaioli, and M. Laurà, "Clinical and electrophysiological aspects of charcot-marie-tooth disease," *NeuroMolecular Med.*, vol. 8, no. 1–2, pp. 3–22, 2006.
- [122] R. Prior, L. Van Helleputte, V. Benoy, and L. Van Den Bosch, "Defective axonal transport: A common pathological mechanism in inherited and acquired peripheral neuropathies," *Neurobiol. Dis.*, vol. 105, pp. 300–320, 2017.
- [123] P. C. Tsai *et al.*, "A recurrent WARS mutation is a novel cause of autosomal dominant distal hereditary motor neuropathy," *Brain*, vol. 140, no. 5, pp. 1252–1266, 2017.
- [124] Z. Mo *et al.*, "Aberrant GlyRS-HDAC6 interaction linked to axonal transport deficits in Charcot-Marie-Tooth neuropathy," *Nat. Commun.*, vol. 9, no. 1, 2018.
- [125] N. Wei, Q. Zhang, and X. L. Yang, "Neurodegenerative Charcot–Marie–Tooth disease as a case study to decipher novel functions of aminoacyl-tRNA synthetases," *J. Biol. Chem.*, vol. 294, no. 14, pp. 5321–5339, 2019.
- [126] S. J. Grice *et al.*, "Dominant, toxic gain-of-function mutations in gars lead to non-cell autonomous neuropathology," *Hum. Mol. Genet.*, vol. 24, no. 15, pp. 4397–4406, 2015.
- [127] K. L. Seburn, L. A. Nangle, G. A. Cox, P. Schimmel, and R. W. Burgess, "An Active Dominant Mutation of Glycyl-tRNA Synthetase Causes Neuropathy in a Charcot-Marie-Tooth 2D Mouse Model," *Neuron*, vol. 51, no. 6, pp. 715–726, 2006.
- [128] W. W. Motley *et al.*, "Charcot-marie-tooth-linked mutant GARS is toxic to peripheral neurons independent of wild-type GARS levels," *PLoS Genet.*, vol. 7, no. 12, p. e1002399, 2011.
- [129] A. S. T. Smith *et al.*, "HDAC6 Inhibition Corrects Electrophysiological and Axonal Transport Deficits in a Human Stem Cell-Based Model of Charcot-Marie-Tooth Disease (Type 2D)," *Adv. Biol.*, vol. 6, no. 2, p. 2101308, 2022.
- [130] N. R. Graff-Radford and B. K. Woodruff, "Frontotemporal dementia," *Semin. Neurol.*, vol. 27, no. 1, pp. 48–57, Feb. 2007.

- [131] M. T. Giordana, P. Ferrero, S. Grifoni, A. Pellerino, A. Naldi, and A. Montuschi, "Dementia and cognitive impairment in amyotrophic lateral sclerosis: A review," *Neurol. Sci.*, vol. 32, no. 1, pp. 9–16, Feb. 2011.
- [132] M. Boivin *et al.*, "Reduced autophagy upon C9ORF72 loss synergizes with dipeptide repeat protein toxicity in G4C2 repeat expansion disorders," *EMBO J.*, vol. 39, no. 4, Feb. 2020.
- [133] M. DeJesus-Hernandez *et al.*, "Expanded GGGGCC Hexanucleotide Repeat in Noncoding Region of C9ORF72 Causes Chromosome 9p-Linked FTD and ALS," *Neuron*, vol. 72, no. 2, pp. 245–256, Oct. 2011.
- [134] W. Dong *et al.*, "Knock in of a hexanucleotide repeat expansion in the C9orf72 gene induces ALS in rats," *Anim. Model. Exp. Med.*, vol. 3, no. 3, pp. 237–244, Sep. 2020.
- [135] R. Balendra and A. M. Isaacs, "C9orf72-mediated ALS and FTD: multiple pathways to disease," *Nat. Rev. Neurol.*, vol. 14, no. 9, pp. 544–558, Sep. 2018.
- [136] S. Wang *et al.*, "Nuclear export and translation of circular repeat-containing intronic RNA in C9ORF72-ALS/FTD," *Nat. Commun.*, vol. 12, no. 1, p. 4908, Aug. 2021.
- [137] N. Ramesh *et al.*, "RNA dependent suppression of C9orf72 ALS/FTD associated neurodegeneration by Matrin-3," *Acta Neuropathol. Commun.*, vol. 8, no. 1, p. 177, Dec. 2020.
- [138] Z. T. McEachin, J. Parameswaran, N. Raj, G. J. Bassell, and J. Jiang, "RNA-mediated toxicity in C9orf72 ALS and FTD," *Neurobiol. Dis.*, vol. 145, p. 105055, Nov. 2020.
- [139] V. V. Belzil *et al.*, "Reduced C9orf72 gene expression in c9FTD/ALS is caused by histone trimethylation, an epigenetic event detectable in blood," *Acta Neuropathol.*, vol. 126, no. 6, pp. 895–905, Dec. 2013.
- [140] T. F. Gendron and L. Petrucelli, "Disease mechanisms of c9orf72 repeat expansions," *Cold Spring Harb. Perspect. Med.*, vol. 8, no. 4, Apr. 2018.
- [141] Y. Sonobe, G. Ghadge, K. Masaki, A. Sendoel, E. Fuchs, and R. P. Roos, "Translation of dipeptide repeat proteins from the C9ORF72 expanded repeat is associated with cellular stress," *Neurobiol. Dis.*, vol. 116, pp. 155–165, Aug. 2018.
- [142] A. Schmitz, J. Pinheiro Marques, I. Oertig, N. Maharjan, and S. Saxena, "Emerging Perspectives on Dipeptide Repeat Proteins in C9ORF72 ALS/FTD," *Front. Cell. Neurosci.*, vol. 15, Feb. 2021.
- [143] D. A. Solomon *et al.*, "A feedback loop between dipeptide-repeat protein, TDP-43 and karyopherin-α mediates C9orf72-related neurodegeneration," *Brain*, vol. 141, no. 10, pp. 2908–2924, Oct. 2018.
- [144] B. D. Freibaum and J. P. Taylor, "The role of dipeptide repeats in C9ORF72-related ALS-FTD," Front. Mol. Neurosci., vol. 10, p. 35, 2017.
- [145] R. Tabet *et al.*, "CUG initiation and frameshifting enable production of dipeptide repeat proteins from ALS/FTD C9ORF72 transcripts," *Nat. Commun.*, vol. 9, no. 1, p. 152, Jan. 2018.
- [146] D. A. Solomon, R. Smikle, M. J. Reid, and S. Mizielinska, "Altered Phase Separation and Cellular Impact in C9orf72-Linked ALS/FTD," *Front. Cell. Neurosci.*, vol. 15, p. 664151, 2021.
- [147] B. K. Jensen *et al.*, "Synaptic dysfunction induced by glycine-alanine dipeptides in C9orf72- ALS / FTD is rescued by SV 2 replenishment," *EMBO Mol. Med.*, vol. 12, no. 5, May 2020.
- [148] R. Rossi, S. Arjmand, S. L. Bærentzen, A. Gjedde, and A. M. Landau, "Synaptic Vesicle Glycoprotein 2A: Features and Functions," *Front. Neurosci.*, vol. 16, p. 864514, 2022.
- [149] J. Pelletier and N. Sonenberg, "Internal initiation of translation of eukaryotic mRNA directed by a

- sequence derived from poliovirus RNA," Nature, vol. 334, no. 6180, pp. 320-325, Jul. 1988.
- [150] T. Endoh, Y. Kawasaki, and N. Sugimoto, "Suppression of gene expression by G-quadruplexes in open reading frames depends on G-quadruplex stability," *Angew. Chemie Int. Ed.*, vol. 52, no. 21, pp. 5522–5526, May 2013.
- [151] M. Wojciechowska, M. Olejniczak, P. Galka-Marciniak, M. Jazurek, and W. J. Krzyzosiak, "RAN translation and frameshifting as translational challenges at simple repeats of human neurodegenerative disorders," *Nucleic Acids Res.*, vol. 42, no. 19, pp. 11849–11864, Oct. 2014.
- [152] H. Liu *et al.*, "A Helicase Unwinds Hexanucleotide Repeat RNA G-Quadruplexes and Facilitates Repeat-Associated Non-AUG Translation," *J. Am. Chem. Soc.*, vol. 143, no. 19, pp. 7368–7379, May 2021.
- [153] Y. Sonobe *et al.*, "A C. elegans model of C9orf72-associated ALS/FTD uncovers a conserved role for eIF2D in RAN translation," *Nat. Commun.*, vol. 12, no. 1, p. 6025, Oct. 2021.
- [154] K. M. Green *et al.*, "RAN translation at C9orf72-associated repeat expansions is selectively enhanced by the integrated stress response," *Nat. Commun.*, vol. 8, no. 1, p. 2005, Dec. 2017.
- [155] T. Krishnamoorthy, G. D. Pavitt, F. Zhang, T. E. Dever, and A. G. Hinnebusch, "Tight Binding of the Phosphorylated α Subunit of Initiation Factor 2 (eIF2α) to the Regulatory Subunits of Guanine Nucleotide Exchange Factor eIF2B Is Required for Inhibition of Translation Initiation," *Mol. Cell. Biol.*, vol. 21, no. 15, pp. 5018–5030, Aug. 2001.
- [156] S. K. Young and R. C. Wek, "Upstream open reading frames differentially regulate genespecific translation in the integrated stress response," J. Biol. Chem., vol. 291, no. 33, pp. 16927–16935, Aug. 2016.
- [157] A. Sendoel *et al.*, "Translation from unconventional 5' start sites drives tumour initiation," *Nature*, vol. 541, no. 7638, pp. 494–499, Jan. 2017.
- [158] S. R. Starck *et al.*, "Translation from the 5' untranslated region shapes the integrated stress response," *Science* (80-.)., vol. 351, no. 6272, Jan. 2016.
- [159] S. K. Young, T. D. Baird, and R. C. Wek, "Translation regulation of the glutamyl-prolyl-tRNA synthetase gene EPRS through bypass of upstream open reading frames with noncanonical initiation codons," *J. Biol. Chem.*, vol. 291, no. 20, pp. 10824–10835, May 2016.
- [160] R. Dafinca *et al.*, "C9orf72 Hexanucleotide Expansions Are Associated with Altered Endoplasmic Reticulum Calcium Homeostasis and Stress Granule Formation in Induced Pluripotent Stem Cell-Derived Neurons from Patients with Amyotrophic Lateral Sclerosis and Frontotemporal Dementia," *Stem Cells*, vol. 34, no. 8, pp. 2063–2078, Aug. 2016.
- [161] J. X. Lu *et al.*, "Axonal mRNA localization and local translation in neurodegenerative disease," *Neural Regen. Res.*, vol. 16, no. 10, pp. 1950–1957, 2021.
- [162] S. Maday, A. E. Twelvetrees, A. J. Moughamian, and E. L. F. Holzbaur, "Axonal Transport: Cargo-Specific Mechanisms of Motility and Regulation," *Neuron*, vol. 84, no. 2, pp. 292–309, Oct. 2014.
- [163] J. N. Savas *et al.*, "A role for Huntington disease protein in dendritic RNA granules," *J. Biol. Chem.*, vol. 285, no. 17, pp. 13142–13153, Apr. 2010.
- [164] C. Bagni, F. Tassone, G. Neri, and R. Hagerman, "Fragile X syndrome: Causes, diagnosis, mechanisms, and

- therapeutics," J. Clin. Invest., vol. 122, no. 12, pp. 4314–4322, Dec. 2012.
- [165] A. Entezam *et al.*, "Regional FMRP deficits and large repeat expansions into the full mutation range in a new Fragile X premutation mouse model," *Gene*, vol. 395, no. 1–2, pp. 125–134, Jun. 2007.
- [166] U. Brykczynska *et al.*, "CGG Repeat-Induced FMR1 Silencing Depends on the Expansion Size in Human iPSCs and Neurons Carrying Unmethylated Full Mutations," *Stem Cell Reports*, vol. 7, no. 6, pp. 1059–1071, Dec. 2016.
- [167] D. Devys, Y. Lutz, N. Rouyer, J. P. Bellocq, and J. L. Mandel, "The FMR-1 protein is cytoplasmic, most abundant in neurons and appears normal in carriers of a fragile X premutation," *Nat. Genet.*, vol. 4, no. 4, pp. 335–340, Aug. 1993.
- [168] A. Lai, A. N. Valdez-Sinon, and G. J. Bassell, "Regulation of RNA granules by FMRP and implications for neurological diseases," *Traffic*, vol. 21, no. 7, pp. 454–462, Jul. 2020.
- [169] M. Mofatteh, "mRNA localization and local translation in neurons," *AIMS Neurosci.*, vol. 7, no. 3, pp. 299–310, 2020.
- [170] S. Miller, M. Yasuda, J. K. Coats, Y. Jones, M. E. Martone, and M. Mayford, "Disruption of dendritic translation of CaMKIIα impairs stabilization of synaptic plasticity and memory consolidation," *Neuron*, vol. 36, no. 3, pp. 507–519, Oct. 2002.
- [171] K. H. Zivraj *et al.*, "Subcellular profiling reveals distinct and developmentally regulated repertoire of growth cone mRNAs," *J. Neurosci.*, vol. 30, no. 46, pp. 15464–15478, Nov. 2010.
- [172] Y. Nakahata and R. Yasuda, "Plasticity of spine structure: Local signaling, translation and cytoskeletal reorganization," *Front. Synaptic Neurosci.*, vol. 10, no. AUG, Aug. 2018.
- [173] R. A. C. Roos, "Huntington's disease: A clinical review," *Orphanet J. Rare Dis.*, vol. 5, no. 1, p. 40, Dec. 2010.
- [174] A. Heinz, D. K. Nabariya, and S. Krauss, "Huntingtin and its role in mechanisms of rna-mediated toxicity," *Toxins (Basel).*, vol. 13, no. 7, p. 487, Jul. 2021.
- [175] K. R. Weiss, Y. Kimura, W. C. M. Lee, and J. T. Littleton, "Huntingtin aggregation kinetics and their pathological role in a drosophila Huntington's disease model," *Genetics*, vol. 190, no. 2, pp. 581–600, Feb. 2012.
- [176] M. Bañez-Coronel *et al.*, "RAN Translation in Huntington Disease," *Neuron*, vol. 88, no. 4, pp. 667–677, Nov. 2015.
- [177] P. Rudich, S. Watkins, and T. Lamitina, "PolyQ-independent toxicity associated with novel translational products from CAG repeat expansions," *PLoS One*, vol. 15, no. 4, p. e0227464, Apr. 2020.
- [178] S. G. Campbell, N. P. Hoyle, and M. P. Ashe, "Dynamic cycling of eIF2 through a large eIF2B-containing cytoplasmic body: Implications for translation control," *J. Cell Biol.*, vol. 170, no. 6, pp. 925–934, Sep. 2005.
- [179] M. D. Keefe *et al.*, "Vanishing white matter disease expression of truncated eif2b5 activates induced stress response," *Elife*, vol. 9, pp. 1–27, Dec. 2020.
- [180] H. D. Ryoo and D. Vasudevan, "Two distinct nodes of translational inhibition in the Integrated Stress Response," *BMB Rep.*, vol. 50, no. 11, pp. 539–545, Nov. 2017.

- [181] E. De Nadal, G. Ammerer, and F. Posas, "Controlling gene expression in response to stress," *Nat. Rev. Genet.*, vol. 12, no. 12, pp. 833–845, Dec. 2011.
- [182] S. L. Moon and R. Parker, "EIF2B2 mutations in vanishing white matter disease hypersuppress translation and delay recovery during the integrated stress response," *Rna*, vol. 24, no. 6, pp. 841–852, Jun. 2018.
- [183] M. E. Kuo and A. Antonellis, "Ubiquitously Expressed Proteins and Restricted Phenotypes: Exploring Cell-Specific Sensitivities to Impaired tRNA Charging," *Trends Genet.*, vol. 36, no. 2, pp. 105–117, 2020.
- [184] E. Storkebaum, "Peripheral neuropathy via mutant tRNA synthetases: Inhibition of protein translation provides a possible explanation," *BioEssays*, vol. 38, no. 9, pp. 818–829, Sep. 2016.
- [185] P. Schimmel, "Aminoacyl tRNA synthetases: general scheme of structure-function relationships in the polypeptides and recognition of transfer RNAs.," *Annu. Rev. Biochem.*, vol. 56, no. 1, pp. 125–158, Jun. 1987.
- [186] M. Ibba and D. Soll, "Aminoacyl-tRNA synthesis," Annu. Rev. Biochem., vol. 69, no. 1, pp. 617–650, 2000.
- [187] N. Sonenberg and A. G. Hinnebusch, "Regulation of Translation Initiation in Eukaryotes: Mechanisms and Biological Targets," *Cell*, vol. 136, no. 4, pp. 731–745, 2009.
- [188] L. A. Nangle, W. Zhang, W. Xie, X. L. Yang, and P. Schimmel, "Charcot-Marie-Tooth disease-associated mutant tRNA synthetases linked to altered dimer interface and neurite distribution defect," *Proceedings of the National Academy of Sciences of the United States of America*, vol. 104, no. 27. pp. 11239–11244, 2007.
- [189] S. Niehues *et al.*, "Impaired protein translation in Drosophila models for Charcot-Marie-Tooth neuropathy caused by mutant tRNA synthetases," *Nat. Commun.*, vol. 6, 2015.
- [190] E. Storkebaum *et al.*, "Dominant mutations in the tyrosyl-tRNA synthetase gene recapitulate in Drosophila features of human Charcot-Marie-Tooth neuropathy," *Proc. Natl. Acad. Sci. U. S. A.*, vol. 106, no. 28, pp. 11782–11787, Jul. 2009.
- [191] C. A. Froelich and E. A. First, "Dominant intermediate charcot-marie-tooth disorder is not due to a catalytic defect in tyrosyl-tRNA synthetase," *Biochemistry*, vol. 50, no. 33, pp. 7132–7145, 2011.
- [192] I. Erdmann *et al.*, "Cell-selective labelling of proteomes in Drosophila melanogaster," *Nat. Commun.*, vol. 6, no. 1, p. 7521, 2015.
- [193] D. C. Dieterich *et al.*, "In situ visualization and dynamics of newly synthesized proteins in rat hippocampal neurons," *Nat. Neurosci.*, vol. 13, no. 7, pp. 897–905, 2010.
- [194] A. Zuko *et al.*, "tRNA overexpression rescues peripheral neuropathy caused by mutations in tRNA synthetase," *Science* (80-.)., vol. 373, no. 6559, pp. 1161–1166, 2021.
- [195] F. Achilli *et al.*, "An ENU-induced mutation in mouse glycyl-tRNA synthetase (GARS) causes peripheral sensory and motor phenotypes creating a model of Charcot-Marie-Tooth type 2D peripheral neuropathy," *DMM Dis. Model. Mech.*, vol. 2, no. 7–8, pp. 359–373, 2009.
- [196] K. H. Morelli *et al.*, "Allele-specific RNA interference prevents neuropathy in Charcot-Marie-Tooth disease type 2D mouse models," *J. Clin. Invest.*, vol. 129, no. 12, pp. 5568–5583, 2019.
- [197] A. P. Schuller and R. Green, "Roadblocks and resolutions in eukaryotic translation," *Nat. Rev. Mol. Cell Biol.*, vol. 19, no. 8, pp. 526–541, Aug. 2018.

- [198] M. Graille and B. Séraphin, "Surveillance pathways rescuing eukaryotic ribosomes lost in translation," *Nat. Rev. Mol. Cell Biol.*, vol. 13, no. 11, pp. 727–735, 2012.
- [199] C. A. P. Joazeiro, "Ribosomal stalling during translation: Providing substrates for ribosome-associated protein quality control," *Annu. Rev. Cell Dev. Biol.*, vol. 33, no. 1, pp. 343–368, 2017.
- [200] R. Ishimura *et al.*, "Ribosome stalling induced by mutation of a CNS-specific tRNA causes neurodegeneration," *Science* (80-.)., vol. 345, no. 6195, pp. 455–459, 2014.
- [201] A. J. Inglis *et al.*, "Activation of GCN2 by the ribosomal P-stalk," *Proc. Natl. Acad. Sci. U. S. A.*, vol. 116, no. 11, pp. 4946–4954, 2019.
- [202] H. P. Harding *et al.*, "The ribosomal P-stalk couples amino acid starvation to GCN2 2 activation in mammalian cells," *Elife*, vol. 8, no. NA, p. NA-NA, Nov. 2019.
- [203] C. C. C. Wu, A. Peterson, B. Zinshteyn, S. Regot, and R. Green, "Ribosome Collisions Trigger General Stress Responses to Regulate Cell Fate," *Cell*, vol. 182, no. 2, pp. 404-416.e14, 2020.
- [204] E. L. Spaulding *et al.*, "The integrated stress response contributes to tRNA synthetase—associated peripheral neuropathy," *Science* (80-.)., vol. 373, no. 6559, pp. 1156–1161, 2021.
- [205] J. Corzo and M. Santamaria, "Time, the forgotten dimension of ligand binding teaching," *Biochem. Mol. Biol. Educ.*, vol. 34, no. 6, pp. 413–416, 2006.
- [206] G. Zhang, I. Fedyunin, O. Miekley, A. Valleriani, A. Moura, and Z. Ignatova, "Global and local depletion of ternary complex limits translational elongation," *Nucleic Acids Res.*, vol. 38, no. 14, pp. 4778–4787, 2010.
- [207] S. Kirchner *et al.*, "Alteration of protein function by a silent polymorphism linked to tRNA abundance," *PLoS Biol.*, vol. 15, no. 5, pp. e2000779-NA, 2017.
- [208] C. Polte *et al.*, "Assessing cell-specific effects of genetic variations using tRNA microarrays," *BMC Genomics*, vol. 20, no. 8, pp. 1–12, 2019.
- [209] F. Tameire *et al.*, "ATF4 couples MYC-dependent translational activity to bioenergetic demands during tumour progression," *Nat. Cell Biol.*, vol. 21, no. 7, pp. 889–899, 2019.
- [210] S. Amirbeigiarab *et al.*, "Invariable stoichiometry of ribosomal proteins in mouse brain tissues with aging," *Proc. Natl. Acad. Sci. U. S. A.*, vol. 116, no. 45, pp. 22567–22572, 2019.
- [211] H. Guo, N. T. Ingolia, J. S. Weissman, and D. P. Bartel, "Mammalian microRNAs predominantly act to decrease target mRNA levels," *Nature*, vol. 466, no. 7308, pp. 835–840, Aug. 2010.
- [212] A. Dobin *et al.*, "STAR: Ultrafast universal RNA-seq aligner," *Bioinformatics*, vol. 29, no. 1, pp. 15–21, 2013.
- [213] L. F. Lareau, D. H. Hite, G. J. Hogan, and P. O. Brown, "Distinct stages of the translation elongation cycle revealed by sequencing ribosome-protected mRNA fragments," *Elife*, vol. 2014, no. 3, pp. e01257-NA, 2014.
- [214] A. Bartholomäus and Z. Ignatova, "Codon Resolution Analysis of Ribosome Profiling Data," *Methods Mol. Biol.*, vol. 2252, no. NA, pp. 251–268, 2021.
- [215] E. Storkebaum *et al.*, "Dominant mutations in the tyrosyl-tRNA synthetase gene recapitulate in Drosophila features of human Charcot-Marie-Tooth neuropathy," *Proc. Natl. Acad. Sci. U. S. A.*, vol. 106, no. 28, pp. 11782–11787, 2009.

- [216] A. Jordanova *et al.*, "Disrupted function and axonal distribution of mutant tyrosyl-tRNA synthetase in dominant intermediate Charcot-Marie-Tooth neuropathy," *Nat. Genet.*, vol. 38, no. 2, pp. 197–202, 2006.
- [217] E. T. Larson *et al.*, "The double-length tyrosyl-tRNA synthetase from the eukaryote leishmania major forms an intrinsically asymmetric pseudo-dimer," *J. Mol. Biol.*, vol. 409, no. 2, pp. 159–176, Jun. 2011.
- [218] M. Tsunoda *et al.*, "Structural basis for recognition of cognate tRNA by tyrosyl-tRNA synthetase from three kingdoms," *Nucleic Acids Res.*, vol. 35, no. 13, pp. 4289–4300, 2007.
- [219] T. D. Bird, Charcot-Marie-Tooth (CMT) Hereditary Neuropathy Overview. 1993.
- [220] S. Bervoets *et al.*, "Transcriptional dysregulation by a nucleus-localized aminoacyl-tRNA synthetase associated with Charcot-Marie-Tooth neuropathy," *Nat. Commun.*, vol. 10, no. 1, pp. 1–14, 2019.
- [221] M. Safro and L. Klipcan, "The mechanistic and evolutionary aspects of the 2'- and 3'-OH paradigm in biosynthetic machinery," *Biol. Direct*, vol. 8, no. 1, p. 17, Jul. 2013.
- [222] K. A. Dittmar, J. M. Goodenbour, and T. Pan, "Tissue-specific differences in human transfer RNA expression," *PLoS Genet.*, vol. 2, no. 12, pp. 2107–2115, 2006.
- [223] M. Santra and B. Bagchi, "Catalysis of tRNA aminoacylation: Single turnover to steady-state kinetics of tRNA synthetases," *J. Phys. Chem. B*, vol. 116, no. 39, pp. 11809–11817, Oct. 2012.
- [224] J. Nijssen, J. Aguila, R. Hoogstraaten, N. Kee, and E. Hedlund, "Axon-Seq Decodes the Motor Axon Transcriptome and Its Modulation in Response to ALS," *Stem Cell Reports*, vol. 11, no. 6, pp. 1565–1578, 2018.
- [225] C. M. Fusco *et al.*, "Neuronal ribosomes exhibit dynamic and context-dependent exchange of ribosomal proteins," *Nat. Commun.*, vol. 12, no. 1, 2021.
- [226] Y. Fonkeu *et al.*, "How mRNA Localization and Protein Synthesis Sites Influence Dendritic Protein Distribution and Dynamics," *Neuron*, vol. 103, no. 6, pp. 1109-1122.e7, Sep. 2019.
- [227] M. Giustetto *et al.*, "Axonal transport of eukaryotic translation elongation factor 1α mRNA couples transcription in the nucleus to long-term facilitation at the synapse," *Proc. Natl. Acad. Sci. U. S. A.*, vol. 100, no. 23, pp. 13680–13685, Nov. 2003.
- [228] B. Koltun *et al.*, "Measuring mRNA translation in neuronal processes and somata by tRNA-FRET," *Nucleic Acids Res.*, vol. 48, no. 6, pp. E32–E32, 2020.
- [229] S. M. II, S. J. Cho, D. H. Seog, and R. Walikonis, "Neuronal activation increases the density of eukaryotic translation initiation factor 4E mRNA clusters in dendrites of cultured hippocampal neurons," *Exp. Mol. Med.*, vol. 41, no. 8, pp. 601–610, 2009.
- [230] L. Morant, M. L. Erfurth, and A. Jordanova, "Drosophila models for charcot-marie-tooth neuropathy related to aminoacyl-trna synthetases," *Genes (Basel).*, vol. 12, no. 10, p. 1519, Sep. 2021.
- [231] M. M. Shipley, C. A. Mangold, and M. L. Szpara, "Differentiation of the SH-SY5Y human neuroblastoma cell line," *J. Vis. Exp.*, vol. 2016, no. 108, Feb. 2016.
- [232] P. Reinhardt *et al.*, "Derivation and Expansion Using Only Small Molecules of Human Neural Progenitors for Neurodegenerative Disease Modeling," *PLoS One*, vol. 8, no. 3, p. e59252, Mar. 2013.
- [233] J. Kovalevich and D. Langford, "Considerations for the use of SH-SY5Y neuroblastoma cells in

- neurobiology," Methods Mol. Biol., vol. 1078, pp. 9-21, 2013.
- [234] S. C. Dolfi *et al.*, "The metabolic demands of cancer cells are coupled to their size and protein synthesis rates," *Cancer Metab.*, vol. 1, no. 1, p. 20, Dec. 2013.
- [235] H. Zhang, Z. W. Zhou, and L. Sun, "Aminoacyl-tRNA synthetases in Charcot–Marie–Tooth disease: A gain or a loss?," *J. Neurochem.*, vol. 157, no. 3, pp. 351–369, May 2021.
- [236] A. Antonellis *et al.*, "Glycyl tRNA synthetase mutations in Charcot-Marie-Tooth disease type 2D and distal spinal muscular atrophy type V," *Am. J. Hum. Genet.*, vol. 72, no. 5, pp. 1293–1299, May 2003.
- [237] M. M. Shipley, C. A. Mangold, and M. L. Szpara, "Differentiation of the SH-SY5Y human neuroblastoma cell line," *J. Vis. Exp.*, vol. 2016, no. 108, 2016.
- [238] S. B. Yamada et al., "RPS25 is required for efficient RAN translation of C9orf72 and other neurodegenerative disease-associated nucleotide repeats," Nat. Neurosci., vol. 22, no. 9, pp. 1383– 1388, Sep. 2019.
- [239] C. L. Simms, L. L. Yan, J. K. Qiu, and H. S. Zaher, "Ribosome Collisions Result in +1 Frameshifting in the Absence of No-Go Decay," *Cell Rep.*, vol. 28, no. 7, pp. 1679-1689.e4, Aug. 2019.
- [240] M. G. Kearse and J. E. Wilusz, "Non-AUG translation: A new start for protein synthesis in eukaryotes," *Genes Dev.*, vol. 31, no. 17, pp. 1717–1731, Sep. 2017.
- [241] K. Ichihara *et al.*, "Combinatorial analysis of translation dynamics reveals eIF2 dependence of translation initiation at near-cognate codons," *Nucleic Acids Res.*, vol. 49, no. 13, pp. 7298–7317, Jul. 2021.
- [242] C. J. Reyes, K. Asano, P. K. Todd, C. Klein, and A. Rakovic, "Repeat-Associated Non-AUG Translation of AGAGGG Repeats that Cause X-Linked Dystonia-Parkinsonism," *Mov. Disord.*, vol. 37, no. 11, pp. 2284–2289, Nov. 2022.
- [243] M. Eshraghi *et al.*, "Mutant Huntingtin stalls ribosomes and represses protein synthesis in a cellular model of Huntington disease," *Nat. Commun.*, vol. 12, no. 1, p. 1461, Mar. 2021.
- [244] D. Blocquel *et al.*, "CMT disease severity correlates with mutation-induced open conformation of histidyl-tRNA synthetase, not aminoacylation loss, in patient cells," *Proc. Natl. Acad. Sci. U. S. A.*, vol. 116, no. 39, pp. 19440–19448, Sep. 2019.
- [245] K. L. Seburn, L. A. Nangle, G. A. Cox, P. Schimmel, and R. W. Burgess, "An Active Dominant Mutation of Glycyl-tRNA Synthetase Causes Neuropathy in a Charcot-Marie-Tooth 2D Mouse Model," *Neuron*, vol. 51, no. 6, pp. 715–726, Sep. 2006.
- [246] W. He *et al.*, "CMT2D neuropathy is linked to the neomorphic binding activity of glycyl-tRNA synthetase," *Nature*, vol. 526, no. 7575, pp. 710–714, 2015.
- [247] C. Hubbert *et al.*, "HDAC6 is a microtubule-associated deacetylase," *Nature*, vol. 417, no. 6887, pp. 455–458, 2002.
- [248] B. Ozes *et al.*, "AAV1.NT-3 gene therapy in a CMT2D model: phenotypic improvements in GarsP278KY/mice," *Brain Commun.*, vol. 3, no. 4, p. fcab252, 2021.
- [249] J. Cassereau *et al.*, "Mitochondrial dysfunction and pathophysiology of Charcot-Marie-Tooth disease involving GDAP1 mutations," *Exp. Neurol.*, vol. 227, no. 1, pp. 31–41, 2011.
- [250] G. López-Doménech et al., "Loss of Dendritic Complexity Precedes Neurodegeneration in a Mouse Model

- with Disrupted Mitochondrial Distribution in Mature Dendrites," *Cell Rep.*, vol. 17, no. 2, pp. 317–327, 2016.
- [251] W. Xie, L. A. Nangle, W. Zhang, P. Schimmel, and X. L. Yang, "Long-range structural effects of a Charcot-Marie-Tooth disease-causing mutation in human glycyl-tRNA synthetase," *Proceedings of the National Academy of Sciences of the United States of America*, vol. 104, no. 24. pp. 9976–9981, 2007.
- [252] H.-C. Lee *et al.*, "Released Tryptophanyl-tRNA Synthetase Stimulates Innate Immune Responses against Viral Infection," *J. Virol.*, vol. 93, no. 2, Jan. 2019.
- [253] A. Nie, B. Sun, Z. Fu, and D. Yu, "Roles of aminoacyl-tRNA synthetases in immune regulation and immune diseases," *Cell Death Dis.*, vol. 10, no. 12, p. 901, Nov. 2019.
- [254] P. Yao and P. L. Fox, "Aminoacyl-tRNA synthetases in medicine and disease," *EMBO Mol. Med.*, vol. 5, no. 3, pp. 332–343, Mar. 2013.
- [255] L. Sun *et al.*, "CMT2N-causing aminoacylation domain mutants enable Nrp1 interaction with AlaRS," *Proc. Natl. Acad. Sci. U. S. A.*, vol. 118, no. 13, Mar. 2021.
- [256] D. Blocquel *et al.*, "Alternative stable conformation capable of protein misinteraction links tRNA synthetase to peripheral neuropathy," *Nucleic Acids Res.*, vol. 45, no. 13, pp. 8091–8104, 2017.
- [257] J. M. Han, J. Y. Kim, and S. Kim, "Molecular network and functional implications of macromolecular tRNA synthetase complex," *Biochem. Biophys. Res. Commun.*, vol. 303, no. 4, pp. 985–993, Apr. 2003.
- [258] S. V. Kyriacou and M. P. Deutscher, "An Important Role for the Multienzyme Aminoacyl-tRNA Synthetase Complex in Mammalian Translation and Cell Growth," *Mol. Cell*, vol. 29, no. 4, pp. 419–427, Feb. 2008.
- [259] C. M. Zhang, J. J. Perona, K. Ryu, C. Francklyn, and Y. M. Hou, "Distinct Kinetic Mechanisms of the Two Classes of Aminoacyl-tRNA Synthetases," *J. Mol. Biol.*, vol. 361, no. 2, pp. 300–311, 2006.
- [260] V. S. Reed, M. E. Wastney, and D. C. H. Yang, "Mechanisms of the transfer of aminoacyl-tRNA from aminoacyl-tRNA synthetase to the elongation factor 1α," J. Biol. Chem., vol. 269, no. 52, pp. 32932–32936, Dec. 1994.
- [261] E. S. Babaylova *et al.*, "MRNA regions where 80S ribosomes pause during translation elongation in vivo interact with protein uS19, a component of the decoding site," *Nucleic Acids Res.*, vol. 48, no. 2, pp. 912–923, Jan. 2020.
- [262] A. M. Smith, M. S. Costello, A. H. Kettring, R. J. Wingo, and S. D. Moore, "Ribosome collisions alter frameshifting at translational reprogramming motifs in bacterial mRNAs," *Proc. Natl. Acad. Sci. U. S. A.*, vol. 116, no. 43, pp. 21769–21779, Oct. 2019.
- [263] L. Houston, E. M. Platten, S. M. Connelly, J. Wang, and E. J. Grayhack, "Frameshifting at collided ribosomes is modulated by elongation factor eEF3 and by integrated stress response regulators Gcn1 and Gcn20," *Rna*, vol. 28, no. 3, pp. 320–339, Mar. 2022.
- [264] K. S. Vassilenko, O. M. Alekhina, S. E. Dmitriev, I. N. Shatsky, and A. S. Spirin, "Unidirectional constant rate motion of the ribosomal scanning particle during eukaryotic translation initiation," *Nucleic Acids Res.*, vol. 39, no. 13, pp. 5555–5567, Jul. 2011.
- [265] K. Li, J. Kong, S. Zhang, T. Zhao, and W. Qian, "Distance-dependent inhibition of translation initiation by downstream out-of-frame AUGs is consistent with a Brownian ratchet process of ribosome scanning,"

- Genome Biol., vol. 23, no. 1, p. 254, Dec. 2022.
- [266] A. Riba, N. Di Nanni, N. Mittal, E. Arhné, A. Schmidt, and M. Zavolan, "Protein synthesis rates and ribosome occupancies reveal determinants of translation elongation rates," *Proc. Natl. Acad. Sci. U. S. A.*, vol. 116, no. 30, pp. 15023–15032, Jul. 2019.
- [267] N. T. Ingolia, L. F. Lareau, and J. S. Weissman, "Ribosome profiling of mouse embryonic stem cells reveals the complexity and dynamics of mammalian proteomes," *Cell*, vol. 147, no. 4, pp. 789–802, 2011.
- [268] S. Lee, B. Liu, S. Lee, S. X. Huang, B. Shen, and S. B. Qian, "Global mapping of translation initiation sites in mammalian cells at single-nucleotide resolution," *Proc. Natl. Acad. Sci. U. S. A.*, vol. 109, no. 37, Sep. 2012.
- [269] S. Kumari, A. Bugaut, J. L. Huppert, and S. Balasubramanian, "An RNA G-quadruplex in the 5' UTR of the NRAS proto-oncogene modulates translation," *Nat. Chem. Biol.*, vol. 3, no. 4, pp. 218–221, Apr. 2007.
- [270] C. Schaeffer, B. Bardoni, J. L. Mandel, B. Ehresmann, C. Ehresmann, and H. Moine, "The fragile X mental retardation protein binds specifically to its mRNA via a purine quartet motif," *EMBO J.*, vol. 20, no. 17, pp. 4803–4813, Sep. 2001.
- [271] S. Wagner *et al.*, "Selective Translation Complex Profiling Reveals Staged Initiation and Co-translational Assembly of Initiation Factor Complexes," *Mol. Cell*, vol. 79, no. 4, pp. 546-560.e7, Aug. 2020.

9 - List of hazardous substances

The table below provides an overview about the substances which were used during this thesis. They are characterized by GHS pictograms, signal words, hazard and precautionary statements.

Substance	Pictogram	Signal word	Hazard statements	Precautionary statements
2-[4-(2-hydroxyethyl)piperazin- 1-yl] ethane-sulfonic acid (HEPES)		Not a dang	erous substance accor	ding to GHS
2-Mercaptoethanol		Danger	301+331, 310, 315, 317, 318, 373, 410	273, 280, 302+352, 304+340, 305+351+338, 308+310
Acetone	(1)	Danger	225, 319, 336	201, 305+351+338, 370+378, 403+235
Acrylamide/Bisacrylamide	\$	Danger	302+332, 315, 317, 319, 340, 350, 361f, 372	201, 261, 280, 304+340+312, 305+351+338, 308+313
Agarose		Not a dangerous substance according to GHS		
Ammonium acetate		Not a dangerous substance according to GHS		
Ammonium persul- fate	(1)	Danger	272, 302, 315, 317, 319, 334, 335	220, 261, 280, 305+351+338, 342+311
Ampicillin	\$	Danger	315,317, 319,334,335	261, 280, 305+351+338, 342+311
Bromophenol blue		Not a dangerous substance according to GHS		
Cycloheximide		Danger	300, 341, 360D, 411	202, 264, 270, 273, 280, 301, 310

CHIR99021		Danger	300, 315, 319, 335	301, 310	
Chloramphenicol	&	Warning	351	280	
Chloroform		Danger	302, 331, 315, 319, 351, 361d, 336, 372	261, 281, 305+351+338, 311	
Creatine phosphate		Not a dangerous substance according to GHS			
D-Glucose	Not a dangerous substance according to GHS				
Dimethyl sulfoxide		Not a dangerous substance according to GHS			
Dimethyl sulfate		Danger	301, 314, 317, 330, 341, 350	201, 280, 301+330+331, 302+352, 304+340, 305+351+338, 308+310	
Dithiothreitol	()	Warning	302, 315, 319, 335	261, 305+351+338	
Ethanol	⋄ (!)	Danger	225, 319	210, 240, 305+351+3 38, 403+233	
Ethylenediaminetetraacetic acid	\$ (!)	Warning	319, 332, 373	280, 304+340, 312, 305+351+3 38, 337+313	
Folinic acid	\$	Danger	315, 317, 319, 334, 335		

Substance	Pictogram	Signal word	Hazard statements	Precautio nary statem ents		
Formamide		Danger	315, 360D, 373	201, 314		
Glycerol		Not a dang	Not a dangerous substance according to GHS			
Glycine	<u>(1)</u>	Warning	315, 319, 335	261, 305+351+3 38		
Hydrogen peroxide (30%)		Danger	302, 318	280, 305 +35 1+3 38, 313		
Imidazole		Danger	360D, 302, 314	201, 280, 301+330 +331, 305+351 +338, 308+310		
Isopropyl alcohol	⋄ ••••••••••••••••••••••••••••••••••••	Danger	225, 319, 336	210, 233, 240, 305+351 +338, 403+235		
Isopropyl β- Dthiogalactopyranoside	(1)	Warning	319, 351	281, 305+351+3 38		
L-(+)-Arabinose		Not a dang	Not a dangerous substance according to GHS			
LB-Agar		Not a dang	Not a dangerous substance according to GHS			
LB-Medium		Not a dang	Not a dangerous substance according to GHS			
Magnesium acetate		Not a dangerous substance according to GHS				
Magnesium chloride		Not a dangerous substance according to GHS				
Monopotassium glutamate	2	Not a dang	Not a dangerous substance according to GHS			
Nickel NTA Resin [Thermo Fisher]		Not a dang	gerous substance according t	o GHS		

N-Methylisatoic anhydride	Warning	315, 319, 335	261, 305+351+338		
p-Coumaric acid	Warning	315, 319, 335	261, 305+351+338		
PEG 8000	Not a dar	Not a dangerous substance according to GHS			
Phenol	Danger	301+311+331, 314, 341, 373, 411	260, 280, 301+330+ 31+310, 303+361+ 53, 304+340+ 10, 305+351+ 38		
Phosphoenolpyruvate	Not a dar	Not a dangerous substance according to GHS			
Potassium acetate	Not a dar	Not a dangerous substance according to GHS			
Potassium chloride	Not a dar	Not a dangerous substance according to GHS			
Potassium dihydrogen phosphate	Not a dar	Not a dangerous substance according to GHS			
Purmorphamine	Not a dar	Not a dangerous substance according to GHS			
Puromycin- Dihydrochloride	Warning	H302	P301 + P312 + P330		
RedSafe	Not a dar	Not a dangerous substance according to GHS			
Sodium acetate	Not a dar	Not a dangerous substance according to GHS			
Sodium azide	Danger	300+310, 373, 410	273, 280, 301+310+330, 302+352+310, 391, 501		
Sodium chloride	Not a dar	Not a dangerous substance according to GHS			
Sodium dodecyl sulfate	Danger	228, 302+332, 315, 318, 335, 412	210, 261, 280 301+312+330 305+351+33 +310, 370+378		

Substance	Pictogram	Signal word	Hazard statements	Precautionary statements	
Sodium hydrogen phosphate		Not a dangerous substance according to GHS			
Spermidine	(e	Danger	314	280, 305+351+338, 310	
SYBR Gold	(N)	Warning	227	210, 280, 370+378	
Tetramethylethylenediamine	(!)	Danger	225, 332, 302, 314	210, 280, 305+351+338, 310	
Thiamine		Not a danger	Not a dangerous substance according to GHS		
TRIS acetate		Not a dangerous substance according to GHS			
Trisodium citrate		Not a dangerous substance according to GHS			
Triton X-100		Danger	302, 315, 318, 410	264, 273, 280, 301, 312, 302, 352, 305, 351, 338	
TRIzol		Danger	301+311+331, 314, 335, 341, 373, 412	201, 261, 264, 280, 273, 301+310, 302+352, 303+361+353, 304+340, 305+351+338	
Tyrosine		Danger	318	280, 305+351+338	
Tween 20		Not a dangerous substance according to GHS			
Urea		Not a dangerous substance according to GHS			
Xylene cyanol FF	<u>(1)</u>	Warning	315, 319, 335	261, 305+351+338	

Acknowledgements

I want to express my thanks to Prof. Dr. Zoya Ignatova, not only for her insight and guidance during this work, but also providing me this great opportunity to work in a fascinating project, with the trust she granted me in allowing me the freedoms to pursue my own scientific curiosity and interests, greatly aiding me in my own scientific advancement.

I would like to thank Prof. Dr. Erik Storkebaum, Radboud University, for his consistently helpful scientific insight and discussions, that have proved invaluable during this long and fruitful collaborative work. My other collaborators in this project, Prof. Dr. Ya-Ming Hou and Prof. Dr. Andreas Hermann, Universität Rostock, were also of great help in my project, and could not have been completed without them. And a thanks to Dr. Hannes Glaß for sharing his knowledge on the culturing and differentiation of the smNPC cells. I would also like to thank Dr. Marie Sissler for taking the time to reviewing my thesis.

Lastly, I would also like to thank the fantastic group of the Ignatova lab, both former and current members. Carrying out a PhD is often times gruelling work, but it is made infinitely more tolerable when surrounded by intelligent people who can help ease the burden and make a host of great memories with. I would like to thank Leonardo Santos for his consistently great work in all of the bioinformatic analysis. My special thanks go to Nikhil Bharti and Moritz Freyberg, for the long hours of discussion, advice, and many, many scientific arguments that were invaluable in helping to bounce around ideas and help solidify my thoughts.

Eidesstattliche Versicherung

Eidesstattliche Versicherung

Hiermit versichere ich an Eides statt, die vorliegende Dissertationsschrift selbst verfasst und

keine anderen als die angegebenen Hilfsmittel und Quellen benutzt zu haben. Die

eingereichte schriftliche Fassung entspricht der auf dem elektronischen Speichermedium.

Die Dissertation wurde in der vorgelegten oder einer ähnlichen Form nicht schon einmal in

einem früheren Promotionsverfahren angenommen oder als ungenügend beurteilt.

Affidavit

I hereby declare in lieu of an oath that I have written this dissertation thesis myself and that I

have not used any aids and sources other than those indicated. The submitted written version

corresponds to the one on the electronic storage medium.

The dissertation has not already been accepted in the form presented or in a similar form in

a previous doctoral procedure or has not been assessed as insufficient.

Hamburg, 6th June, 2023

Unterschrift der Doktorandin / des Doktoranden